Inorganic Chemistry

pubs.acs.org/IC

Review

$[Ru(bpy)_3]^{2+}$: The Ongoing Story of a Photochemical Icon

This review article is in dialogue with the review article 10.1021/acs.inorgchem.5c03471.

Céline Bourgois, Ludovic Troian-Gautier,* and Winald R. Kitzmann*

Cite This: *Inorg. Chem.* 2026, 65, 7549–7577

Read Online

ACCESS | Metrics & More | Article Recommendations | Supporting Information

ABSTRACT: $[Ru(bpy)_3]^{2+}$ has long served as the archetypal coordination complex for probing inorganic photophysics and photochemistry. Its intense visible MLCT absorption, quantitative intersystem crossing, and microsecond ^{3}MLCT lifetime established it as a benchmark photosensitizer across energy conversion, sensing, and catalysis. This review complements a recent historical perspective on $[Ru(bpy)_3]^{2+}$ by providing a contemporary view of its use as a versatile platform for advanced photochemical design. We first discuss updated views of its excited-state landscape, including refined descriptions of metal-centered states, minimum-energy crossing points, and photodissociation pathways, as well as the profound influence of counterions and microenvironments on excited-state energetics, stability, and reactivity. We then survey emerging applications, multiphoton solvated electron generation, mechanochemical ball-mill photoredox catalysis, and spin-forbidden red-light excitation. Next, we examine polynuclear complexes and dyads derived from the $[Ru(bpy)_3]^{2+}$ scaffold, emphasizing delocalized and antidissipative ^{3}MLCT states, long-lived charge separation, and integration into biohybrid or supramolecular architectures. Finally, we outline "real-life" applications in industrial photoredox chemistry, electrochemiluminescence immunoassays, oxygen sensing, and photodynamic therapy, and we position $[Ru(bpy)_3]^{2+}$ alongside emerging photosensitizers based on earth-abundant metals. Rather than being superseded, $[Ru(bpy)_3]^{2+}$ now functions as both a robust technological workhorse and an indispensable reference for next-generation photocatalyst design.

1. INTRODUCTION AND SCOPE

Tris(2,2′-bipyridine)ruthenium(II), $[Ru(bpy)_3]^{2+}$, is widely regarded as the prototypical coordination complex for the exploration of inorganic photochemistry and photophysics.[1−6] Its status as a model compound is due to the combination of several critical features: a strong visible-light absorption band characterized by metal-to-ligand charge transfer (MLCT) transitions, quantitative intersystem crossing (ISC) from singlet to triplet states, and a microsecond lifetime of the ^{3}MLCT excited state.[6,7] Over the years, $[Ru(bpy)_3]^{2+}$ has established itself as *the* reference[8−10] and has been utilized as both an educational tool[11] and a practical photosensitizer (PS),[7] facilitating discoveries in fields that range from solar energy conversion to electrochemiluminescence (ECL) sensing.[12−17]

The photophysical and photochemical behavior of $[Ru(bpy)_3]^{2+}$ is dominated by its MLCT states (Figure 1). Photoexcitation initially produces a singlet MLCT state (^{1}MLCT), which undergoes ultrafast intersystem crossing to yield the triplet MLCT state (^{3}MLCT).[10] This state perdures for ∼1 μs and constitutes the primary reactive species exploited in electron and energy transfer processes.[18] Its relatively long lifetime allows bimolecular quenching processes to occur efficiently, enabling both oxidative and reductive electron transfer pathways, as well as energy transfer reactions, such as the sensitization of singlet oxygen.[7,19] However, the performance of $[Ru(bpy)_3]^{2+}$ is also limited by the accessibility of metal-centered (MC) excited states.[20] Although these states lie at higher energy levels, they can be thermally populated, providing deactivation channels that compete with the productive reactivity of the MLCT.[20] In some cases, the MC state population can even lead to ligand dissociation or irreversible degradation, thereby compromising long-term stability.[21−23] The balance between maintaining an accessible and long-lived MLCT state while suppressing detrimental MC population thus remains a central design challenge.[24]

In this context, theoretical and computational chemistry have become crucial. Developments in time-dependent density functional theory (TD-DFT) and multiconfigurational ap-

Received: January 29, 2026
Revised: March 12, 2026
Accepted: March 19, 2026
Published: April 2, 2026

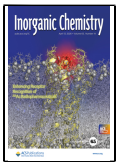

https://doi.org/10.1021/acs.inorgchem.6c00560
Inorg. Chem. 2026, 65, 7549−7577

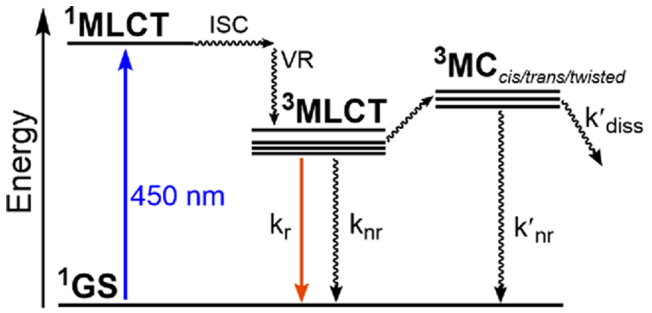

Figure 1. Simplified photophysical scheme of $[Ru(bpy)_3]^{2+}$. Light excitation populates a singlet metal-to-ligand charge transfer (^{1}MLCT) state that, after intersystem crossing (ISC) and vibrational relaxation (VR) populates the manifold of photoactive ^{3}MLCT state. For $[Ru(bpy)_3]^{2+}$, four distinct ^{3}MLCT states have been observed.[25] The ^{3}MLCT state can deactivate to the ground state through radiative and nonradiative decay (with the corresponding radiative (k_r) and nonradiative (k_{nr}) rate constants), or via population of higher-energy triplet metal-centered (^{3}MC) states that can also lead to ligand-loss chemistry, with the corresponding dissociation rate constant (k'_{diss}). The ^{3}MC manifold has recently been proposed to be composed of three distinct states (*cis*, *trans* and *twisted*) that are close in energy.[26−28]

proaches have allowed for more accurate mapping of the MLCT−MC energy gap and enhanced our understanding of ISC and the pathways involved in excited-state relaxation.[21,22,28,29] These insights not only shed light on the fundamental aspects of excited-state dynamics but also serve as a predictive tool for the strategic design of modified ligands, customized environments, and hybrid materials that stabilize the MLCT states. The synergy between experimental approaches and theoretical models is therefore key to addressing long-standing issues of excited-state deactivation and to developing strategies that extend the utility of $[Ru(bpy)_3]^{2+}$ in modern photochemical applications.

While the fundamental photophysical properties of $[Ru(bpy)_3]^{2+}$ are well established,[10,18,30] the past decade has witnessed a resurgence of innovation in this area. Contemporary research has shifted from discovering entirely new properties to developing strategies that exploit, control, and extend the known excited-state reactivity of these complexes within modern chemical contexts. The development and wider access to advanced experimental techniques capable of resolving events on extremely short time scales, such as femtosecond transient absorption spectroscopy[31] or time-resolved X-ray absorption spectroscopy,[32−34] have significantly enhanced our ability to elucidate excited-state landscapes and reactivity. Based on this knowledge acquired over past decades, novel avenues have recently emerged with use of the $[Ru(bpy)_3]^{2+}$ motif in polynuclear complexes,[35−41] dyads,[42−46] or within structured environments, such as metal−organic frameworks,[47] porous polymers,[48−51] and conductive supports.[52−54] This heterogenization has improved recyclability,[55,56] enhanced robustness under operational conditions,[45] and created new opportunities for the integration of $[Ru(bpy)_3]^{2+}$-type structures into photocatalytic devices.[46] Moreover, recent studies have highlighted the significant impact of the local microenvironment, including counterions,[57−60] solvent polarity,[61−67] and encapsulating matrices[68−70] on excited-state energetics and lifetimes. These findings demonstrate that photoredox efficiency and selectivity can often be tuned without altering the ligand framework, underscoring the versatility of local condition engineering as a means of controlling reactivity.

Within this review,[71] we will not provide a comprehensive survey of $[Ru(bpy)_3]^{2+}$'s widespread use as a photosensitizer in organic transformations, but we will rather spotlight recent experimental and theoretical breakthroughs that have opened new conceptual directions, expanded the mechanistic landscape, and inspired innovative strategies in photochemistry. The review also examines its industrial applications and concludes with a perspective that positions this established archetype alongside emerging photosensitizers based on earth-abundant elements.

2. INNOVATIVE APPROACHES TO $[RU(BPY)_3]^{2+}$ PHOTOCHEMISTRY AND PHOTOPHYSICS

2.1. Revisiting Metal-Centered Excited States

The defining feature of $[Ru(bpy)_3]^{2+}$ is its long-lived luminescence from ^{3}MLCT excited states.[10] Decades of research have been spent to understand what sets $[Ru(bpy)_3]^{2+}$ apart from other transition metal complexes that lack some of these favorable ground- and excited-state properties.[6,18,30,72] In particular, understanding the mechanism of nonradiative excited-state deactivation represents an important avenue to develop better chromophores.[30] In $[Ru(bpy)_3]^{2+}$, the barrier for the deactivation of the ^{3}MLCT state was determined as 3,800 cm^{-1} using temperature-dependent luminescence lifetime measurements.[73,74] This activation energy was assigned to the ^{3}MLCT−^{3}MC energy gap or the barrier for the ^{3}MLCT−^{3}MC internal conversion.[73,74] Recently, this model has been called into question as temperature-dependent lifetimes of $[Ru(bpy)_3]^{2+}$ were revisited computationally by González et al.[29] Instead of solely considering the ^{3}MC state as one state, the authors computed deactivation pathways along the ^{3}MC-*trans*, ^{3}MC-*cis*, and the ^{3}MC-*twist* geometries, which differ in their molecular structure and *d*-orbital occupation.[29] DFT calculations revealed that the experimentally determined activation energy corresponded to the energetic span between the ^{3}MLCT state and the minimum-energy crossing points (MECP) of the different ^{3}MC states with the singlet ground state.[29] The authors found that the contribution of the previously invoked ^{3}MC-*trans* state in the deactivation process was actually minimal due to its high-energy ^{3}MECP.[29]

Apart from facilitating nonradiative relaxation, population of the ^{3}MC states in $[Ru(bpy)_3]^{2+}$ can also lead to photodissociation. Under green light irradiation the photodecomposition quantum yield is 0.02%.[75] While this process is undesirable for most applications like sensing or photocatalysis, it shows great promise for the local delivery of therapeutics, e.g. by releasing a nitrile or pyridine ligands.[76−80] Thus, understanding the deciding factors for photodissociation is crucial for optical applications of photoactive metal complexes. Dixon et al. investigated the microscopic mechanism of light-driven ligand release in $[Ru(bpy)_3]^{2+}$ using DFT calculations.[22,28,81] The authors focused on the ^{3}MC manifold and identified a monophotonic and a biphotonic pathway. Interestingly, after the absorption of a single photon, all elementary steps of the dissociation process including the coordination of solvent molecules can occur in the triplet manifold.[22] Alternatively, $[Ru(bpy)_3]^{2+}$ can undergo a stepwise dissociation process. After absorption of the first photon, one pyridyl unit is substituted by a solvent molecule forming

https://doi.org/10.1021/acs.inorgchem.6c00560
Inorg. Chem. 2026, 65, 7549−7577

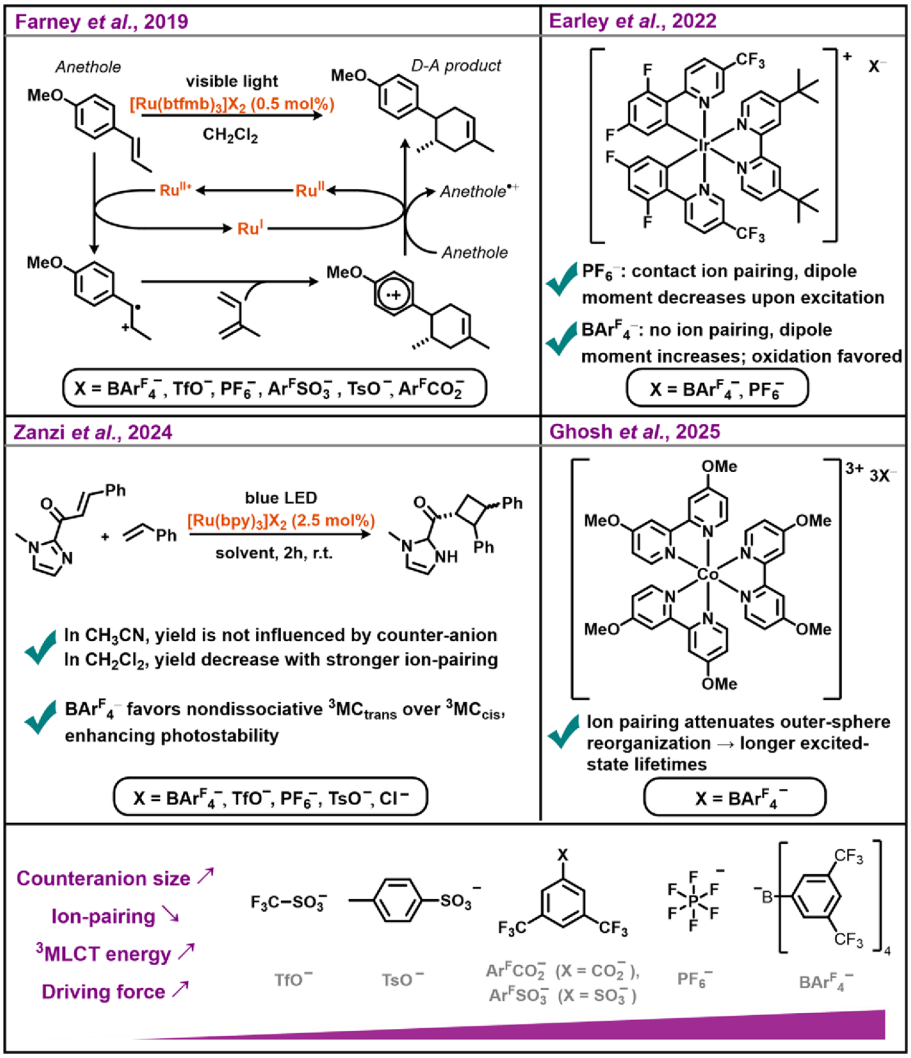

Figure 2. Recent studies that have highlighted the importance of counterions in photophysical and photochemical processes. See text for details.[57−60]

Table 1. Counteranion Effect on the Radical Cation Diels−Alder Cycloaddition as well as on the Photophysical and Electrochemical Properties of $[Ru(btfmb)_3]^{2+}$[57]

anions	λ_{abs} (nm)	λ_{em} (nm, eV)	τ (ns)	$E([Ru]^{2+/+})$ (V vs SCE)	$E([Ru]^{2+*/+})$ (V vs SCE)	NMR yield of the Diels−Alder product
$BAr^F_4{}^-$	453	576, 2.17	520	−0.65	+1.52	98 (20 min)
PF_6^-	458	605, 2.05	860	−0.89	+1.16	n. d.
$Ar^FSO_3^-$	458	618, 2.01	950	−0.93	+1.08	14 (24 h)
TsO^-	458	625, 1.99	n. d.	−0.95	+1.04	2 (24 h)

$[Ru(bpy)_2(\kappa^1\text{-bpy})(MeCN)]^{2+}$. The ligand then fully dissociates after this intermediate absorbs a second photon. The authors highlight that associative mechanisms could also be at play with experimental conditions likely having a large impact on the observed pathways.[22]

2.2. Counterion Effects

Photoredox catalysis has emerged as a powerful tool in organic synthesis over the past two decades, with transition metal polypyridyl complexes playing a pivotal role in this field.[82,83] Their ability to drive photoinduced electron and energy transfer processes has made them useful in various applications, including light-to-chemical energy conversion, which has redefined the realm of organic synthesis.[84] Despite the extensive research on ligand modifications and their effects on catalyst efficiency, a crucial aspect remained largely unexplored, i.e. the influence of the photocatalyst's counterion(s).

In 2019, Farney et al. demonstrated that counteranions have a dramatic impact on the rate of photocatalytic radical cation Diels−Alder reactions catalyzed by $[Ru(btfmb)_3]^{2+}$ (btfmb = 4,4′-bis(trifluoromethyl)-2,2′-bipyridyl; Figure 2).[57] A detailed analysis revealed that the identity of the counteranion influenced multiple steps in the catalytic cycle. Most notably, photocatalysts with noncoordinating counteranions yielded a more photooxidizing ^{3}MLCT excited state and improved the radical chain propagation steps, resulting in higher conversion and higher yields (Table 1). This counteranion effect was proposed to arise from Coulombic ion-pairing interactions between the counteranion and both the cationic photoredox

https://doi.org/10.1021/acs.inorgchem.6c00560
Inorg. Chem. 2026, 65, 7549−7577

catalyst and the radical cation intermediate. The solvent also plays a crucial role as Coulomb interactions dominate in nonpolar solvents, such as dichloromethane, where ion-pairing is stronger than in high-dielectric solvents, such as acetonitrile.[57]

For different $[Ru(btfmb)_3]^{2+}$ salts, the ground-state absorption maxima (λ_{abs}) are almost unaffected by the nature of the counteranion (Table 1).[57] However, the electrochemical properties are sensitive to it, as counteranions of lower Lewis basicity led to an anodic shift in the ground-state reduction potentials $E([Ru]^{2+/+})$ (Table 1). This shift is most pronounced for the $BAr^F{}_4^-$ salt which was rationalized with the weak electrostatic stabilization of the $\{[Ru^{II}(btfmb)_3]^{2+}[BAr^F{}_4]^-\}$ ion-pair making its reduction energetically more favorable, e.g. compared to the tightly bound tosylate anion.[57]

The nature of the counterion also significantly affects the ^{3}MLCT excited state of $[Ru(btfmb)_3]^{2+}$. The photoluminescence maximum (λ_{em}) blue-shifts by almost 50 nm (~0.18 eV) when going from the tosylate to the $BAr^F{}_4^-$ salt (Table 1).[57] The authors postulated that this shift results from the symmetry breaking that occurs when exciting from the GS (D_3 symmetry) to the ^{3}MLCT state (C_2 symmetry).[85,86] This transition is associated with a substantial dipole moment which is influenced by charge-dipole interactions of the complex with the counteranion. Consequently, weakly coordinating anions destabilize the ^{3}MLCT state, leading to an enhanced excited-state reduction potential through the synergistic effect on both a higher ^{3}MLCT energy and less negative ground-state potential (Table 1). It is important to note that the excited-state lifetime decreased with less coordinating anions (Table 1), which can potentially impact performance in photoredox reactions.[87] However, no such effect was observed in case of the Diels–Alder reaction of anethole (Figure 2).[57] On the contrary, the reaction was the most efficient for the $BAr^F{}_4$ salt,[57] highlighting that the higher driving force for electron transfer is the main factor leading to rapid photoinitiation and low reaction times.[87] The authors also found that the slower reaction rates associated with coordinating counteranions could be mitigated using a hydrogen-bonding anion binder, such as thiophosphotriamide derivatives, which attenuate deleterious ion-pairing interactions in the case of $Ar^FSO_3^-$. This strategy proved to be very efficient, as product yields could be increased from 5 to 99% in the presence of 20 mol % of the ion-binder.[57] These findings not only elucidate a previously underappreciated aspect of photoredox catalysis but also suggest novel strategies for optimizing organic reactions using transition-metal photocatalysts.

While the studies discussed above have identified counterion identity as a crucial element in modulating electron-transfer processes, more recent investigations have revealed its importance in energy transfer catalysis.[59] In 2024, Zanzi et al. reported that the choice of counterion substantially impacted the efficiency of triplet–triplet energy transfer processes (TTEnT) from $[Ru(bpy)_3](X)_2$ to cinnamoyl-type substrates (Figure 2). Their photophysical insights agreed with previous results on electron transfer reactivity and also led to higher yields when using low-coordinating anions in nonpolar solvents.[59] Quenching rate constants of the $BAr^F{}_4^-$ salt increased by a factor of 100 compared to tosylate. The improvement in performance can again be found in the higher energy of the ^{3}MLCT states when ion-pairing is weak, leading to a higher driving force for the energy transfer.[59]

Interestingly, counteranions also affect the photostability of $[Ru(bpy)_3]^{2+}$ which is crucial for achieving high turnover numbers (TON) in photocatalysis.[59] As previously discussed, ligand loss is mainly promoted by the ^{3}MC-*cis* state where the d_{x2-y2} is occupied, while the ^{3}MC-*trans* state with an occupied d_{z2} orbital is nondissociative.[22] The bulky $BAr^F{}_4^-$ counterions form a "clip-like" configuration around the metal complex which stabilizes the nondissociative ^{3}MC-*trans* states leading to higher photostability than in the $[PF_6]^-$ case where these ^{3}MC states are much closer in energy. The combination of faster quenching kinetics and higher photostability led to an impressive TON of 1040 for a [2 + 2] photocycloaddition reaction using $[Ru(bpy)_3](BAr^F{}_4)_2$.[59]

The significance of the effect of counterions on photocatalysis was reinforced and expanded on in studies beyond ruthenium complexes. In 2022, Rumbles and co-workers demonstrated that ion-pair reorganization in $[Ir^{III}(dF(CF_3)ppy)_2(dtbpy)]X$ complexes directly regulates photoredox reactivity (Figure 2).[58] The extent of contact versus solvent-separated ion pairing alters the dipole moments and reorganization energies of the excited state, thereby shifting the balance between oxidative and reductive pathways.[58] Most recently, complementary work by McCusker and co-workers revealed that ion pairing also modulates excited-state lifetimes of $[Co^{III}(4,4'\text{-OMe-bpy})_3](BArF_4)_3$ using NMR and ultrafast time-resolved absorption spectroscopy (Figure 2).[60] Supported by DFT calculations, they suggested that ion-pairing leads to an attenuation of outer-sphere contributions to the total reorganization energy and was largely responsible for the observed increase in excited-state lifetime under conditions in which contact ion pairs are the dominant species.[60]

Taken together, these studies highlight ion-pair engineering as a versatile and powerful lever to tune excited-state energetics, reaction pathways, and catalyst stability. This body of work transforms counterions from innocent bystanders into a tool for optimizing both photoredox and energy transfer photocatalysis.

2.3. Reaction Mechanisms Beyond Conventional Photoredox Catalysis

Photoredox catalysis has evolved from mechanistic curiosity to a central pillar of synthetic chemistry.[88] Conventional photoredox catalysis typically relies on single-photon excitation followed by electron or energy transfer to drive redox processes in solution.[89] Although this strategy has enabled a broad range of transformations, it remains limited by the intrinsic photophysical properties of the photosensitizers and the energetic reach of visible light. Recent studies have begun to challenge these boundaries by exploiting unconventional reaction media, excitation regimes, and mechanistic paradigms. These approaches no longer treat the photocatalyst as a static entity but as part of a dynamic system whose photophysical and redox properties can be engineered through its microenvironment, energy input, or even spin configuration. For example, multiphoton processes,[90] mechanochemical activation,[91] and spin-forbidden excitations[92] now enable the use of milder conditions, longer irradiation wavelengths, and solvent-free systems while achieving transformations that previously required high-energy input.

2.3.1. Intermediates in Photoredox Catalysis and Solvated Electron Generation. The singly reduced form of $[Ru(bpy)_3]^{2+}$, i.e. $[Ru(bpy)_2(bpy^{\bullet-})]^+$, is a common intermediate in photoredox catalysis.[89] This species can be easily

https://doi.org/10.1021/acs.inorgchem.6c00560
Inorg. Chem. 2026, 65, 7549–7577

generated in situ by irradiating $[Ru(bpy)_3]^{2+}$ in the presence of an electron donor such as triethylamine or ascorbic acid and typically acts as a reductant in photocatalytic reactions. Recently, this intermediate has been isolated by Scott et al. and thoroughly characterized.[93,94] Its EPR spectrum with a g-factor of 2.002 is consistent with a bipyridine radical anion.[93] Single-crystal analysis revealed that the extra electron is localized on a single bipyridine in the solid state. The isolation of $[Ru(bpy)_2(bpy^{\bullet-})]^+$ also allowed to probe its reactivity. It is capable of reducing iodobenzene in the ground state, while visible light irradiation unlocks reduction of bromobenzene.[93] This highlights that $[Ru(bpy)_2(bpy^{\bullet-})]^+$ itself can be photoactive which needs to be considered when proposing photochemical mechanisms involving $[Ru(bpy)_3]^{2+}$ in the presence of electron donors.[93]

Fascinatingly, $[Ru(bpy)_2(bpy^{\bullet-})]^+$ can also release solvated electrons ($e^{\bullet-}_{aq}$) when photoexcited.[95] Solvated electrons are the simplest reductants in chemistry showing a remarkable reduction potential of −2.9 V vs SHE in acetonitrile.[96,97] Multiple reactions have been developed to capitalize on solvated electrons, such as the Birch reduction or the degradation of halogenated organic molecules, which is attractive for the degradation of polyfluoroalkyl substances (PFAS).[98−102] While many techniques have been developed to generate solvated electrons (pulse radiolysis, electrolysis, or flash photolysis in the UV−C range), they all require a high energy input to generate this highly reactive species.[97] To overcome this energetic limitation, the most promising strategy is to employ two successive single-photon absorptions and store the energy of the first photon in an intermediate state. Over the years, this mechanism was implemented using different approaches.

The oxidative quenching route (Figure 3, oxidative route) was investigated by Goez et al. at the beginning of the century.[103] Here, the ^{3}MLCT state of $[Ru(bpy)_3]^{2+}$ was directly photoionized using a second more energetic photon (355 nm) to give $e^{\bullet-}_{aq}$ and the oxidized complex $[Ru(bpy)_3]^{3+}$. The catalytic cycle was proposed to be completed by the reduction of $[Ru(bpy)_3]^{3+}$ by water acting as a sacrificial electron donor.[103] Despite its simplicity, this system suffers from many limitations, as it still requires high-flux and high-energy light sources to photoionize $[Ru(bpy)_3]^{2+*}$ as the lifetime of its ^{3}MLCT state is too short to allow for photon pooling using low-flux light sources like LEDs or the sun. Moreover, the photoionization efficiency of 2.3% was also fairly low for practical synthetic applications on a laboratory-scale.[103]

To decouple the photoionization process from the ^{3}MLCT lifetime, the energy of the first photon can be stored in a long-lived monoreduced intermediate instead (Figure 3, reductive route). Specifically, $[Ru(bpy)_3]^{2+}$ is excited to its ^{3}MLCT state which then undergoes reductive quenching by a sacrificial electron donor and generates the corresponding reduced complex, $[Ru(bpy)_2(bpy^{\bullet-})]^+$.[95] This species is stable and absorbs in the visible spectral range. Upon subsequent photoexcitation a solvated electron can be released, thereby closing the catalytic cycle.[95] Naumann et al. demonstrated this strategy using nontoxic and bioavailable ascorbate as sacrificial electron donor.[104,106] To increase its reductive ability, they employed its dianionic form Asc^{2-}, which required working under strongly basic conditions (pH 12.7). The general principle can also be applied to other electron donors such as 4-methoxy phenolate and urate dianions.[107] Since photoexcitation of $[Ru(bpy)_3]^{2+}$ produces the ^{3}MLCT quantitatively,

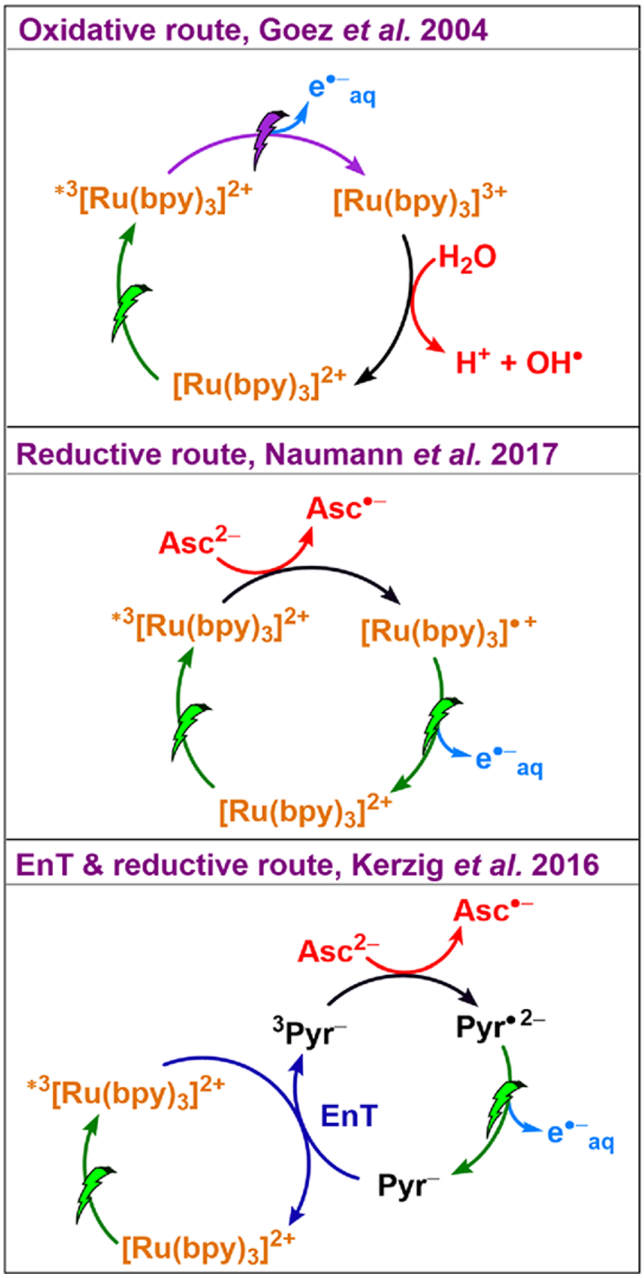

Figure 3. Recent studies and mechanistic pathways leading to the formation of solvated electrons. See text for additional details.[103−105]

the production of solvated electrons is limited by the quenching efficiency with ascorbate and the quantum yield of photoionization of $[Ru(bpy)_2(bpy^{\bullet-})]^+$ in the reductive scheme.[104] Owing to the suitable reduction potential of Asc^{2-}, the quenching rate constant (7×10^9 M^{-1} s^{-1}) and overall cage escape yield (38%) of the photoreduction were high. Hence, the limiting step in this system was the quantum yield for the photoionization of $[Ru(bpy)_2(bpy^{\bullet-})]^+$, which was only 1.3%. Therefore, most absorption events of $[Ru(bpy)_2(bpy^{\bullet-})]^+$ did not produce the desired solvated electrons, even with the high power densities of a laser.

To fix the inefficient photoionization, $[Ru(bpy)_2(bpy^{\bullet-})]^+$ was replaced by a monoreduced polyaromatic chromophore as a source for solvated electrons (Figure 3, EnT & reductive route), specifically the radical anion of pyrene-1-carboxylate ($Pyr^{\bullet2-}$) which features a four times higher photoionization

https://doi.org/10.1021/acs.inorgchem.6c00560
Inorg. Chem. 2026, 65, 7549−7577

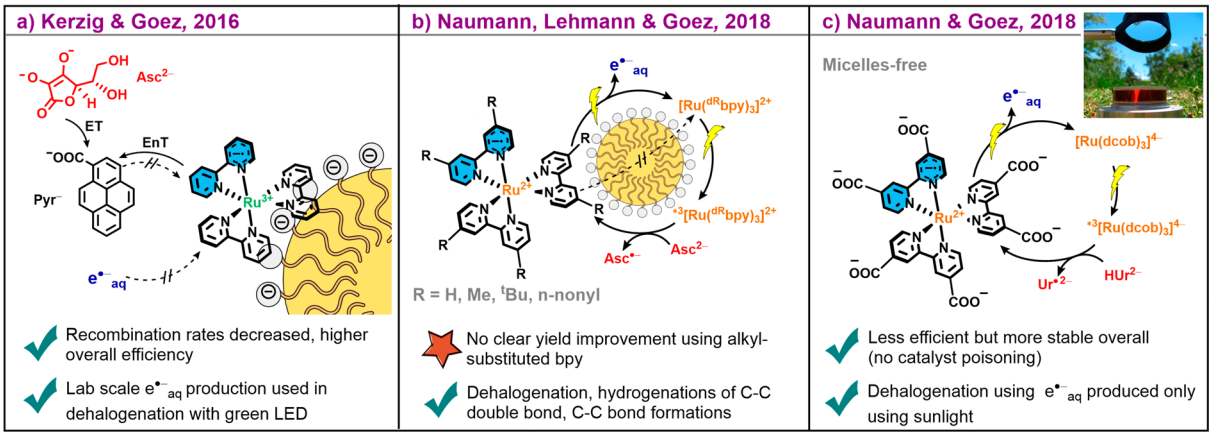

Figure 4. Recent studies showcasing the production of solvated electrons in micellar systems (panel a and b) or via electrostatic interactions between the photosensitizer and the quencher (panel c). ^{3}MLCT states are indicated with a 2,2′-bipyridine highlighted in blue and Ru^{3+} (green, panel a) whereas reduced complexes have a Ru^{2+} (orange, panel b and c).[105,108,109] The photograph on the right is adapted with permission from ref 109 (Copyright 2018, John Wiley and Sons) and showcases the formation of solvated electrons using focused sunlight irradiation. See text for additional details.

quantum yield of 5.4%.[105] This radical anion can be formed from Pyr^- by photoreduction of its long-lived triplet excited state $^3Pyr^-$ by Asc^{2-}. As direct excitation of Pyr^- requires UV light and the intersystem crossing is inefficient, $[Ru(bpy)_3]^{2+}$ was kept as a green light absorbing sensitizer that generates $^3Pyr^-$ in larger yields via dexter energy transfer. Although the photoionization step was designed to regenerate the stable ground-state catalyst Pyr^- from its radical anion form ($Pyr^{\bullet 2-}$), under the experimental conditions (532 nm excitation), only two-thirds of $Pyr^{\bullet 2-}$ undergo photoionization while the rest gets protonated by the solvent. Even if quantitative regeneration was achieved using a wavelength closer to the absorption maximum of $Pyr^{\bullet 2-}$ (504 nm), this would require two different light sources for both excitations. Additionally, side reaction such as oxidation of $Pyr^{\bullet 2-}$ by photoexcited photosensitizer lowered the overall yield of solvated electrons.[105]

To solve stability and side reaction issues, Kerzig and Goez introduced negatively charged micelles to the system.[108] In this environment, the positively charged photosensitizer accumulates on the micelle surface which maintains the reaction between $[Ru(bpy)_3]^{2+}$ and Pyr^- to form $^3Pyr^-$ as these monoanionic species can shuttle between the Stern layer and the aqueous bulk (Figure 4a). However, polyanionic species like Asc^{2-} and $Pyr^{\bullet 2-}$ are repelled by the negative charge on the micelle surface which drastically slows down competing electron transfer side reactions by 2 orders of magnitude. Overall, the micellar environment almost doubled the maximum concentration of the solvated electron precursor ($Pyr^{\bullet 2-}$) and extended its lifetime by a factor of 30. In this system, the limiting step is no longer the production of the electron precursor ($Pyr^{\bullet 2-}$) but only the photoionization quantum yield.[108]

This general strategy of using a supramolecular environment to decrease side-reaction rates was applied in several studies to achieve higher production of solvated electrons while simultaneously decreasing the required light intensity. In a first synthetic application, an LED was sufficient to drive a cross-coupling reaction via solvated electrons.[107] $[Ru(bpy)_3]^{2+}$ was used as a photosensitizer, protected by an anionic micelle, while urate dianion (Ur^{2-}) acted as the sacrificial electron donor confined to the aqueous bulk. Ur^{2-} was carefully chosen as it decreases unproductive charge recombination. Its oxidized form ($Ur^{\bullet -}$) undergoes deprotonation which generates a dianion that is repelled by the micelles, lowering recombination rates and enabling cross-coupling reactions.[107]

In this context, Goez and co-workers also studied the effect of the photosensitizer's structure on the overall photocatalytic performance (Figure 4b).[108] While they did not find a straightforward single-cause relationship, the study demonstrated several synthetic applications of $[Ru(^{Me}bpy)_3]^{2+}$ (^{Me}bpy = 4,4′-dimethyl-2,2′-bipyridine) under irradiation with a green LED. The generated hydrated electrons acted as "superreductants" and drove reactions that are typically impervious to standard photoredox catalysts, e.g. dehalogenation of alkyl and aryl chlorides and fluorides, hydrogenation of carbon−carbon double bonds and self-/cross-coupling reactions.[108]

Although the micellar method has proven to be effective, it has certain drawbacks. The typical SDS surfactant needs to be used in large amounts and is not sufficiently biodegradable.[109] Additionally, the product has to be isolated from the surfactant. It is also possible that reactants or products accumulate in the micelles which can either deactivate the catalyst or reduce the effectiveness of capturing hydrophilic solvated electrons. Therefore, Naumann and Goez chose to revisit the nonmicellized system.[109] By considering the positive effects of electrostatic repulsion, they engineered a tetraanionic photosensitizer, $[Ru(dcob)_3]^{4-}$ (dcob = 2,2′-bipyridine-4,4′-dicarboxylate) that repels the sacrificial electron donor. To avoid recombination, repulsion between intermediates had to remain as high as possible, which is why dianionic urate was chosen as sacrificial electron donor. $[Ru(dcob)_3]^{4-}$ also showed a higher photostability than $[Ru(bpy)_3]^{2+}$ as its activation barrier for the ^{3}MLCT−^{3}MC internal conversion is 20 kJ mol^{-1} larger than in $[Ru(bpy)_3]^{2+}$ in both water and SDS media.[109] Although the quenching rate constant of the negatively charged catalyst was lower than that of the micelle-based system, this higher stability resulted in a greater total electron output over time, making it the best overall sensitizer.[109] Moreover, transformations involving less hydrophilic substrates profit from the absence of micellar barriers because e^-_{aq} resides in the aqueous phase, and similarly cross-couplings proceed more smoothly when both components have unhindered access to each other. It also allows the use of

https://doi.org/10.1021/acs.inorgchem.6c00560
Inorg. Chem. 2026, 65, 7549−7577

supramolecular carriers such as cyclodextrins for water-insoluble substrates, as demonstrated by the dechlorination of 1-chloronaphthalene and the drug diclofenac, which is notoriously difficult to eliminate during wastewater treatment. In an impressive demonstration of its performance, the catalytic system using $[Ru(dcob)_3]^{4-}$ even decomposed chloroacetate using focused sunlight (Figure 4c).[109] This process required no active cooling, stirring, or oxygen exclusion. The field experiment, which required only a clear sky and a lens, successfully detoxified 80% of the harmful organochloride within 6 h.[109]

The generation of solvated electrons using $[Ru(bpy)_3]^{2+}$ started off as an interesting proof-of-concept that required high-intensity light sources but careful design of molecular interactions in the catalytic system unlocked super-reductive reactivity accessible with commercial green LEDs and even sunlight.

2.3.2. Ball-Milling Photoredox Chemistry. A mechanochemical reaction is defined by the International Union of Pure and Applied Chemistry (IUPAC) as a "chemical reaction that is induced by the direct absorption of mechanical energy" and was recognized in 2019 as one of the ten chemical innovations that could change the world.[110] Among the prevalent methodologies in mechanochemistry, ball milling is the most common approach.[91] Beyond the primary argument for removing environmentally detrimental solvents, mechanochemical reactions facilitated by ball milling can yield products that might not be attainable through solution-phase chemistry because of the poor solubility of the initial reagents or the instability of products in solution.[111−115] The solvent can also hinder the speed of product formation because of the statistical diffusion of reactants; as such, mechanochemical techniques can significantly accelerate this process. However, there is no ideal set of milling conditions for all mechanochemical reactions, and optimization is required.[91,116] With the advancement of time-resolved in situ monitoring, such as Raman spectroscopy[117−119] and X-ray diffraction,[120,121] mechanochemistry is experiencing a resurgence, and applications in photocatalysis are no exception. This includes the mechanochemical synthesis of photosensitizers[122,123] and the performance of photochemical reactions inside a ball mill.[122]

In 2025, Bantreil et al. developed a mechanochemical method for the synthesis of ruthenium trisbipyridyl complexes and demonstrated their application as catalysts in light-driven reductive dehalogenation reactions performed in a ball-mill.[122] The combination of mechanochemistry with visible light has been scarcely reported in the literature, and even more rarely in the case of photocatalysis, the first example being published in 2017 on an eosin Y catalyst.[124] Compared to other metals such as iron, the mechanosynthesis of ruthenium complexes like $[Ru(bpy)_3]^{2+}$ is relatively underexplored.[116,123,125] Initial experiments led to the unwanted formation of $[Fe(bpy)_3]^{2+}$ via the redox reaction between $RuCl_3$ and the elemental iron from the stainless steel balls.[122] The use of harder tungsten carbide provided more energetic impacts and avoided this side reaction. The authors further optimized the reaction conditions using ethanol as both a reducing agent and a liquid-assisted grinding agent. The addition of 1 M NaOH was also found to facilitate the reduction of Ru(III) to Ru(II), significantly improving conversion. The optimized conditions were successfully applied to the synthesis of complexes with substituted bipyridines and 1,10-phenanthroline (phen).[122] Except for $[Ru(phen)_3]^{2+}$, the mechanochemical approach proved to be more efficient than traditional solution-based methods, offering higher yields, shorter reaction times, and less waste.[122]

In a next step, the same authors performed the photocatalytic reductive dehalogenation of α-chloroesters under ball milling conditions.[122] For this to work, the ball mill needed to be made of transparent materials like poly(methyl methacrylate) (PMMA), quartz, sapphire, or as chosen in this study chemically resistant epoxy resin.[122] The reaction was performed using a ruthenium polypyridine photosensitizer, diisopropylethylamine (DIPEA), and a Hantzsch amide as the reducing agent under blue LED irradiation. Complete conversion was achieved using *N*,*N*-dimethylacetamide as a liquid additive. Control experiments underscored the necessity of both the photosensitizer and light, as their absence led to poor (10%) and no conversion, respectively. Unfortunately, the control experiment with irradiation but without ball-milling has not been reported.[122] $[Ru(bpy)_3][PF_6]_2$ emerged as the most active photosensitizer, providing the highest reaction conversion. These optimized conditions were successfully applied to a range of α-chloro and α-bromo esters and amides.[122] Overall, this mechanochemical photoredox method drastically reduced the reaction time from 24 h in solution to just 3.5 h and simplified the purification process significantly.[122]

We expect that the combination of these two high-energy processes, i.e. light excitation and high mechanical impacts, will fashion exciting new reactivity in the future. In any case, this approach can help reduce waste and simplify purification procedures.

2.3.3. Spin-Forbidden Excitation. In the context of photoredox catalysis, $[Ru(bpy)_3]^{2+}$ is typically used with blue light excitation e.g. at 450 nm to excite ^{1}MLCT transitions with high molar absorption coefficients of up to 14,400 M^{-1} cm^{-1}.[10,126] The downside of this excitation scheme is that a large part of the excitation energy (ca. 25%) is lost during the relaxation to the photoactive triplet state.[92] To circumvent this issue, the Rovis group has explored the direct excitation of ^{3}MLCT states in osmium(II) complexes using red light.[92] Due to the large spin−orbit coupling these spin-forbidden singlet−triplet transitions have appreciable molar absorption coefficients of up to 4,000 M^{-1} cm^{-1}.[92,126] For ruthenium(II) based systems, charge injection in dye-sensitized solar cells under red light irradiation has been discussed in the past,[127−130] but spin-forbidden transition have only recently been leveraged for photoredox catalysis.[92,131]

Unlike osmium(II) complexes, the lighter ruthenium(II) complexes have not been considered for efficient spin-forbidden excitation due to the lack of distinct ^{3}MLCT absorption bands.[86] In a study by Romero and co-workers, $[Ru(bpy)_3]^{2+}$ was supposed to serve as a negative control for a red-light-driven aza-Henry reaction but surprisingly demonstrated catalytic activity under red light (730 nm), yielding 20% of the product.[132] This result was unexpected as $[Ru(bpy)_3]^{2+}$ only exhibits molar absorption coefficients smaller than 100 M^{-1} cm^{-1} at wavelengths greater than 600 nm. High-throughput experimentation using $[Ru(bpy)_3]^{2+}$ as photosensitizer was used to screen different counterions, catalyst loadings, solvents, and irradiation wavelengths. The final optimized batch conditions were identified as 10 mol % of $[Ru(bpy)_3]Cl_2$ with 10 equiv of nitromethane in DMSO under 660 nm irradiation for 40 h, achieving 53% isolated yield.[132]

https://doi.org/10.1021/acs.inorgchem.6c00560
Inorg. Chem. 2026, 65, 7549−7577

To understand the unexpected reactivity, several possibilities of external bias were systematically ruled out, namely photocatalytic activity arising from impurities, the potential formation of an electron donor−acceptor complex with starting materials, and the presence of higher-energy light components in the irradiation source.[132] The authors also excluded contributions from two-photon absorption because the reaction yield and emission intensity of $[Ru(bpy)_3]^{2+}$ showed a linear correlation with the light power, indicating a monophotonic process. The hypothesis of the spin-forbidden transition is also consistent with the relatively high photocatalyst loading required during the reaction screening, as it compensates for the low molar absorption coefficient at this wavelength range ($\varepsilon_{660nm} \sim 45\ M^{-1}\ cm^{-1}$ in DMSO).[132]

On the flip side, this high catalyst loading prevented meaningful transient absorption measurements due to significant inner filter effects that limited the transmission of probe light in the UV−vis spectral range.[132] Emission decay rates and spectra were consistent across different excitation conditions (450, 600, 610 nm), suggesting that the same ^{3}MLCT excited state was generated under both red and blue light excitation. Therefore, the observed absorption was attributed to direct $^1A_1 \rightarrow {}^3$MLCT excitation, and the observed anti-Stokes emission (excitation at 660 nm with emission peaking at 610 nm) was rationalized to stem from hot-band absorption from higher vibrational levels of the electronic ground state (Figure 5).[132]

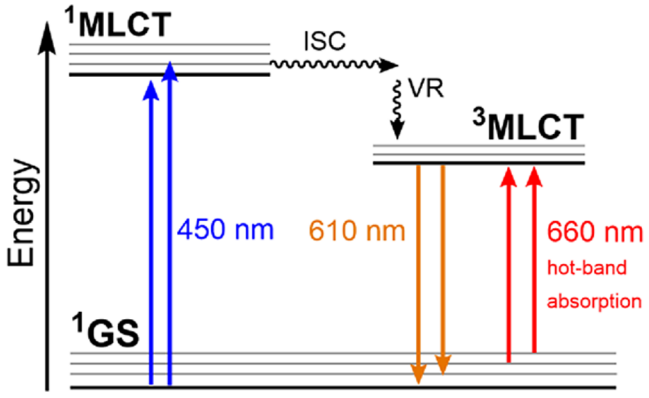

Figure 5. Simplified energy diagram of $[Ru(bpy)_3]^{2+}$. Excitation of the $^1A_1$ ground state with 450 nm light populates the ^{1}MLCT excited-state (blue arrows). After intersystem crossing (ISC) and vibrational relaxation (VR) from the ^{1}MLCT to ^{3}MLCT states, radiative decay from the ^{3}MLCT occurs with an emission peak centered at 610 nm. Direct excitation of $[Ru(bpy)_3]^{2+}$ into the spin-forbidden $^1A_1 \rightarrow {}^3$MLCT absorption band with lower energy light is possible from vibrationally excited levels of the electronic ground state, also called hot-band absorption (red arrows).[132]

Finally, the applicability of this red-light-driven photocatalysis using $[Ru(bpy)_3]^{2+}$ was demonstrated across a wide range of transformations, including reductive quenching, oxidative quenching, and energy transfer.[132] To mitigate the disadvantage of the high catalyst loading, a recycling strategy was successfully implemented by immobilizing $[Ru(bpy)_3]Cl_2$ on silica. This heterogeneous photocatalyst showed comparable yields and could be recycled for at least four successive runs without any loss of efficiency.[132]

2.3.4. Photochemistry in the Biological Realm. Photoredox catalysis gives rise to interesting reactivity and can be performed under mild conditions.[88] As $[Ru(bpy)_3]^{2+}$ is both water-soluble and water-stable, such reactions can in principle also be performed in biological systems. Such a bioorthogonal approach can be used to couple photoredox catalysis with enzyme reactivity and help interrogate intracellular processes, for example through protein labeling and ligand uncaging.[133] In the following section, we highlight recent examples of bioorthogonal chemistry approaches involving $[Ru(bpy)_3]^{2+}$. For a more in-depth discussion, we refer readers to recent reviews on the topic.[133−135]

Photochemical reactions can be used to probe protein interactions inside cells. An emergent technique in this area is called proximity labeling.[134] Here, a reactive species is locally released upon a trigger (e.g., light) and unselectively labels neighboring proteins. The labeling range is determined by the lifetime of the reactive species (e.g., 4 μs for $^1O_2$).[134] After the labeling step, the protein mixture can be analyzed and proteins that were close to each other can be identified by their tag. Several platforms for light-driven proximity labeling have been developed over the years.[134] Early studies around 2000 established $[Ru(bpy)_3]^{2+}$ as a photocatalyst for the cross-linking of proteins via phenoxyl radicals formed from tyrosine groups.[136] More selective labeling and inactivation of specific proteins can be achieved by linking the ruthenium complex to a protein binder.[137] Irradiation with light leads to the formation of both phenoxyl radicals and singlet oxygen which inactivates the protein. By trapping the phenoxyl radicals with a suitable radical trap, the protein can be labeled instead.[137] The ruthenium photocatalyst and the ligand can also be colocalized on magnetic beads in a more modular approach. For example in one study, irradiation led to sensitization of singlet oxygen and nucleophilic tagging of histidine residues in bound proteins when combined with a suitable labeling agent.[138]

Apart from labeling, photochemistry can also be used to synthesize molecules in cells. For example, in a proof-of-principle study, indoles were successfully synthesized in cells in a bond-forming reaction.[139] The system combined an organic azide as an exogenous substrate with $[Ru(bpy)_3]^{2+}$ as photosensitizer.[139] In the future, photocatalytic systems could be engineered in a way that they only react in specific cells to unlock a new mode of cancer cell labeling. Another promising avenue is pairing the versatility of photocatalysis with the selectivity of enzymatic reactions. Such tandem catalysis could be used to activate prodrugs or fluorophore precursors.[140]

2.4. Polynuclear Complexes Based on the $[Ru(bpy)_3]^{2+}$ Motif

The conceptual roots of polynuclear ruthenium assemblies can be traced back to the Creutz−Taube complex, a landmark mixed-valence compound that was used to demonstrate efficient electronic communication between two ruthenium centers through a bridging ligand.[141,142] This discovery established the fundamental framework for intramolecular electron transfer and inspired the subsequent design of more elaborate metal-bridged architectures.[35,143−158] These systems were primarily regarded as model compounds to study charge delocalization and intervalence charge transfer rather than as functional photocatalysts. The focus remained on static electronic communication rather than dynamic photochemical reactivity, and a detailed understanding of how nuclearity could enhance stability or direct excited-state pathways was still missing. Nonetheless, these studies laid an essential

https://doi.org/10.1021/acs.inorgchem.6c00560
Inorg. Chem. 2026, 65, 7549−7577

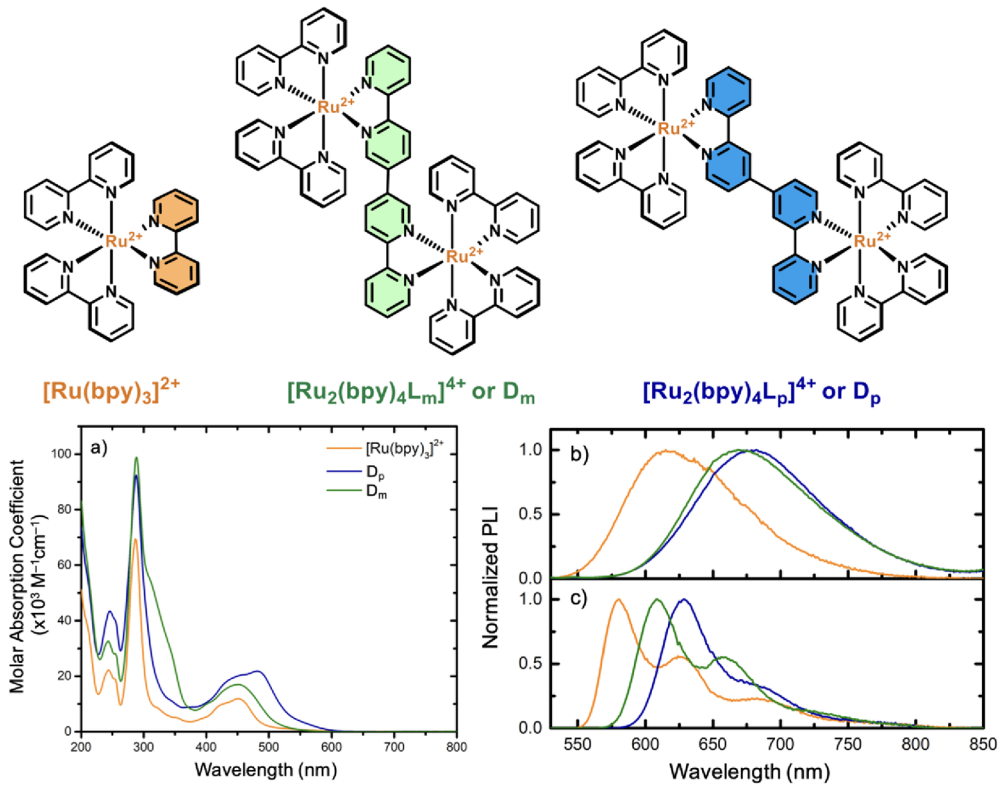

Figure 6. Top: Molecular structures of $[Ru(bpy)_3]^{2+}$ and dinuclear analogs. Bottom: (a) UV−vis absorption spectra and normalized steady-state photoluminescence spectra in acetonitrile (b) at room temperature and (c) in frozen butyronitrile matrix at 77 K. Adapted with permission from ref 40. Copyright 2020 Royal Chemical Society.

Table 2. Photophysical Properties of the Binuclear and Trinuclear Complexes and $[Ru(bpy)_3]^{2+}$ Recorded in Argon Purged Acetonitrile Solution[38,40,a]

	binuclear		trinuclear				reference
	D_p	D_m	T_{mp}	T_{mm}	T_{pm}	T_{pp}	$[Ru(bpy)_3]^{2+}$
λ_{max}^{Abs} (nm) [ε_{max} ($M^{-1}cm^{-1}$)]	481 [21 800]	451 [17 000]	475 [42 200]	445 [29 500]	485 [31 200]	484 [40 100]	450 [12 000]
λ_{max}^{Em} (nm)[b]	682	670	721	698	683	684	615
τ (ns)	2350	580	298	312	623	1815	890
Φ_{PL}[c]	0.077	0.034	0.009	0.014	0.048	0.121	0.094
$\lambda_{max}^{Em,77K}$ (nm)[b,d]	629	610	662	633	635	641	579

[a] λ_{max}^{Abs} = absorption peak maximum, λ_{max}^{Em} = emission peak maximum, τ = excited-state lifetime, Φ_{PL} = photoluminescence quantum yield, $\lambda_{max}^{Em,77K}$ = emission peak maximum at 77 K. [b] Excitation at 450 nm. [c] $[Ru(bpy)_3]^{2+}$ in air-equilibrated acetonitrile used as reference (Φ_{PL} = 0.018). [d] Butyronitrile rigid matrix.

foundation for the rational design of multinuclear frameworks, establishing key design principles such as orbital overlap through π-conjugated bridges and the role of redox asymmetry to control the direction and rate of intramolecular electron transfer.

Recently, there has been a renewed interest in polynuclear ruthenium complexes, driven by advances in time-resolved spectroscopy and computational modeling. These technologies have enabled a comprehensive understanding of energy and electron transfer mechanisms within polynuclear complexes. As will be described here, more recent work also demonstrated that engineering these metal-to-metal interactions can offer significant advantages for photoredox catalysis such as extending the excited-state lifetimes, improving photostability, and even controlling dissipative pathways to gain in redox power, benefits that are largely out of reach for their mononuclear counterparts.

2.4.1. Photophysical Effects of Delocalized Excited States. In 2020, Elias and co-workers reported a study on binuclear ruthenium complexes bridged by a bis-2,2′-bipyridine ligand, which was connected either through the *para* position (ligand L_p, forming complex D_p) or the *meta* position (ligand L_m, forming complex D_m), Figure 6.[40] The dinuclear complexes showed higher molar absorption coefficients compared to the parent complex $[Ru(bpy)_3]^{2+}$ (Figure 6a). In addition, the lowest-energy MLCT absorption band red-shifted by 30 nm in D_p compared to $[Ru(bpy)_3]^{2+}$ whereas no shift was observed in D_m.[40] Nevertheless, the photoluminescence red-shifted in both D_p and D_m, with D_p showing a higher photoluminescence quantum yield than D_m (Table 2). The excited-state lifetime of D_p (2.3 μs) was surprisingly long, more than double that of $[Ru(bpy)_3]^{2+}$ (890 ns), whereas D_m exhibited the shortest excited-state lifetime (580 ns) in the series, highlighting that the bridging position between the two bipyridine moieties had a decisive influence

https://doi.org/10.1021/acs.inorgchem.6c00560
Inorg. Chem. 2026, 65, 7549−7577

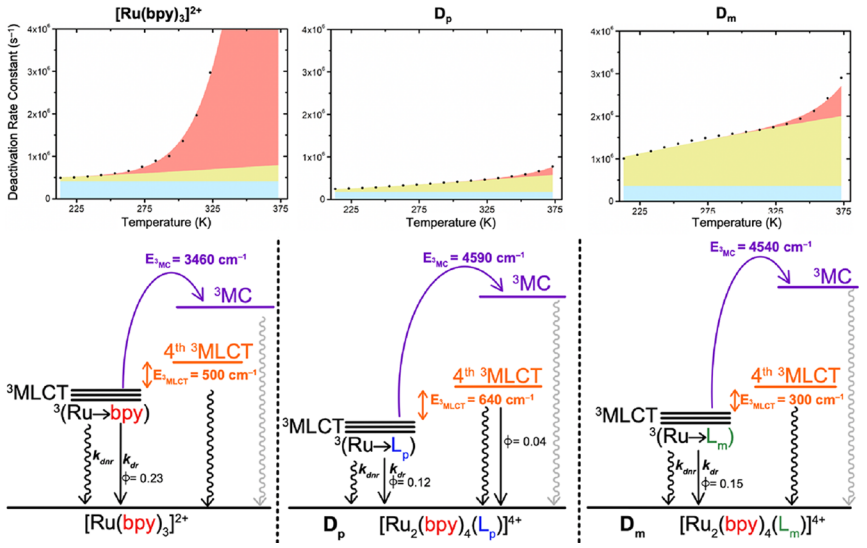

Figure 7. Top: Excited-state deactivation rate constants for complexes $[Ru(bpy)_3]^{2+}$, $\mathbf{D_p}$ and $\mathbf{D_m}$ with direct radiative and nonradiative rate constants ($k_{dr} + k_{dnr}$, blue area), thermally activated deactivation via the upper lying ^{3}MLCT (k_{3MLCT}, yellow area), thermally activated deactivation via the higher-energy ^{3}MC (k_{3MC}, red area) and experimental data (dotted line). Bottom: Proposed photophysical schemes for $[Ru(bpy)_3]^{2+}$, $\mathbf{D_p}$ and $\mathbf{D_m}$. Adapted with permission from ref 40. Copyright 2020, Royal Society of Chemistry.

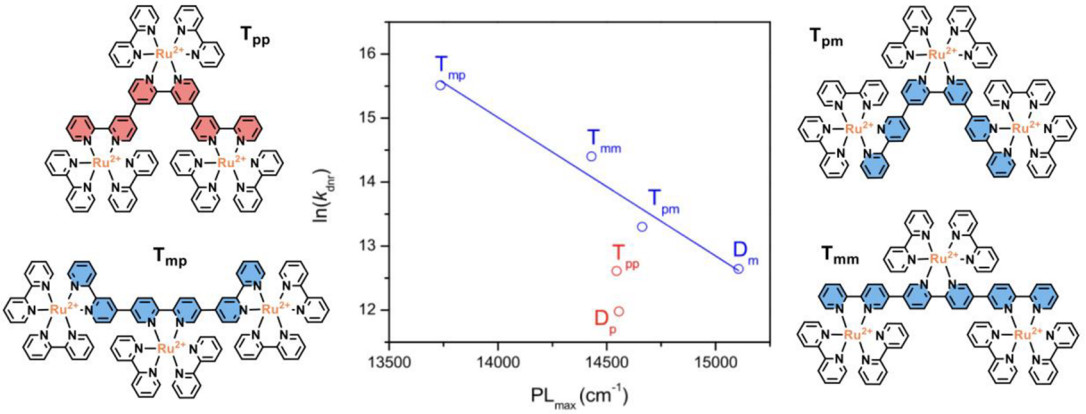

Figure 8. Molecular structures of trinuclear ruthenium(II) complexes and logarithmic plot of nonradiative rate constant vs photoluminescence band maximum PL_{max} according to the energy-gap law[74] for dinuclear and trinuclear complexes at 213 K in butyronitrile solution. The blue line represents the linear fit for $\mathbf{T_{pm}}$, $\mathbf{T_{mp}}$, $\mathbf{T_{mm}}$ and $\mathbf{D_m}$ according to $\ln(k_{dnr}) = c - \frac{\gamma E_0}{\hbar\omega_M}$ with a slope of −500 cm^{-1}. Adapted from ref 38. Copyright 2021 American Chemical Society.

on the photophysical properties of the resulting dinuclear assembly.[40]

Franck−Condon line shape analysis of the 77 K luminescence spectra was used to investigate excited-state geometries (Figure 6c).[40] At this low temperature, the transition from the excited state to the ground state primarily occurs through direct radiative (k_{dr}) and nonradiative (k_{dnr}) deactivation, as thermally activated deactivation processes are considered negligible. This assumption allows to extract the Huang−Rhys factor (S_M), which indicates the geometric distortion between the ground and excited states. S_M was significantly smaller for D_p (0.46) compared to D_m (0.71) and $[Ru(bpy)_3]^{2+}$ (0.82). This smaller S_M value for D_p suggests a less distorted and more delocalized excited state, which leads to a decrease in the direct nonradiative deactivation rate (k_{dnr}) and, thus, a longer excited-state lifetime.[40]

Variable-temperature photoluminescence measurements were conducted to understand the excited-state deactivation pathways for complexes D_p and D_m and the reference $[Ru(bpy)_3]^{2+}$.[40] As expected, the excited-state lifetimes and absolute PL quantum yields for both dinuclear complexes decreased as the temperature increased. The three complexes displayed the same two thermally activated relaxation pathways. The first pathway was associated with a higher activation energy ($\Delta E_{3MC} > 3000$ cm^{-1}) and was attributed to the population of the ^{3}MC state, which relaxes to the ground state with the rate constant k_{3MC} (Figure 7, red area). The second pathway had a lower activation energy ($\Delta E_{3MLCT} \sim 300-1000$ cm^{-1}) and involved relaxation via a higher-energy ^{3}MLCT excited state with the rate constant k_{3MLCT} (Figure 7, yellow area). While the activation energies are similar between the three complexes, their contributions are different. Specifically, deactivation via the ^{3}MC pathway was found to be very pronounced for $[Ru(bpy)_3]^{2+}$ at room temperature (48%), while it was negligible for the dinuclear complexes D_p and D_m (<0.5%). Moreover, both direct (k_{dr}, k_{dnr}) and activated (k_{3MC} and k_{3MLCT}) deactivation rates were significantly enhanced in D_m compared to D_p. This explained the shorter excited-state

https://doi.org/10.1021/acs.inorgchem.6c00560
Inorg. Chem. 2026, 65, 7549−7577

lifetime of D_m and highlights the crucial role of bridging ligand geometry. Collectively, these results demonstrate that dinuclear complexes can disfavor nonradiative relaxation pathways which eventually can lead to enhanced photostability.[40]

Finally, it was observed that the photoluminescence maxima shifted for D_p when the temperature was changed from 213 to 373 K whereas only broadening were observed for D_m (data not shown).[40] For both D_m and $[Ru(bpy)_3]^{2+}$, the temperature-dependent PL quantum yields were accurately modeled using only the lowest ^{3}MLCT excited state as luminescent state, which indicated that the thermally activated relaxation pathway involving the upper-lying ^{3}MLCT state is either very weakly or nonluminescent.[40] In contrast, for D_p a blue-shift was observed in its photoluminescence spectrum with increasing temperature from 213 to 373 K, suggesting that the higher-energy ^{3}MLCT excited state, that is populated thermally, is also luminescent and emits at a higher energy (Figure 7). This was further supported by the fact that the temperature-dependent PL quantum yields for D_p could only be accurately modeled when an additional radiative deactivation pathway from the thermally activated ^{3}MLCT state was included. In conclusion, the combination of the smaller nonradiative pathway rate constants and the presence of two luminescent ^{3}MLCT states in D_p resulted in a photoluminescence quantum yield more than double that of D_m, and only slightly less than that of $[Ru(bpy)_3]^{2+}$.[40]

The strong effect of ligand connectivity on photophysical properties persists in trinuclear complexes.[38] Here, several different isomers with different bridging ligands were investigated (T_{mp}, T_{mm}, T_{pm}, T_{pp}, Figure 8). Strikingly, complex T_{pp} with the connection of three 2,2′-bipyridine fragments via the *para* position showed stronger molar absorption coefficients at longer wavelengths, possessed a longer excited-state lifetime and a higher photoluminescence quantum yield than $[Ru(bpy)_3]^{2+}$ (Table 2). The other bridging ligands yielded trinuclear complexes (T_{pm}, T_{mp}, T_{mm}) that exhibited shorter excited-state lifetimes and lower photoluminescence quantum yields than those of the parent complex.[38] T_{pp} showed a much slower nonradiative relaxation rate constant k_{dnr} than expected from the red-shifted emission according to the energy gap law (Figure 8).[38] This anormal behavior of T_{pp} was attributed to a highly delocalized excited state as evidenced by its low Huang−Rhys factor S_M of 0.33, which reduces geometric distortion and vibrational overlap between the ground and excited states.[38]

In general, the trinuclear complexes differed from $[Ru(bpy)_3]^{2+}$ in their deactivation pathways. All investigated trinuclear complexes showed deactivation via a higher-energy ^{3}MLCT state in thermal equilibrium in temperature dependent luminescence lifetime and quantum yield experiments.[38] Deactivation via ^{3}MC states was absent even at room temperature, contributing to the higher photostability of the trinuclear complexes compared to $[Ru(bpy)_3]^{2+}$. The authors also observed that the decrease in the overall photoluminescence quantum yield with increasing temperature was less pronounced than the decrease in τ. This discrepancy indicates that the thermally activated deactivation pathway must have a significant radiative component, similar to the emissive higher-energy ^{3}MLCT excited state in the dinuclear complex D_p. Finally, *para* connectivity of the peripheral 2,2′-bipyridines (T_{pp}, T_{mp}) resulted in an increased energy gap E_{3MLCT} between the lower and upper ^{3}MLCT states, which in turn decreased the relative kinetic rate of deactivation compared to the complexes with *meta*-connectivity (T_{pm}, T_{mm}).[38]

2.4.2. Antidissipative Behavior of Polynuclear Ru(II) Photosensitizers. In both natural and artificial photosynthesis, high-energy excited states rapidly relax by internal conversion (IC) and vibrational relaxation (VR), typically losing 20−30% of the photon energy before any productive chemistry can occur.[92,159] To harness this energy for solar fuels or photoredox catalysis, one must deliberately slow down IC between higher-energy (HE) and lower-energy (LE) ^{3}MLCT states by engineering weak excited-state electronic coupling and non-negligible activation barriers for IC (Figure 9). Cadranel and co-workers recently discovered such an antidissipative strategy using polynuclear ruthenium complexes enabling more efficient solar energy conversion.[36]

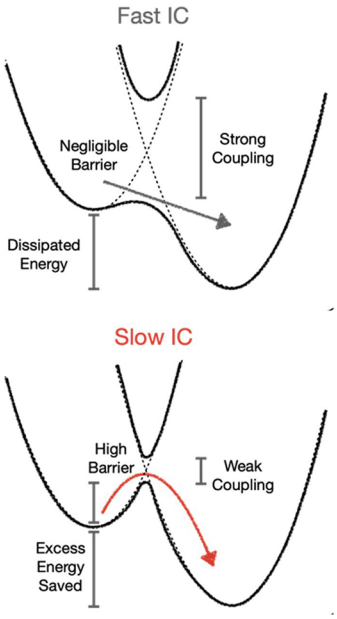

Figure 9. Schematic representation of excited state relaxation with strong electronic coupling between excited states and fast IC in traditional energy conversion (top) and with weak electronic coupling between the excited states and slow IC for antidissipative energy conversion (bottom). Adapted with permission from ref 160. Copyright 2022, Royal Society of Chemistry.

Specifically, the authors revisited the binuclear and trinuclear Ru(II) polypyridine complexes D_p, D_m and T_{mm} (Figures 6 and 8). In the *para*-linked dimer (D_p), strong excited-state electronic coupling led to rapid (sub-ps) IC to the LE ^{3}MLCT(L_p) state localized on the bridging ligand, and classical Kasha behavior.[36] In contrast, in the *meta*-linked dimer (D_m) and the trinuclear analogue (T_{mm}), weak coupling between chromophores produced two distinct long-lived ^{3}MLCT states: a lower-energy state centered on the bridging ligand (^{3}MLCT(L_m)) and a HE state with the spin density located on an ancillary bpy ligand (^{3}MLCT(bpy)). Using a combination of electrochemistry, steady-state emission and femto- to nanosecond transient absorption spectroscopy, the authors mapped out the energetic and kinetic landscape of these complexes. Franck−Condon line shape analysis of 77 K emission spectra gave triplet energies of 16,400 cm^{-1} for ^{3}MLCT(L_m) and ∼17,200 cm^{-1} for ^{3}MLCT(bpy), i.e. an energy gap of 800−

https://doi.org/10.1021/acs.inorgchem.6c00560
Inorg. Chem. 2026, 65, 7549−7577

1,400 cm^{-1} (100−170 meV) between LE and HE states. Temperature-dependent ns-transient absorption spectroscopy yielded activation barriers for the HE→LE IC of ∼2,000 cm^{-1} and pre-exponential factors ∼5 × 10^{11} s^{-1}, corresponding to IC rate constants on the order of 10^7 s^{-1} at room temperature. As a result, ^{3}MLCT(bpy) lifetimes are on the 10−20 ns scale, while ^{3}MLCT(L_m) lifetimes amount to hundreds of ns.[36]

Remarkably, both HE and LE states are long-lived enough to participate in bimolecular electron transfer.[36] Proof-of-concept quenching experiments with tritolylamine (TTA) as an electron donor showed that both ^{3}MLCT(bpy) and ^{3}MLCT-(L_m) can be intercepted by electron transfer before IC occurs, generating distinct reduced photosensitizers with different reducing powers. The HE-derived reduced species is about 140 meV more reducing than the one derived from the LE state. This demonstrates the central antidissipative idea: by introducing an activated, slow IC channel between coexisting ^{3}MLCT states, one can "trap" and chemically exploit HE states before excess energy is dissipated.[36]

Building directly on this framework, the authors investigated the detailed nature and localization of the HE states, and if they can be modulated by tuning of the ancillary ligands.[35] Specifically, the authors investigated derivatives of D_m (Figure 6) of the general structure $[Ru_2(L_m)(bpy^R)_4]^{4+}$ with different substitution patterns on the ancillary bpy^R ligands (R = H, 4,4′-Me, 5,5′-Me, 4,4′-MeO, 4,4′-CF_3).[35] This allowed them to modulate the relative energies of bridge- vs ancillary-centered ^{3}MLCT states while preserving the weak coupling topological motif previously described. With electron-donating substituents (R = H, 4,4′-Me, 5,5′-Me, 4,4′-MeO), the first two reduction waves at −0.56 and −0.76 V vs SCE corresponded to successive one-electron reductions of the L_m bridge, whereas ancillary ligands were reduced at more negative potentials.[35] In contrast, for R = 4,4′-CF_3 the first two reductions occur on the ancillary CF_3-substituted bpy at −0.38 V vs SCE, showing that strong electron acceptors can localize the LUMO on the ancillary ligands.[35]

The luminescence decay was biexponential for all complexes except $[Ru_2(L_m)(bpy^{4,4\text{-}CF3})_4]^{4+}$, featuring a short (5−40 ns) and a long component (100−350 ns).[35] Time-resolved emission spectroscopy showed that these correspond to two distinct phosphorescence bands separated by 430−980 cm^{-1}, similar to the HE/LE pair described previously. The ligand centered radical anions associated with the two ^{3}MLCT states were assigned in fs/ns-transient absorption spectroscopy via their characteristic absorption signatures.[35]

Overall, antidissipative behavior was found for $[Ru_2(L_m)(bpy^R)_4]^{4+}$ with unsubstituted bipyridine and electron-donating derivatives. In this case both HE and LE states are localized on the bridging ligand, with the LE state being more delocalized over the quaterpyridine backbone.[35] The HE→LE IC thus corresponds to an intraligand electron transfer within L_m. This intraligand electron transfer is remarkably slow (5−40 ns), giving ample time for the HE ^{3}MLCT to participate in bimolecular reactions.[35] With the strongly electron-withdrawing substituent CF_3, the situation flips and the ancillary-centered ^{3}MLCT($bpy^{4,4\text{-}CF3}$) state is stabilized and becomes the LE excited state. In this case, the L_m-centered HE state decays on the sub-ps time scale, with a negligible barrier to IC, and the antidissipative character is lost. Hence, overly strong acceptors as ancillary ligands funnel the excited state away from the antidissipative bridge and must be avoided.[35]

Finally, antidissipative reductive and oxidative photoreactivity was demonstrated using complex $[Ru_2(L_m)(bpy)_4]^{4+}$ and $[Ru_2(L_m)(bpy^{MeO})_4]^{4+}$ and TTA and benzoquinone as quenchers.[35] TTA as a reductive quencher reacted with both the HE and LE ^{3}MLCT(L_m) states with nearly diffusion-controlled rate constants (10^8−10^9 M^{-1} s^{-1}), forming distinct charge-separated species with different radical-anion signatures.[35] With benzoquinone as electron acceptor, HE states act as slightly stronger photoreductants. However, the effect was modest as the energy gap between HE and LE amounted to only 400 cm^{-1}. No photoproduct could be detected, likely due to low cage escape and fast geminate charge recombination.[35]

2.4.3. Polynuclear Complexes in Photoredox Catalysis. The studies discussed above provide a direct structure−property relationship between bridge topology, excited-state delocalization, and photostability, leading to a solid mechanistic understanding for exploring polynuclear systems in light-driven applications. In the context of photoredox catalysis, binuclear (D_p), trinuclear (T_{pp}) and quadrinuclear (Q_{ppp}) complexes with *para*-connectivity were successfully used in a reductive dehalogenation reaction.[39] The investigated reaction requires the excited ruthenium complex to be reductively quenched by an electron donor, so that the reduced photosensitizer can then reduce the substrate 4-bromobenzyl-2-chloro-2-phenylacetate initiating its dehalogenation.[39] The polynuclear photosensitizers D_p, T_{pp}, and Q_{ppp} consistently exhibited superior catalytic performance compared to the mononuclear photosensitizer $[Ru(bpy)_3]^{2+}$ under equimolar [Ru] concentrations, especially under irradiation with low-energy light (Table 2).[39]

Due to their red-shifted absorption bands, polynuclear photosensitizers demonstrated remarkable efficiency using low-energy green and orange LEDs (>90% in 7 h, Table 3).[39] In contrast, $[Ru(bpy)_3]^{2+}$ was rather ineffective, yielding only 49% after 72 h of irradiation with orange light, in line with its smaller molar absorption coefficient at the irradiation wavelength.[39] Furthermore, the polynuclear complexes are stronger photooxidants than $[Ru(bpy)_3]^{2+}$ owing to their at least 300 mV higher ground-state reduction potentials.[39] This shift in potentials overcompensates the lower excited-state energies of the polynuclear complexes. Consequently, the thermodynamic

Table 3. Yields for the Dehalogenation of 4-Bromobenzyl-2-chloro-2-phenylacetate under Different Reaction Conditions[39]

	[PS] (mol %)	Eq. Ru center (mol %)	white light (6500 K)[a]	blue (470 nm)[a]	green (525 nm)[a]	orange (590 nm)[a]
$[Ru(bpy)_3]^{2+}$	2.50	2.5	77%	80% (5 h)	78% (7 h)	49% (72 h)[b]
D_p	1.25	2.5	92%	91% (2 h)	91% (2.5 h)	91% (6.5 h)
T_{pp}	0.83	2.5	91%	93% (2 h)	93% (2.5 h)	94% (7 h)
Q_{ppp}	0.63	2.5	93%	95% (2 h)	96% (2.5 h)	95% (7 h)

[a]Isolated yields of 4-bromobenzyl-2-phenylacetate after column chromatography. Time required for full conversion determined by ^{1}H NMR given in brackets. [b]Incomplete conversion with 33% of starting material recovered.

https://doi.org/10.1021/acs.inorgchem.6c00560
Inorg. Chem. 2026, 65, 7549−7577

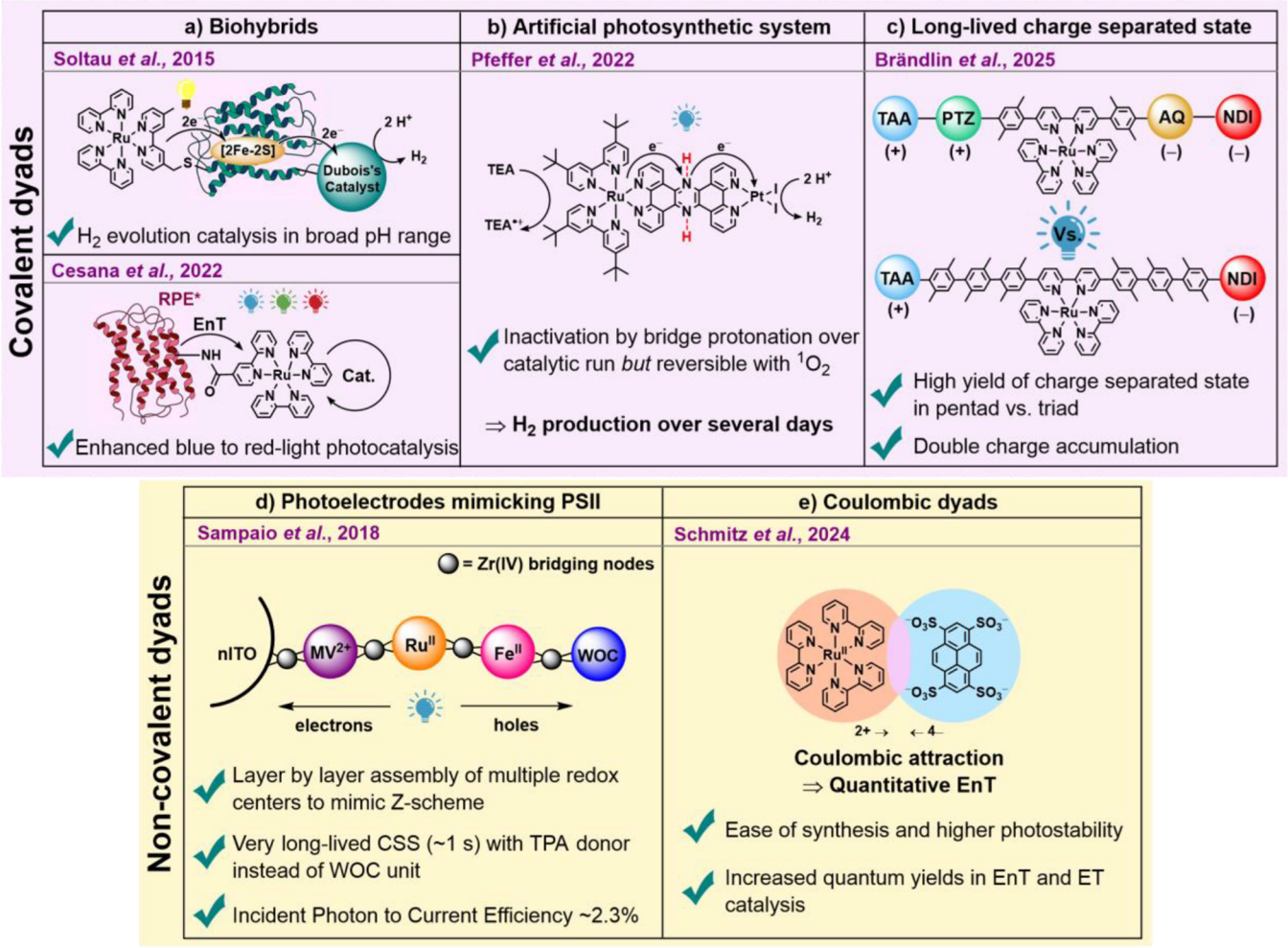

Figure 10. Representative examples of covalent (top) and noncovalent (bottom) dyads for electron or energy transfer applications. (WOC = water oxidation catalyst). See text for additional details.[43,45,55,172−174]

driving force for the initial electron transfer from the sacrificial donors to the polynuclear photosensitizers is higher which leads to higher quenching rate constants compared to $[Ru(bpy)_3]^{2+}$. Finally, the polynuclear complexes are more photostable than the parent complex because nonradiative relaxation via the ^{3}MC states is negligible for D_p, T_{pp} and Q_{ppp} (see Section 2.4.1).[39] Overall, the polynuclear complexes showed a better performance as photocatalysts compared to $[Ru(bpy)_3]^{2+}$.[39]

2.5. Dyads

The foundational concepts of ruthenium-based dyads extend back to the second half of the 20th century following the discovery of the Creutz-Taube ion.[141,142] These initial studies frequently involved $[Ru(bpy)_3]^{2+}$ chromophores linked to quinones,[161−164] aromatic derivatives[161−165] and biomolecules.[166−170] Although the term "dyad" was not yet used during these initial studies, the core idea was evident: pairing a photosensitizer with another redox-active component to facilitate intramolecular electron transfer.[171] Initially, these systems operated as mechanistic platforms to explore long-range electron transfer, bridge-mediated coupling, and thermodynamic asymmetry, forming the conceptual basis for contemporary dyad design. In recent years, the degree of molecular control and purpose-driven engineering has advanced significantly, and dyads have transitioned from model compounds to precisely calibrated photochemical tools.

2.5.1. Covalent Dyads. Over the past decade, the development of Ru-based covalent dyads has been increasingly guided by the principles of natural photosynthesis.[175] In biological systems, efficient charge separation relies on a remarkably coordinated sequence of events: photoexcitation is followed by rapid and directional electron transfer, stabilization of spatially separated charges, minimization of energy-wasting decay pathways, and embedding of these elementary steps in a modular protein scaffold.[175] These design principles have inspired chemists to build artificial molecular architectures in which a photosensitizer is covalently linked to an electron or energy acceptor, donor, or catalytic unit with finely tuned geometric and electronic properties. The goal remains the same as in natural photosynthesis, i.e. to generate long-lived charge-separated states with minimal recombination and enough driving force to fuel downstream chemistry.

Recently, biological scaffolds have not only been used as conceptual blueprints but also as functional architectures capable of stabilizing charge-separated states, enforcing redox gradients, or preorganizing chromophores and catalytic motifs.[55,172,176] In such biohybrid systems, a ruthenium complex is covalently linked to a protein or peptide matrix that acts simultaneously as structural support and electronic

https://doi.org/10.1021/acs.inorgchem.6c00560
Inorg. Chem. 2026, 65, 7549−7577

regulator. Some representative examples come from Utschig and co-workers, who used small, soluble proteins such as ferredoxin (Fd) and flavodoxin (Fld) as templates to assemble Ru-polypyridine chromophores together with Co- and Ni-DuBois-type catalysts (Figure 10a).[172,176] These constructs mimic key features of photosystem I, enabling photochemical H_2 generation from water. Notably, the protein environment renders the otherwise insoluble Ni catalyst active in aqueous media over an exceptionally broad pH range (3.5−12).[176] Time-resolved spectroscopic techniques revealed that the protein matrix is responsible for distinct electron-transfer pathways, sequential versus direct, depending on the native cofactors, and stabilizes charge-separated states on the millisecond time scale, long enough to drive productive catalysis. This work provides a benchmark for how protein scaffolds can protect, solubilize, and electronically regulate molecular catalysts under conditions where they would otherwise fail.

Biohybrids have also emerged as valuable platforms for photoredox catalysis. In 2022, Cesana and co-workers introduced a markedly different design in which $[Ru(bpy)_3]^{2+}$ complexes were covalently attached to the light-harvesting protein R-phycoerythrin (RPE), yielding RPE-$(Ru)_n$ (Figure 10a).[55] Here, the ruthenium complex serves exclusively as the catalytic unit, while the protein acts as a broadband light-harvesting unit that sensitizes its ^{3}MLCT state. Efficient energy transfer from the RPE antenna to the bound ruthenium complexes was confirmed spectroscopically and enabled catalytic activity at wavelengths less accessible to free $[Ru(bpy)_3]^{2+}$, including green (513 nm) and even red light (630 nm).[55] In two model transformations, a thiol−ene coupling and a cysteinyl-desulfurization, the biohybrid not only allowed red-light reactivity but also delivered substantially higher product yields than the catalyst alone under its optimal blue-light conditions. Additionally, the large size of RPE-$(Ru)_n$ (∼240 kDa) allowed for easy recovery of the biohybrid by centrifugation and recycling with minimal loss of efficiency, thereby blending the benefits of homogeneous and heterogeneous catalysis.[55]

The RPE-biohybrid places $[Ru(bpy)_3]^{2+}$ in an atypical role as a catalytic center rather than as the photosensitizer.[55] However, the majority of covalent dyads still follow the classical scheme in which a ruthenium(II) polypyridyl unit performs both light-harvesting and directional charge transfer. Within this more conventional framework, Rau and co-workers developed a particularly influential Ru−tpphz−Pt dyad (tpphz = tetrapyrido[3,2-a:2′,3′-c:3″,2″-h:2‴,3‴-j]phenazine, Figure 10b), demonstrating how precise chromophore−catalyst coupling can govern photostability, self-repair, and multi-electron reactivity.[45]

The earliest molecular devices capable of photochemical hydrogen evolution emerged in the mid-2000s. Sakai and co-workers, in 2006, reported a Ru−Pt dyad that produced H_2 using EDTA as a sacrificial electron donor,[177,178] and in parallel Rau introduced the related Ru−tpphz−Pd system.[179,180] Shortly thereafter, Hammarström and co-workers examined a Pd-based Ru−chromophore dyad and provided direct evidence that, under catalytic conditions, the Pd center readily decomposes to form colloidal Pd nanoparticles that are solely responsible for H_2 evolution.[181] While similar mechanistic ambiguity was later observed in Ru−tpphz−Pd systems, the corresponding Pt analogues remained molecular and photoactive on the time scale of the experiments.[182] This contrasting behavior was rationalized by the lower energy of the dissociative metal-centered states in Pd complexes relative to Pt, which facilitates ligand loss upon excitation and accelerates decomposition.

To develop artificial photosynthetic systems toward practical implementation, it is essential to understand and manage catalyst deactivation pathways. Nature addresses photodamage not by preventing it entirely but by repairing key components in situ. Inspired by this paradigm, Rau and co-workers developed assemblies capable of controlled, chemically driven repair during operation.[45] Such strategies require that the catalytic center remain structurally intact, underscoring the importance of the metal identity in determining the long-term function of Ru-based dyads. In 2022, Rau and co-workers showed that the Ru−tpphz−Pt dyad deactivated over time not because of irreversible decomposition, but due to a reversible hydrogenation of the tpphz bridging ligand.[45] This modification suppresses the essential photoinduced electron transfer from the Ru chromophore to the Pt catalytic center, thereby halting hydrogen evolution. Identification of this deactivation pathway enabled repair through the oxidative dehydrogenation of the hydrogenated ligand using singlet oxygen, generated in situ by the Ru photosensitizer under irradiation in the presence of air.[45] Implementing the repair cycle extended the operational lifetime of the dyad from approximately 2 days to several weeks (over 400 h), yielding cumulative TON values exceeding 3,000.[45] While this represents a major step forward in the development of regenerative systems, the repair cycle still required several additional steps (removal of solvent and additives, redissolution, reaction with $^1O_2$) increasing cost and adding sources of contaminations.[45]

Having established how covalent dyads like the Ru−tpphz−Pt system can be engineered for robustness and in situ repair,[45] the next frontier lies in extending the lifetime and magnitude of charge separation itself. In this context, Wenger and co-workers have recently reported molecular dyads that can accumulate multiple separated charges and store photochemical potential over extended time scales, an essential step toward artificial Z-scheme and solar fuel systems (Figure 10c).[173] A primary challenge is that photoinduced charges tend to recombine spontaneously, wasting much of the absorbed photon energy. While increasing the distance between charges can slow this recombination down, it typically reduces the efficiency of the initial charge separation step.[183] Wenger and co-workers addressed this trade-off by incorporating redox-active relay stations that enable a multistep "hopping" sequence rather than relying on single-step tunneling through passive spacers.[173] In a recent study, they showed that a pentad (D_2−D_1−PS−A_1−A_2) containing such relays maintains a charge-separation quantum yield of ∼60% over a donor−acceptor distance of 44 Å, compared to ∼5% for a comparable triad containing only passive linkers (Figure 11). The lifetime of the resulting charge-separated state was also extended from 28 μs (triad) to 120 μs (pentad), owing to strongly reduced back-electron transfer rates. These improvements were attributed to the redox-active intermediates D_1 and A_1, which enable efficient multistep hopping during charge separation but do not facilitate charge recombination. The authors emphasize that focusing on quantum yields, rather than exclusively on kinetic rate constants, is critical because efficiencies inherently reflect dark recombination events that are otherwise easily overlooked.[173] Such long-lived charge-separated states are particularly valuable under low-intensity solar irradiation,

https://doi.org/10.1021/acs.inorgchem.6c00560
Inorg. Chem. 2026, 65, 7549−7577

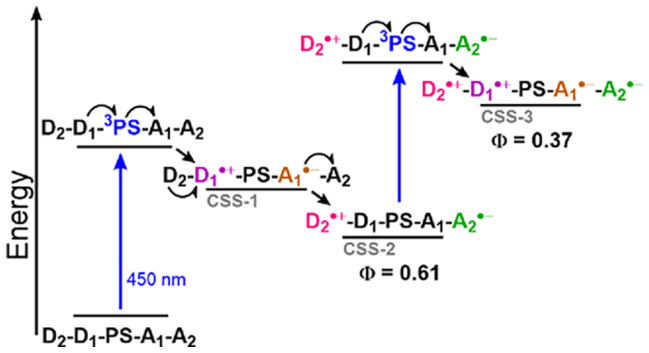

Figure 11. Energy level diagrams of the key photoproducts and their corresponding energies in a covalent pentad. The first charge-separated state (CSS-1) spontaneously evolves onward to form CSS-2. Secondary excitation of CSS-2 leads to the formation of CSS-3 with two separated pairs of charges. The two ϕ values indicate quantum yields for the formation of the corresponding CSS, as determined by relative actinometry.[173]

where sequential excitation becomes necessary for accumulating multiple redox equivalents. A common limitation of molecular dyads is that after the first charge-separation event, absorption of a second photon often triggers fast charge recombination instead of further charge buildup.[184−186] In the pentad system, however, the first photogenerated electron−hole pair rapidly separates over a large distance, restoring the photosensitizer's local electronic environment and allowing a second productive excitation.[173]

As outlined in Figure 11, the first excitation of the pentad forms an initial charge-separated state (CSS-1: $D_2-D_1^{\bullet+}-PS-A_1^{\bullet-}-A_2$), which evolves into a more stable and long-lived state (CSS-2: $D_2^{\bullet+}-D_1-PS-A_1-A_2^{\bullet-}$) within 10 ns. A second excitation of the photosensitizer in the CSS-2 state initiates the formation of a doubly charge-separated state (CSS-3), where two positive charges are on the donor side ($D_1^{\bullet+}$ and $D_2^{\bullet+}$) and two negative charges are on the acceptor side ($A_1^{\bullet-}$ and $A_2^{\bullet-}$). This final photoproduct formed with an overall quantum yield of 37% and persisted for more than 100 ns, thereby storing approximately 3.0 eV of energy. This work represents a significant advancement in achieving sequential, light-driven accumulation of two electrons and two holes in a fully molecular system without sacrificial agents.

2.5.2. Noncovalent Dyads. Noncovalent dyads represent a complementary design strategy in which photosensitizers and redox-active partners are brought into functional contact not through covalent linkers, but through a variety of weak interactions such as electrostatic attraction, hydrogen bonding, π-stacking, or surface coordination motifs. These assemblies preserve the essential features of the dyad architectures, i.e. proximity, directionality, and controlled electron transfer, while avoiding the synthetic constraints and conformational rigidity of covalently tethered systems. As such, noncovalent dyads offer a versatile platform for studying and controlling photoinduced transfer processes, including in emerging PSII-mimetic systems and inorganic−organic hybrid dyads formed by simply mixing ionic chromophores in polar solvents.

Meyer and co-workers focused on the development of molecular photoelectrodes through precise layer-by-layer assembly of chromophore and catalysts on conductive metal oxide surfaces as a powerful strategy for controlling interfacial charge-transfer processes.[174,187−189] They have demonstrated how stepwise construction of molecular architectures on mesoporous indium-doped tin oxide (nanoITO) enables charge separation across nanometer-scale distances with lifetimes far longer than those typically observed in solution or at conductive interfaces.[174,187] The layer-by-layer methodology relies on the strong affinity of phosphonic-acid groups for metal-oxide surfaces and on the use of Zr(IV) ions as bridging nodes that link successive layers.[174,187,190−192] This approach enables the ordered deposition of different molecular components, i.e. electron acceptors, chromophores, electron donors and water-oxidation catalysts, into defined supramolecular stacks extending from the oxide surface.[174,187] Because the assemblies are built on mesoporous nanoITO films composed of 20 nm particles and containing large internal pore volumes, each hierarchical structure can form not only on the external film surfaces but also within the internal porous network, ensuring high loadings and large interfacial area.

As such, a five-component assembly consisting of a nanoITO electrode, a surface-bound methylviologen electron acceptor (MV), a ruthenium(II) polypyridyl sensitizer (S), an iron(II) terpyridyl donor (Fe), and a terminal triphenylamine (TPA) electron donor where anchored in a layer-by-layer fashion via Zr bridges to generate the nanoITO|MV−S−Fe−TPA architecture with an overall molecular length estimated at 6 nm (Figure 10d).[174] While on semiconductor oxides such sensitizer assemblies often suffer from ultrafast recombination, the authors demonstrated that the conductive nanoITO interface supported long-lived charge separation. Spectroelectrochemistry measurements confirmed the reduction potentials of each component that efficiently created a free-energy gradient that was used to drive electrons toward the oxide surface and holes outward, rendering interfacial charge transfer directionally favorable.[174] Transient absorption spectroscopy revealed the success of this design. Excitation of the ruthenium chromophore initiated an ultrafast charge-transfer cascade, resulting in electron injection into the MV/ITO surface and rapid hole diffusion toward the distal TPA donor. Remarkably, this process produces a charge-separated state that persists for almost one second, i.e. six orders of magnitude longer than for the sensitizer alone on nanoITO.[174] The recombination kinetics were fully first-order, indicating a well-defined interfacial configuration rather than the distributed kinetics characteristic of sensitized semiconductor electrodes. The long lifetime arises not from the semiconductor's properties alone but rather from the large spatial separation between the injected electron and the oxidized electron donor, which drastically reduces the electronic coupling that governs back-electron transfer.[193,194]

Using the same layer-by-layer approach, Meyer and co-workers then replaced the model TPA electron donor by a ruthenium-based water oxidation catalyst to generate the nanoITO|MV−S−Fe−Ru(catalyst) photoelectrode (Figure 10d).[187] This assembly intentionally bears analogy to Photosystem II: the MV layer plays the role of the primary quinone acceptor, the $[Ru(bpy)_3]^{2+}$-based chromophore mimics the P680 special pair, the Fe electron donor emulates the redox-active tyrosine that relays oxidative equivalents and the distal Ru catalyst occupies the position of the oxygen-evolving complex. As in the earlier study, the layer-by-layer design dramatically extended the lifetime of the charge-separated states. With the complete MV−S−Fe−Ru architecture, the reduced oxide and oxidized catalyst remain separated for several seconds.[187] This persistence of redox equivalents on

https://doi.org/10.1021/acs.inorgchem.6c00560
Inorg. Chem. 2026, 65, 7549−7577

both ends of the supramolecular chain is essential for catalytic turnover, since water oxidation requires the accumulation of multiple oxidative equivalents at the catalytic site.[195−197] Under steady-state visible-light illumination with an applied bias, the photoelectrode produced oxygen with incident photon-to-current efficiencies reaching 2.3% at 440 nm.[187]

Taken together, these studies demonstrate that layer-by-layer molecular engineering on conductive metal oxides enables a level of functional control impossible with randomly adsorbed dyes or with covalently linked supramolecular assemblies. By dictating the spatial and electronic arrangement of each redox-active component, a system that reproduces key features of natural photosynthetic machinery was developed.[187] The layer-by-layer approach thus provides a versatile platform where multiple components can be engineered with a level of precision that approaches the functional logic of natural photosynthetic assemblies.

A complementary and increasingly attractive strategy to dyads is exploiting coulomb interactions to assemble photosensitizer−acceptor pairs. In this design, a positively charged photosensitizer associates spontaneously with a negatively charged chromophore or quencher, forming a dynamic encounter complex that can mediate rapid and directional electron or energy transfer. The assemblies are formed in situ without additional synthetic effort and their components remain modular and exchangeable. Recent studies from Kerzig and co-workers have demonstrated how such Coulombic dyads can deliver photophysical and photocatalytic performance equal to, or even surpassing, covalent dyads (Figure 10e).[42−44] In one example, mixing a cationic ruthenium complex ($[Ru(phen)_3]^{2+}$) with an anionic pyrene derivative (pyrene-1,3,6,8-tetrasulfonic acid, PTS^{4-}) led to a Coulombic dyad in water.[43] Strong ground-state association between the oppositely charged partners enabled ultrafast, static Dexter energy transfer, funneling visible-light excitation of the ruthenium(II) complex into the long-lived triplet state of the pyrene unit ($^3PTS^{4-}$). This process occurred with nearly quantitative efficiency and yielded a triplet lifetime of 355 μs, over 300 times longer than the parent metal complex (1.1 μs).[43] The extended lifetime translated directly into greater catalytic performance, as shown across multiple reductive and oxidative photoreactions where the Coulombic dyad outperformed both free $[Ru(phen)_3]^{2+}$ and the analogous covalently linked dyad.[43] Earlier work had observed similar behavior with the monoanionic pyrene derivative (PMS),[43,44] but the tetraanionic system exhibited markedly higher quenching efficiency.[43]

Building on this concept, the group extended the Coulombic-dyad strategy to $[Os(phen)_3]^{2+}$ paired with the perylenetetracarboxylate anion (PTC^{4-}), aiming to overcome the intrinsic limitations of osmium photosensitizers in singlet-oxygen generation.[42] Osmium complexes can be directly excited into their triplet manifolds with red light, which is ideal for energy efficiency and deep medium penetration, but their short excited-state lifetimes (77 ns) limit diffusion-controlled reactions. A Coulombic dyad with PTC^{4-} showed ultrafast (∼100 ps) energy transfer from the osmium complex to the organic acceptor, generating a long-lived ^3PTC state (τ = 219 μs).[42] This state reacted with O_2 almost quantitatively, resulting in a 15.5-fold increase in singlet oxygen production relative to the osmium complex alone. The system proved highly effective in red-light-driven photooxygenations of furfural, 5-HMF, and even DMSO, as well as in degrading environmental pollutants such as glyphosate in wastewater.[42]

A key benefit of using Coulomb interactions to create dyads is that the organic component can be readily exchanged in case it decomposes, keeping the expensive metal complex intact. Covalent dyads on the other hand undergo irreversible deactivation upon oxidation of the organic chromophore. Addition of PTC^{4-} during operation restored the activity immediately, enabling sustained high TOF.[42] Together, these results establish Coulombic dyads as a simple, versatile, and highly efficient alternative to their covalent counterpart, particularly for applications requiring long-lived excited states, deep-penetrating red-light activation, or modular component replacement. Their performance across both synthetic and environmental transformations underscores the broad potential of Coulombic dyads in next-generation photocatalysis.

3. FUTURE PERSPECTIVES

3.1. "Real-Life" Applications

Within the past 90 years since its discovery, $[Ru(bpy)_3]^{2+}$ evolved from a scientific curiosity to a cornerstone of photophysics and photochemistry research.[2,198] Its favorable optical properties enabled its critical role in driving several research fields. The impact of $[Ru(bpy)_3]^{2+}$ reaches beyond the academic landscape into "real-world" applications. The following section aims at highlighting past and present commercial applications of $[Ru(bpy)_3]^{2+}$ and its current trends.

A patent search on $[Ru(bpy)_3]^{2+}$ (see SI for details) yielded 1650 patents in 920 simple families. The earliest patent originated from 1962 and focused on the synthesis of bipyridine metal complexes as antimicrobial agents.[199] Since the 1990s the number of patents on $[Ru(bpy)_3]^{2+}$ has increased exponentially (Figure 12). Clustering of the patents revealed that the key application areas are photoredox catalysis and electrochemiluminescence (ECL) sensing. While the total number of patents in both categories is similar, photoredox catalysis saw the steepest rise in the past 10 years, with 66% of the patents being published in the past 5 years.

This development comes to no surprise considering that photoredox catalysis dramatically expanded synthetic methodology and facilitated several reactions relevant to the pharmaceutical industry.[82,84] A major boost to this development has been that photocatalysts such as $[Ru(bpy)_3]^{2+}$ were made commercially available soon after their potential became apparent.[200] A major challenge for the industrial use of photoredox chemistry lies in the upscaling of these reactions.[201] Unlike thermal reactions where heat can be uniformly applied to a large reactor aided by fast mixing, photoredox reactions only occur at parts of the reaction mixture that light can reach. According to the Lambert−Beer law, light has a very shallow penetration depth in highly absorbing mixtures. For a photoredox reaction this means that radicals are only generated in a thin outer layer, regardless of the size of the reactor, if irradiation occurs from the outside of said reaction.[202] In 2022, researchers at Abbvie reported one of the first commercial-scale photoredox reactions using LED plug flow and laser-based continuous stirred tank photoreactors.[203] Their target reaction was the trifluoromethylation of 2-chlorothiophenol using $[Ru(bpy)_3]^{2+}$ as a photosensitizer. After photoexcitation, $[Ru(bpy)_3]^{2+*}$ generated iodine radicals from iodide to start a radical chain reaction. After the

https://doi.org/10.1021/acs.inorgchem.6c00560
Inorg. Chem. 2026, 65, 7549−7577

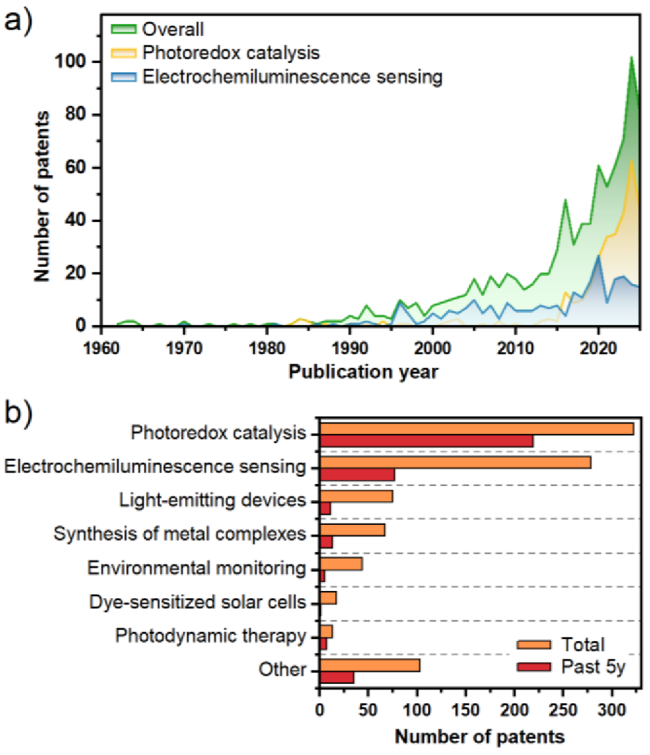

Figure 12. Patent search results on $[Ru(bpy)_3]^{2+}$. (a) Total number of simple patent families over time. (b) Number of patents families in different categories. See SI for details on patent search and analysis.

optimization of reaction conditions, the authors were able to access over 500 kg of the desired product. Due to the radical chain mechanism, only 0.01 mol % of $[Ru(bpy)_3]^{2+}$ were necessary to drive the reaction.[203]

The second largest area of application for $[Ru(bpy)_3]^{2+}$ are commercial automated immunoassays, such as the cobase/Elecsys assays developed by Roche.[204] These assays are used for the sensitive quantification of biomarkers such as tumor markers, hormones or viral proteins with small sample volumes.[12] Here, $[Ru(bpy)_3]^{2+}$ acts as a label that is conjugated to an antibody that in turn binds the target analyte. The readout is an electrochemiluminescence (ECL) signal that is generated when an electric potential is applied to the complex in the presence of an electron donor like tripropylamine. The electrochemical oxidation of tripropylamine on the electrode surface leads to redox cycling of $[Ru(bpy)_3]^{2+}$ which eventually populates its luminescent excited state yielding the chemiluminescence readout.[205] A good ECL label needs to balance several properties like turnover, reaction specificity, quantum yield and dynamic range of the luminescence signal.[205] The combination of $[Ru(bpy)_3]^{2+}$ and tripropylamine marked a sweet spot in this property space. So even though other Ru^{II} complexes and purely organic systems like luminol/H_2O_2 have been explored in the past, $[Ru(bpy)_3]^{2+}$/tripropylamine still remains a popular platform for ECL immunosensing applications.[12,204]

$[Ru(bpy)_3]^{2+}$ and its derivatives are also used in commercial sensing applications, specifically for sensing molecular oxygen.[206] Such sensing relies on the collisional quenching of the ^{3}MLCT state by $^3O_2$ forming $^1O_2$. This reaction of the excited state shortens the luminescence lifetime and lowers its intensity. By determining the quenching rate constant (e.g., using Stern−Volmer experiments), the partial pressure or solution concentration of oxygen can be determined from intensity or lifetime data. This sensing mechanism is well established for $[Ru(bpy)_3]^{2+}$[207−209] and several older patents mention using this complex.[207,210−212] However, as the sensor materials are proprietary, companies often only provide vague descriptions such as "ruthenium sensor"[213] and it is thus difficult to tell whether unfunctionalized $[Ru(bpy)_3]^{2+}$ is still being used in commercial sensing devices.

A particularly impactful application of a $[Ru(bpy)_3]^{2+}$ derivative lies in the treatment of cancer using photodynamic therapy (PDT).[214] In one of the operative mechanisms of PDT, a sensitizer releases highly reactive species (e.g., $^1O_2$ or $O_2^{\cdot-}$) at or inside a tumor when irradiated with light. The high spatial control over the treatment limits adverse effects on healthy tissue.[214] TLD1433 is the first ruthenium complex to enter human clinical trials as a PDT agent,[214] which are currently in phase 2 for the treatment of bladder cancer.[215] TLD1433 consists of a ruthenium(II) metal center, two 4,4′-dimethylbipyridine ligands and a substituted phenanthroline ligand with a tethered chain of three α-thiophene units (Figure 13). This molecular design was chosen to enable both light-induced electron transfer reactions and sensitization of singlet oxygen locally at the tumor site. The thiophene units are central to both modes of action. First and foremost, they introduce dark intraligand triplet states (^{3}IL) with $\pi\pi^*$ character. These excited states have an energy of 1.72 eV and thus lie below the complex's ^{3}MLCT states and possess a much longer excited-state lifetime of 48 μs in deaerated water.[216] The ^{3}IL states sensitize singlet oxygen with a unity quantum yield.[217] Second, the electron-rich thiophene units can reductively quench the MLCT state forming an intraligand charger transfer state (^{3}ILCT) that can undergo follow-up electron transfer reactions to damage tumor tissue, e.g. by forming superoxide ($O_2^{\cdot-}$).[214] Interestingly, the ^{3}ILCT state can also react with other sensitizer molecules in their ground state which produces two reactive species − an oxidized and a reduced complex. As each photon can generate more than one reactive species, the photocytotoxicity of TLD1433 is dramatically improved.[214] While most of the excitation energy is funneled into the dark ^{3}IL/^{3}ILCT states, a weak luminescence via the ^{3}MLCT can still be observed (Φ < 0.05%)[216] and used for theranostic imaging.[214] During therapy, the complex is directly applied to the bladder where it accumulates selectively in the cancer tissue and is then

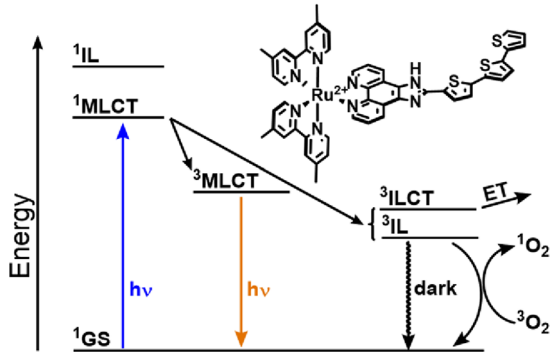

Figure 13. Photophysical scheme of TLD1433. The emissive ^{3}MLCT state can be used for diagnosis and imaging whereas the non-luminescent (dark) ^{3}IL and ^{3}ILCT promote singlet oxygen formation and electron transfer chemistry, respectively.[214]

https://doi.org/10.1021/acs.inorgchem.6c00560
Inorg. Chem. 2026, 65, 7549−7577

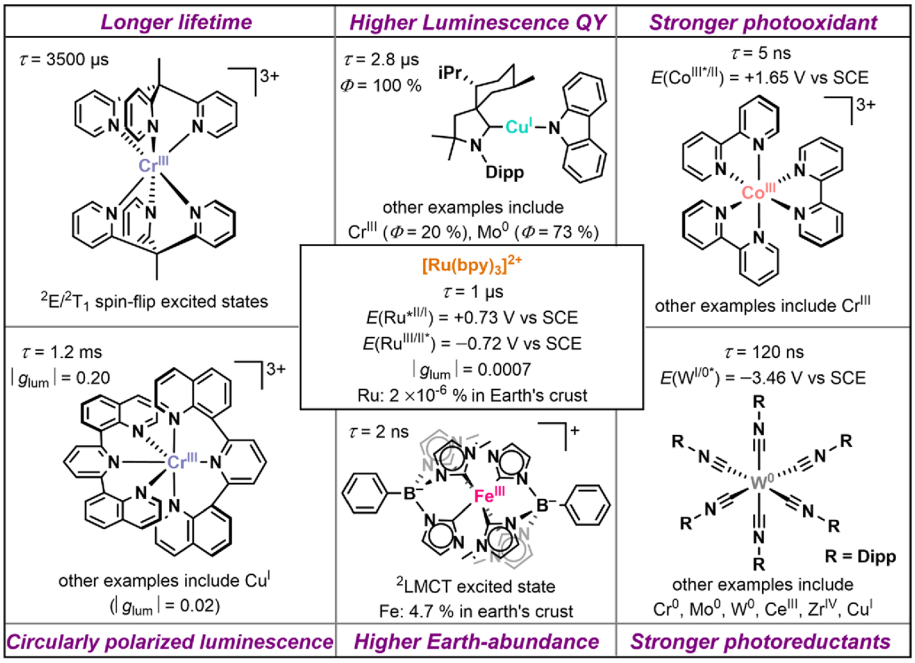

Figure 14. Representative examples of photosensitizers based on earth abundant element that have matched or outcompeted some of the excited-state properties of the prototypical $[Ru(bpy)_3]^{2+}$,[7,224] with regards to lifetime,[225,226] photoluminescence quantum yield,[227−229] photooxidative power,[222] circularly polarized luminescence,[230−233] Earth-abundance[221] and photoreductive power.[223]

irradiated with 520 nm light.[25] While $[Ru(bpy)_3]^{2+}$ itself is not used for this highly specialized application, it is the decades of research on its photophysical and photochemical properties that enabled this new cancer therapy.[214]

3.2. Earth-Abundant Metal Complexes "Surpassing" $[Ru(bpy)_3]^{2+}$

$[Ru(bpy)_3]^{2+}$ has long set the standard for photoactive metal complexes.[1−6] However, the general scarcity of precious metals motivated researchers to explore photoactivity with more abundant metal centers.[218] There have been enormous efforts in the past 10 years to establish such metal complexes with unique photoactivity surpassing the traditional $[Ru(bpy)_3]^{2+}$ family.[218−223] In this section, we spotlight earth-abundant metal complexes that beat that standard in one or more ways, i.e. better light absorption, longer-lived excited states, or greater stability, and explain why those advantages matter.

One of $[Ru(bpy)_3]^{2+}$'s great strengths is its versatility in photochemical reactions. It can act as a photooxidant and a photoreductant with reasonable potentials of +0.73 and −0.72 V vs SCE, respectively.[7] However, this versatility also means that the excited-state energy is broadly distributed between both reactivity modes. As a result, accessing larger potentials with $[Ru(bpy)_3]^{2+}$ requires specialized strategies like reducing the excited state with an electron donor to form $[Ru(bpy)_3]^{+}$ as active species ($E([Ru]^{2+/+}) = -1.3$ V vs SCE)[7] or two-photon processes (e.g., generation of hydrated electrons).[90] There are several complexes with higher photooxidative power than $[Ru(bpy)_3]^{2+}$ such as its long-overlooked cobalt(III) analog $[Co^{III}(bpy)_3]^{3+}$ (Figure 14) and its derivatives that feature dark ^{3}MC excited states which could be described as superoxidants with excited state potentials $E(Co^{III*/II})$ of up to +1.65 V vs SCE.[234,235] These complexes were recently used as photosensitizers for the particularly challenging arylation of amines.[222] Cr^{III} complexes such as $[Cr(phen)_3]^{3+}$ and so-called molecular rubies can also be used as photooxidants (+1.33 to +1.83 V vs SCE).[225,236−239] On the reductive side, there have been plenty of examples, such as copper(I) complexes (up to −2.22 V vs SCE),[240,241] group 6 carbonyl and isonitrile complexes (−1.68 to −3.46 V vs SCE),[75,220,223,229,242,243] zirconium(IV) arylimidazolpyridine complexes (−2.41 to −2.98 V vs SCE)[244,245] and cerium(III) bis(guanidinate) complexes (−3.0 to −3.3 V vs SCE).[246] Especially, zerovalent tungsten complexes of the type $W^0(CN{-}R)_6$ (Figure 14) combine strong photoreductive power (up to −3.46 V vs SCE) with synthetic accessibility, microsecond excited-state lifetimes and enormous molar absorption coefficients (up to 10^5 M^{-1} cm^{-1}).[223]

In areas like sensing and photoredox catalysis, a longer excited-state lifetime leads to better performance and lower costs.[247] The ^{3}MLCT excited-state lifetime of $[Ru(bpy)_3]^{2+}$ with ∼1 μs is long enough for both fundamental photochemical investigations and applications.[7] However, this value has been surpassed by a factor of 3500 by the current record holder $[Cr(tpe)_2]^{3+}$ (Figure 14, tpe = 1,1,1-tris(pyrid-2-yl)ethane) which reached an excited-state lifetime of 3.5 ms in solution at room temperature.[225,226] The reasons for this particularly long lifetime lie in the so-called metal-centered spin-flip states in chromium(III) complexes.[248] These excited states feature the same $(t_{2g})^3$ orbital occupation as the ground state, except that one electron spin is flipped. As a result, the excited state is barely distorted which slows down relaxation to the ground state. The transition to the ground state is also strongly Laporte forbidden. In $[Cr^{III}(tpe)_2]^{3+}$, this effect is further amplified by the perfect inversion symmetry imposed by the ligands.[226] Overall, spin-flip excited states find application in pressure and oxygen sensing,[249] photoredox catalysis,[225,238] as well as qubits using Cr^{IV}, Mo^{IV} and V^{III}.[250−252]

Chromium(III) complexes with the right ligands can also outperform $[Ru(bpy)_3]^{2+}$ with regards to luminescence quantum yields. For example, $[Cr(bpmp)_2]^{3+}$ showed a red

https://doi.org/10.1021/acs.inorgchem.6c00560
Inorg. Chem. 2026, 65, 7549−7577

phosphorescence at 709 nm with an efficiency of 20% (bpmp = 2,6-bis(2-pyridylmethyl)pyridine).[228] Linear copper(I) complexes bearing carbene ligands even reached luminescence quantum yields of unity (Figure 14).[227] Admittedly, both systems feature fundamentally different electronic structures (Cr^{III}: d^3, Cu^{I}: d^{10}) which changes the nature of nonradiative relaxation pathways.[218] However, recent work on molybdenum(0) complexes showed that values up to 73% can be achieved with earth-abundant metal centers isoelectronic to $[Ru(bpy)_3]^{2+}$.[229,253]

The nature of the excited states is central to the emerging field of chiral emitters showing circularly polarized luminescence.[254] This phenomenon has promising applications in the fields of anticounterfeiting, bioimaging, display technology and quantum technology.[255−258] For most technologies, a bright and strongly circularly polarized luminescence is required.[254] The degree of circular polarization is commonly quantified with the dissymmetry factor g_{lum} that ranges from −2 to +2 corresponding to 100% right- and left-handed circular polarization of the emitted light.[254] While $[Ru(bpy)_3]^{2+}$ is chiral and its luminescence is reasonably bright (Φ_{PL} = 9.5%),[9] its performance as a CPL emitter is very poor reaching low $|g_{lum}|$ values of 0.0007.[224,254] This means that the Δ- and Λ-isomers of $[Ru(bpy)_3]^{2+}$ only emit an excess of 0.035% of one handedness of circularly polarized light. The chiroptical properties of an electronic transition depend strongly on its magnetic transition dipole moment, i.e. the rotation of charge during the transition.[259] Unfortunately, the emissive ^{3}MLCT states in $[Ru(bpy)_3]^{2+}$ and similar complexes only show small magnetic transition dipole moments, and hence do not fulfill the selection rules for strong CPL.[254] In contrast, lanthanide complexes can achieve g_{lum} values of up to 1.38 via their f−f transitions.[260] On the side of earth-abundant metals, Cu(I) and Cr(III) complexes (Figure 14) come closest to these dissymmetries, reaching g_{lum} values of 0.02[233] and 0.2,[230−232,261] respectively.

Iron is by far the most abundant transition metal in the Earth's crust.[262] So, from a cost and sustainability perspective there is a strong incentive to develop photoactive iron complexes that rival $[Ru(bpy)_3]^{2+}$ in its photoactivity.[263] The main challenge is the lower intrinsic ligand field splitting in Fe(II) that stabilizes metal-centered excited states which in turn facilitate the rapid deactivation of MLCT excited states.[24,264] Despite intense research efforts over 20 years, so far, only one example of an Fe(II) complex mimicking the electronic structure of $[Ru(bpy)_3]^{2+}$ with a photoreactive ^{3}MLCT state has been reported.[265] However, its excited-state lifetime remains short (∼1 ns) and its excited state energies are low.[265] Further breakthroughs have been achieved by moving away from the d^6 electron configuration. By combining an Fe(III) center (d^5) with strongly σ-donating carbene ligands (Figure 14), photoactive complexes with ^{2}LMCT excited state were obtained.[221,266] As these complexes also feature a doublet ground state, the relaxation of the excited state is spin-allowed leading to relatively short excited-state lifetimes of 2 ns. Recent work demonstrated that these lifetimes and thus the photoactivity can be enhanced dramatically up to 11.5 μs by attaching organic chromophores to the ligands.[267−269] When the energies of the organic triplet state and the ^{2}LMCT state match, energy can be funneled to the organic triplet.[267] Apart from the lifetime, the doublet multiplicity also affects which reactions are possible after photoexcitation[270] as well as the dark thermal processes like charge recombination following photoreactivity.[271−275] For example, complexes with doublet excited states can harvest both singlet and triplet excitons[276] and are promising platforms for photon-upconversion.[268,277−280]

This short overview shows that precious metals are not the sole candidates capable of achieving bright luminescence, strong photoreactivity and long-lived excited states. Metal complexes based on earth abundant elements have become competitive to their precious metal congeners such as $[Ru(bpy)_3]^{2+}$ and in some cases have even surpassed them in their performance. Equipped with the knowledge of the past, exploration of the full chemical space that transition metals have to offer has already begun. There will still be a place for applications of $[Ru(bpy)_3]^{2+}$ in the future, e.g. as a valuable reference compound and benchmark given the vast amounts of data that were collected over the past decades.

4. CONCLUSIONS

The story of tris(2,2′-bipyridine)ruthenium(II) is, in many ways, the story of modern inorganic photochemistry. $[Ru(bpy)_3]^{2+}$ began its life as a model compound for understanding fundamental MLCT photophysics, unity intersystem crossing, a microsecond triplet lifetime, and well-behaved spectroscopy.[6,7,18] Over the past decades, however, it has steadily evolved from "the textbook chromophore" into a flexible platform for engineering reactivity across environments, architectures, and to develop new reaction methodologies. What is still considered as a benchmark now also functions as a highly adaptable scaffold whose properties can be tuned not only through ligand design,[126] but through counterions,[57,59] supramolecular environments,[47,174] polynuclear organization,[35,38,40] and coupling to other functional units.[55,172,176]

High-level calculations and advanced time-resolved spectroscopic techniques have revealed a much more nuanced excited-state landscape that was initially described, in which multiple ^{3}MC states, minimum-energy crossing points, and subtle environmental effects jointly determine nonradiative decay, ligand loss, and photostability.[21−23,28,29,281] These insights do more than refine our understanding of an old system as they provide quantitative design rules for suppressing dissociative pathways or for deliberately exploiting them, for example in light-triggered drug release.[76]

At the same time, what used to be treated as "spectator" components of the system, i.e. counterions[57,59] and to some extend solvent, micellar hosts, or porous supports,[64,66,108,282] have now been redefined as powerful levers for tuning reactivity. Ion pairing now clearly stands alongside ligand modification and solvent choice as a genuine design parameter. By choosing weakly coordinating, bulky anions, researchers have shown that the ^{3}MLCT energy, excited-state reduction potential, quenching kinetics, and even ^{3}MC-state ordering can be manipulated to optimize both electron- and energy-transfer catalysis, as well as to enhance long-term photostability and TON.[43,57,59] This shift in perspective, from ignoring the counterion to engineering the ion pair, exemplifies how deeply the field has begun to interrogate and harness second-sphere effects.

In parallel, new reaction paradigms have greatly expanded the chemical space accessible to $[Ru(bpy)_3]^{2+}$ photochemistry. Multiphoton strategies that use long-lived reduced intermediates or organic relay chromophores now enable the generation of solvated electrons under low-intensity visible light, especially

https://doi.org/10.1021/acs.inorgchem.6c00560
Inorg. Chem. 2026, 65, 7549−7577

when combined with micellar or electrostatically engineered environments that suppress recombination and side reactions.[106,108] Mechanochemical ball-mill photoredox catalysis demonstrates that $[Ru(bpy)_3]^{2+}$-type systems can operate efficiently in nominally "solvent-free" conditions, with dramatically shortened reaction times and greener processing.[122] Spin-forbidden excitation has been leveraged to drive productive photoredox catalysis with red light, broadening the spectral window in which $[Ru(bpy)_3]^{2+}$ can operate and opening opportunities in settings where high-energy photons are undesirable.[132]

The migration of $[Ru(bpy)_3]^{2+}$ into biological contexts further illustrates its flexibility. Its water solubility, robustness, and well-characterized excited-state behavior have enabled applications in proximity labeling[134] and intracellular bond-forming reactions.[139] These developments highlight how the same MLCT platform can be adapted from fundamental spectroscopy to complex cellular environments, provided its local context and partners are judiciously chosen.

Another major conceptual evolution has been the move from mononuclear complexes to polynuclear assemblies and dyads. Dinuclear and trinuclear $[Ru(bpy)_3]^{2+}$-type systems with well-designed bridges can delocalize excited states and suppress population of deactivating ^{3}MC states.[38,40] In some cases, multiple long-lived ^{3}MLCT states coexist and communicate through activated internal conversion, enabling antidissipative behavior in which high-energy states are available long enough to engage in bimolecular electron transfer before relaxing. When deployed in catalysis, these polynuclear systems outperform the parent $[Ru(bpy)_3]^{2+}$ under lower-energy illumination and exhibit markedly higher photostability.[39]

Covalent and noncovalent dyads push this modularity even further. Ru-based covalent dyads, particularly those integrating catalytic centers via bridging ligands, now offer not only long-lived charge separation but also in situ repair strategies that mimic biological self-healing.[45] Biohybrid architectures demonstrate how protein scaffolds can solubilize molecular catalysts, impose redox gradients, and extend operational lifetimes far beyond what is achievable in simple solution.[55,172,176] In a complementary fashion, noncovalent assemblies, whether layer-by-layer constructs on conductive oxides[174,188] or Coulombic dyads in homogeneous solution,[42,43] show that precise spatial and energetic organization does not require covalent bonds. Instead, dynamic supramolecular architectures can deliver extraordinarily long charge-separated lifetimes, red-light reactivity, and straightforward replacement of components when organic partners degrade.

Crucially, $[Ru(bpy)_3]^{2+}$ has not remained confined to academic laboratories. Its role in large-scale photoredox manufacturing,[203] ECL-based clinical diagnostics,[204] oxygen sensing,[206] and photodynamic therapy[214] underscores that its photophysical virtues translate into technological impact. The same features that make it a didactic model also underpin its industrial reliability.

At the same time, the field has moved decisively beyond a ruthenium-centric view. Complexes based on earth-abundant metals now surpass $[Ru(bpy)_3]^{2+}$ in individual metrics such as excited-state redox potentials,[222,223] molar absorption coefficients,[223] excited-state lifetimes,[226] luminescence quantum yields,[227] chiroptical performance,[254] or sustainability.[221] Chiral chromium spin-flip emitters,[232,248] copper and molybdenum complexes with near-unity quantum yields,[227,229,253] and iron-based LMCT systems with doublet excited states[221] collectively demonstrate that many of the principles learned from $[Ru(bpy)_3]^{2+}$ can be revised in these new chemical spaces.

Looking ahead, the enduring relevance of $[Ru(bpy)_3]^{2+}$ will likely rest on two roles. First, it will remain a critical benchmark that anchors methodological advances in spectroscopy, computation, and device engineering. Second, it will continue to serve as a flexible platform for conceptual innovation, from ion-pair engineering and antidissipative architectures to biohybrid catalysis and unconventional reaction media. Even 90 years after its first report,[2,198] $[Ru(bpy)_3]^{2+}$ continues to expand both the breadth of its applications and the depth of our mechanistic understanding, while simultaneously inspiring the next generation of photosensitizers based on earth-abundant elements that will ultimately define a more sustainable future.

■ ASSOCIATED CONTENT

Supporting Information

The Supporting Information is available free of charge at https://pubs.acs.org/doi/10.1021/acs.inorgchem.6c00560.

Description of $[Ru(bpy)_3]^{2+}$ patent search (PDF)

■ AUTHOR INFORMATION

Corresponding Authors

Ludovic Troian-Gautier − *Institute of Condensed Matter and Nanosciences (IMCN), Molecular Chemistry, Materials and Catalysis (MOST), UCLouvain, 1348 Louvain-la-Neuve, Belgium; Wel Research Institute, 1300 Wavre, Belgium;* orcid.org/0000-0002-7690-1361; Email: Ludovic.Troian@uclouvain.be

Winald R. Kitzmann − *Chemistry Department, Massachusetts Institute of Technology, Cambridge, Massachusetts 02139, United States;* orcid.org/0000-0003-0339-2196; Email: kitzmann@mit.edu

Author

Céline Bourgois − *Institute of Condensed Matter and Nanosciences (IMCN), Molecular Chemistry, Materials and Catalysis (MOST), UCLouvain, 1348 Louvain-la-Neuve, Belgium;* orcid.org/0009-0006-1080-6560

Complete contact information is available at: https://pubs.acs.org/10.1021/acs.inorgchem.6c00560

Notes

The authors declare no competing financial interest.

■ ACKNOWLEDGMENTS

C.B. thanks the Belgian National Funds for Scientific Research (F.R.S.-FNRS) for their FNRS Aspirant PhD grant. L.T.-G. is a Chercheur Qualifié of the Fonds de la Recherche Scientifique − FNRS. L.T.-G. gratefully acknowledges UCLouvain and the FNRS for continuous financial support. This work was supported by the Human Frontier Science Program (HFSP) Fellowship LT0010/2024-C (W.R.K.) (DOI: 10.52044/HFSP.LT00102024-C.pc.gr.194466).

■ REFERENCES

(1) Arias-Rotondo, D. M. The Fruit Fly of Photophysics. *Nat. Chem.* **2022**, *14* (6), 716.

(2) Scattolini, G.; Rosichini, A.; Kaul, N. The Many Lives of $[Ru(Bpy)_3]^{2+}$: A Historical Perspective. *Inorg. Chem.* **2025**, *64* (47), 23133−23148.
(3) Juris, A.; Balzani, V.; Barigelletti, F.; Campagna, S.; Belser, P.; von Zelewsky, A. Ru(II) Polypyridine Complexes: Photophysics, Photochemistry, Eletrochemistry, and Chemiluminescence. *Coord. Chem. Rev.* **1988**, *84*, 85−277.
(4) Barigelletti, F.; Juris, A.; Balzani, V.; Belser, P.; Von Zelewsky, A. Excited-State Properties of Complexes of the Tris(Diimine)-Ruthenium(2+) Ion Family. *Inorg. Chem.* **1983**, *22* (22), 3335−3339.
(5) De Armond, M. K.; Myrick, M. L. The Life and Times of $[Ru(Bpy)_3]^{2+}$: Localized Orbitals and Other Strange Occurrences. *Acc. Chem. Res.* **1989**, *22* (10), 364−370.
(6) Thompson, D. W.; Ito, A.; Meyer, T. J. $[Ru(bpy)_3]^{2+*}$ and other remarkable metal-to-ligand charge transfer (MLCT) excited states. *Pure Appl. Chem.* **2013**, *85* (7), 1257−1305.
(7) Arias-Rotondo, D. M.; McCusker, J. K. The Photophysics of Photoredox Catalysis: A Roadmap for Catalyst Design. *Chem. Soc. Rev.* **2016**, *45* (21), 5803−5820.
(8) Müller, P.; Brettel, K. $Ru(Bpy)_3^{2+}$ as a Reference in Transient Absorption Spectroscopy: Differential Absorption Coefficients for Formation of the Long-Lived ^{3}MLCT Excited State. *Photochem. Photobiol. Sci.* **2012**, *11* (4), 632−636.
(9) Suzuki, K.; Kobayashi, A.; Kaneko, S.; Takehira, K.; Yoshihara, T.; Ishida, H.; Shiina, Y.; Oishi, S.; Tobita, S. Reevaluation of Absolute Luminescence Quantum Yields of Standard Solutions Using a Spectrometer with an Integrating Sphere and a Back-Thinned CCD Detector. *Phys. Chem. Chem. Phys.* **2009**, *11* (42), 9850−9860.
(10) Arias-Rotondo, D. M.; McCusker, J. K. An Overview of the Physical and Photophysical Properties of $[Ru(Bpy)_3]^{2+}$. In *Visible Light Photocatalysis in Organic Chemistry*; Stephenson, C.; Yoon, T.; MacMillan, D. W. C., Eds.; Wiley-VCH: Weinheim, Germany, 2018; pp 1−24.
(11) Bolton, E.; Richter, M. M. Chemiluminescence of Tris(2,2'-Bipyridyl)Ruthenium(II): A Glowing Experience. *J. Chem. Educ.* **2001**, *78* (1), 47−48.
(12) Yu, J.; Stankovic, D.; Vidic, J.; Sojic, N. Recent Advances in Electrochemiluminescence Immunosensing. *Sensors & Diagnostics* **2024**, *3* (12), 1887−1898.
(13) Kalyanasundaram, K. Photophysics, Photochemistry and Solar Energy Conversion with Tris(Bipyridyl)Ruthenium(II) and Its Analogues. *Coord. Chem. Rev.* **1982**, *46*, 159−244.
(14) Muñoz-García, A. B.; Benesperi, I.; Boschloo, G.; Concepcion, J. J.; Delcamp, J. H.; Gibson, E. A.; Meyer, G. J.; Pavone, M.; Pettersson, H.; Hagfeldt, A.; Freitag, M. Dye-Sensitized Solar Cells Strike Back. *Chem. Soc. Rev.* **2021**, *50* (22), 12450−12550.
(15) Kirsch-De Mesmaeker, A.; Rochus-Dewitt, M.; Nasielski, J. Photoelectrochemical Transients Induced by Pulsed Laser Illumination of the Tin Dioxide/Tris(2,2'-Bipyridine)Ruthenium(II) Solution Interface at Different pH's. *J. Phys. Chem.* **1986**, *90* (25), 6657−6662.
(16) Brennaman, M. K.; Dillon, R. J.; Alibabaei, L.; Gish, M. K.; Dares, C. J.; Ashford, D. L.; House, R. L.; Meyer, G. J.; Papanikolas, J. M.; Meyer, T. J. Finding the Way to Solar Fuels with Dye-Sensitized Photoelectrosynthesis Cells. *J. Am. Chem. Soc.* **2016**, *138* (40), 13085−13102.
(17) Kuciauskas, D.; Freund, M. S.; Gray, H. B.; Winkler, J. R.; Lewis, N. S. Electron Transfer Dynamics in Nanocrystalline Titanium Dioxide Solar Cells Sensitized with Ruthenium or Osmium Polypyridyl Complexes. *J. Phys. Chem. B* **2001**, *105* (2), 392−403.
(18) Roundhill, D. M. Photochemistry, Photophysics, and Photoredox Reactions of Ru(Bpy) 3 2+ and Related Complexes. In *Photochemistry and Photophysics of Metal Complexes*; Roundhill, D. M., Ed.; Springer: Boston, 1994; pp 165−215.
(19) Jiménez-Hernández, M. E.; Manjón, F.; García-Fresnadillo, D.; Orellana, G. Solar Water Disinfection by Singlet Oxygen Photogenerated with Polymer-Supported Ru(II) Sensitizers. *Sol. Energy* **2006**, *80* (10), 1382−1387.
(20) Kitzmann, W. R.; Heinze, K. Charge-Transfer and Spin-Flip States: Thriving as Complements. *Angew. Chem., Int. Ed.* **2023**, *62* (15), No. e202213207.
(21) Eastham, K.; Scattergood, P. A.; Chu, D.; Boota, R. Z.; Soupart, A.; Alary, F.; Dixon, I. M.; Rice, C. R.; Hardman, S. J. O.; Elliott, P. I. P. Not All ^{3}MC States Are the Same: The Role of $^3MC_{cis}$ States in the Photochemical N∧N Ligand Release from $[Ru(Bpy)_2(N\wedge N)]^{2+}$ Complexes. *Inorg. Chem.* **2022**, *61* (49), 19907−19924.
(22) Soupart, A.; Alary, F.; Heully, J.-L.; Elliott, P. I. P.; Dixon, I. M. Theoretical Study of the Full Photosolvolysis Mechanism of $Ru(Bpy)_3^{2+}$: Providing a General Mechanistic Roadmap for the Photochemistry of $Ru(\hat{N}N)_3^{2+}$-Type Complexes toward Both Cis and Trans Photoproducts. *Inorg. Chem.* **2020**, *59* (20), 14679−14695.
(23) Soupart, A.; Alary, F.; Heully, J.-L.; Elliott, P. I. P.; Dixon, I. M. Recent Progress in Ligand Photorelease Reaction Mechanisms: Theoretical Insights Focusing on Ru(II) ^{3}MC States. *Coord. Chem. Rev.* **2020**, *408*, No. 213184.
(24) Wenger, O. S. Is Iron the New Ruthenium? *Chem.—Eur. J.* **2019**, *25* (24), 6043−6052.
(25) Harriman, A.; Izzet, G. Direct Observation of the Fourth MLCT Triplet State in Ruthenium(II) Tris(2,2′-Bipyridine). *Phys. Chem. Chem. Phys.* **2007**, *9* (8), 944−948.
(26) Lumpkin, R. S.; Kober, E. M.; Worl, L. A.; Murtaza, Z.; Meyer, T. J. Metal-to-Ligand Charge-Transfer (MLCT) Photochemistry: Experimental Evidence for the Participation of a Higher Lying MLCT State in Polypyridyl Complexes of Ruthenium(II) and Osmium(II). *J. Phys. Chem.* **1990**, *94* (1), 239−243.
(27) Harrigan, R. W.; Hager, G. D.; Crosby, G. A. Evidence for Multiple-State Emission from Ruthenium(II) Complexes. *Chem. Phys. Lett.* **1973**, *21* (3), 487−490.
(28) Soupart, A.; Alary, F.; Heully, J.-L.; Elliott, P. I. P.; Dixon, I. M. Exploration of Uncharted ^{3}PES Territory for $Ru(Bpy)_3^{2+}$: A New ^{3}MC Minimum Prone to Ligand Loss Photochemistry. *Inorg. Chem.* **2018**, *57* (6), 3192−3196.
(29) Hernández-Castillo, D.; Nau, R. E. P.; Schmid, M.-A.; Tschierlei, S.; Rau, S.; González, L. Multiple Triplet Metal-Centered Jahn-Teller Isomers Determine Temperature-Dependent Luminescence Lifetimes in $[Ru(Bpy)_3]^{2+}$. *Angew. Chem., Int. Ed.* **2023**, *62* (48), No. e202308803.
(30) Dongare, P.; Myron, B. D. B.; Wang, L.; Thompson, D. W.; Meyer, T. J. [Ru(Bpy)3]2+* Revisited. Is It Localized or Delocalized? How Does It Decay? *Coord. Chem. Rev.* **2017**, *345*, 86−107.
(31) Sakizadeh, J. D.; Weiss, R.; Scholes, G. D.; Kudisch, B. Ultrafast Spectroscopy and Dynamics of Photoredox Catalysis. *Annu. Rev. Phys. Chem.* **2025**, *76*, 203−229.
(32) Ryland, E. S.; Yang, X.; Garratt, D.; Henke, W. C.; Kahraman, A.; Taub, M.; Sachs, M.; Biasin, E.; Hampton, C. Y.; Hoffman, D. J.; Coslovich, G.; Kunnus, K.; Dakovski, G. L.; Mara, M. W.; Chen, L. X.; Mulfort, K. L.; Li, X.; Cordones, A. A. Revealing Parallel Inter- and Intra-Ligand Charge Transfer Dynamics in $[Ru(L)_2(Dppz)]^{2+}$ Molecular Lightswitch with N K-Edge X-Ray Absorption Spectroscopy. *Angew. Chem., Int. Ed.* **2025**, *64* (36), No. e202509496.
(33) Jay, R. M.; Eckert, S.; Van Kuiken, B. E.; Ochmann, M.; Hantschmann, M.; Cordones, A. A.; Cho, H.; Hong, K.; Ma, R.; Lee, J. H.; Dakovski, G. L.; Turner, J. J.; Minitti, M. P.; Quevedo, W.; Pietzsch, A.; Beye, M.; Kim, T. K.; Schoenlein, R. W.; Wernet, P.; Föhlisch, A.; Huse, N. Following Metal-to-Ligand Charge-Transfer Dynamics with Ligand and Spin Specificity Using Femtosecond Resonant Inelastic X-Ray Scattering at the Nitrogen K-Edge. *J. Phys. Chem. Lett.* **2021**, *12* (28), 6676−6683.
(34) Gawelda, W.; Johnson, M.; De Groot, F. M. F.; Abela, R.; Bressler, C.; Chergui, M. Electronic and Molecular Structure of Photoexcited $[Ru^{II}(Bpy)_3]^{2+}$ Probed by Picosecond X-Ray Absorption Spectroscopy. *J. Am. Chem. Soc.* **2006**, *128* (15), 5001−5009.
(35) Chantry, N.; Cotic, A.; De Kreijger, S.; Di Forti, R.; Elias, B.; Troian-Gautier, L.; Cadranel, A. Nature of Anti-Dissipative High-Energy Excited States in Quaterpyridine-Bridged Ruthenium Complexes. *Angew. Chem. Int. Ed* **2025**, *64* (33), No. e202507738.

https://doi.org/10.1021/acs.inorgchem.6c00560
Inorg. Chem. 2026, 65, 7549−7577

(36) Cotic, A.; Cerfontaine, S.; Slep, L. D.; Elias, B.; Troian-Gautier, L.; Cadranel, A. Anti-Dissipative Strategies toward More Efficient Solar Energy Conversion. *J. Am. Chem. Soc.* **2023**, *145* (9), 5163−5173.
(37) Cotic, A.; Cerfontaine, S.; Slep, L. D.; Elias, B.; Troian-Gautier, L.; Cadranel, A. A Photoinduced Mixed Valence Photoswitch. *Phys. Chem. Chem. Phys.* **2022**, *24* (24), 15121−15128.
(38) Cerfontaine, S.; Troian-Gautier, L.; Duez, Q.; Cornil, J.; Gerbaux, P.; Elias, B. MLCT Excited-State Behavior of Trinuclear Ruthenium(II) 2,2′-Bipyridine Complexes. *Inorg. Chem.* **2021**, *60* (1), 366−379.
(39) Cerfontaine, S.; Wehlin, S. A. M.; Elias, B.; Troian-Gautier, L. Photostable Polynuclear Ruthenium(II) Photosensitizers Competent for Dehalogenation Photoredox Catalysis at 590 Nm. *J. Am. Chem. Soc.* **2020**, *142* (12), 5549−5555.
(40) Cerfontaine, S.; Troian-Gautier, L.; Wehlin, S. A. M.; Loiseau, F.; Cauët, E.; Elias, B. Tuning the Excited-State Deactivation Pathways of Dinuclear Ruthenium(II) 2,2′-Bipyridine Complexes through Bridging Ligand Design. *Dalton Trans.* **2020**, *49* (24), 8096−8106.
(41) Langer, M.; Mengele, A. K.; Müller, R.; Wetzel, J. C.; Mayer, J.; Rau, S.; Streb, C. In Situ Formation of an Active Oxygen Evolution Catalyst *via* Photodegradation of $[Ru(Bpy)_3]^{2+}$. *Dalton Trans.* **2025**, *54* (12), 4861−4865.
(42) Schmitz, M.; Naumann, R.; Heinze, K.; Kerzig, C. Efficient Red Light−Driven Singlet Oxygen Photocatalysis with an Osmium-Based Coulombic Dyad. *Angew. Chem., Int. Ed.* **2025**, *64* (35), No. e202502840.
(43) Schmitz, M.; Bertrams, M.-S.; Sell, A. C.; Glaser, F.; Kerzig, C. Efficient Energy and Electron Transfer Photocatalysis with a Coulombic Dyad. *J. Am. Chem. Soc.* **2024**, *146* (37), 25799−25812.
(44) Glaser, F.; Schmitz, M.; Kerzig, C. Coulomb Interactions for Mediator-Enhanced Sensitized Triplet−Triplet Annihilation Upconversion in Solution. *Nanoscale* **2023**, *16* (1), 123−137.
(45) Pfeffer, M. G.; Müller, C.; Kastl, E. T. E.; Mengele, A. K.; Bagemihl, B.; Fauth, S. S.; Habermehl, J.; Petermann, L.; Wächtler, M.; Schulz, M.; Chartrand, D.; Laverdière, F.; Seeber, P.; Kupfer, S.; Gräfe, S.; Hanan, G. S.; Vos, J. G.; Dietzek-Ivanšić, B.; Rau, S. Active Repair of a Dinuclear Photocatalyst for Visible-Light-Driven Hydrogen Production. *Nat. Chem.* **2022**, *14* (5), 500−506.
(46) Amthor, S.; Knoll, S.; Heiland, M.; Zedler, L.; Li, C.; Nauroozi, D.; Tobaschus, W.; Mengele, A. K.; Anjass, M.; Schubert, U. S.; Dietzek-Ivanšić, B.; Rau, S.; Streb, C. A Photosensitizer−Polyoxometalate Dyad That Enables the Decoupling of Light and Dark Reactions for Delayed on-Demand Solar Hydrogen Production. *Nat. Chem.* **2022**, *14* (3), 321−327.
(47) Han, W.-K.; Liu, Y.; Yan, X.; Jiang, Y.; Zhang, J.; Gu, Z.-G. Integrating Light-Harvesting Ruthenium(II)-Based Units into Three-Dimensional Metal Covalent Organic Frameworks for Photocatalytic Hydrogen Evolution. *Angew. Chem., Int. Ed.* **2022**, *61* (40), No. e202208791.
(48) Çeper, T.; Nabiyan, A.; Neumann, C.; Turchanin, A.; Schacher, F. H. Visible-Light-Driven Hydrogen Evolution of PtNP/$[Ru(Bpy)_3]^{2+}$/Polyampholyte Hybrid Hydrogels. *ACS Appl. Polym. Mater.* **2023**, *5* (8), 6493−6503.
(49) Wang, C.-A.; Han, Y.-F.; Nie, K.; Li, Y.-W. Porous Organic Frameworks with Mesopores and $[Ru(Bpy)_3]^{2+}$ Ligand Built-in as a Highly Efficient Visible-Light Heterogeneous Photocatalyst. *Mater. Chem. Front.* **2019**, *3* (9), 1909−1917.
(50) Romanenko, I.; Rajagopal, A.; Neumann, C.; Turchanin, A.; Streb, C.; Schacher, F. H. Embedding Molecular Photosensitizers and Catalysts in Nanoporous Block Copolymer Membranes for Visible-Light Driven Hydrogen Evolution. *J. Mater. Chem. A* **2020**, *8* (13), 6238−6244.
(51) Kund, J.; Kruse, J.-H.; Gruber, A.; Trentin, I.; Langer, M.; Read, C.; Neusser, G.; Blaimer, D.; Rupp, U.; Streb, C.; Leopold, K.; Schacher, F. H.; Kranz, C. Multimodal Analysis of Light-Driven Water Oxidation in Nanoporous Block Copolymer Membranes. *Angew. Chem., Int. Ed.* **2023**, *62* (22), No. e202217196.
(52) Guo, Z.; Dong, S. Electrogenerated Chemiluminescence from $Ru(Bpy)_3^{2+}$ Ion-Exchanged in Carbon Nanotube/Perfluorosulfonated Ionomer Composite Films. *Anal. Chem.* **2004**, *76* (10), 2683−2688.
(53) Farnum, B. H.; Morseth, Z. A.; Lapides, A. M.; Rieth, A. J.; Hoertz, P. G.; Brennaman, M. K.; Papanikolas, J. M.; Meyer, T. J. Photoinduced Interfacial Electron Transfer within a Mesoporous Transparent Conducting Oxide Film. *J. Am. Chem. Soc.* **2014**, *136* (6), 2208−2211.
(54) Farnum, B. H.; Nakada, A.; Ishitani, O.; Meyer, T. J. Bias-Dependent Oxidative or Reductive Quenching of a Molecular Excited-State Assembly Bound to a Transparent Conductive Oxide. *J. Phys. Chem. C* **2015**, *119* (45), 25180−25187.
(55) Cesana, P. T.; Li, B. X.; Shepard, S. G.; Ting, S. I.; Hart, S. M.; Olson, C. M.; Martinez Alvarado, J. I.; Son, M.; Steiman, T. J.; Castellano, F. N.; Doyle, A. G.; MacMillan, D. W. C.; Schlau-Cohen, G. S. A Biohybrid Strategy for Enabling Photoredox Catalysis with Low-Energy Light. *Chem.* **2022**, *8* (1), 174−185.
(56) Amara, Z.; Zimberlin, P.; Atakpa, A. P.; Al Ayi, Y.; Lancel, M. More than Catalyst Recycling: Tuning Synthetic Photocatalytic Processes via Heterogenization on Silica and Alumina. *ACS Org. Inorg. Au* **2026**, *6* (1), 8−22.
(57) Farney, E. P.; Chapman, S. J.; Swords, W. B.; Torelli, M. D.; Hamers, R. J.; Yoon, T. P. Discovery and Elucidation of Counteranion Dependence in Photoredox Catalysis. *J. Am. Chem. Soc.* **2019**, *141* (15), 6385−6391.
(58) Earley, J. D.; Zieleniewska, A.; Ripberger, H. H.; Shin, N. Y.; Lazorski, M. S.; Mast, Z. J.; Sayre, H. J.; McCusker, J. K.; Scholes, G. D.; Knowles, R. R.; Reid, O. G.; Rumbles, G. Ion-Pair Reorganization Regulates Reactivity in Photoredox Catalysts. *Nat. Chem.* **2022**, *14* (7), 746−753.
(59) Zanzi, J.; Pastorel, Z.; Duhayon, C.; Lognon, E.; Coudret, C.; Monari, A.; Dixon, I. M.; Canac, Y.; Smietana, M.; Baslé, O. Counterion Effects in $[Ru(Bpy)_3](X)_2$-Photocatalyzed Energy Transfer Reactions. *JACS Au* **2024**, *4* (8), 3049−3057.
(60) Ghosh, A.; Holmes, D.; McCusker, J. K. Probing the Influence of Ion-Pairing on Ligand-Field Excited-State Dynamics. *Chem. Sci.* **2025**, *16* (35), 16110−16120.
(61) Troian-Gautier, L.; Marcélis, L.; Winter, J. D.; Gerbaux, P.; Moucheron, C. Two Ruthenium Complexes Capable of Storing Multiple Electrons on a Single Ligand − Photophysical, Photochemical and Electrochemical Properties of $[Ru(Phen)_2(TAPHAT)]^{2+}$ and $[Ru(Phen)_2(TAPHAT)Ru(Phen)_2]^{4+}$. *Dalton Trans.* **2017**, *46* (44), 15287−15300.
(62) Hoff, D. A.; Silva, R.; Rego, L. G. C. Subpicosecond Dynamics of Metal-to-Ligand Charge-Transfer Excited States in Solvated $[Ru(Bpy)_3]^{2+}$ Complexes. *J. Phys. Chem. C* **2011**, *115* (31), 15617−15626.
(63) Sun, Y.; Turro, C. Highly Solvent Dependent Luminescence from $[Ru(Bpy)_n(Dppp_2)_{3-n}]^{2+}$ (n = 0−2). *Inorg. Chem.* **2010**, *49* (11), 5025−5032.
(64) Stark, C. W.; Trummal, A.; Uudsemaa, M.; Pahapill, J.; Rammo, M.; Petritsenko, K.; Sildoja, M.-M.; Rebane, A. Solute-Solvent Electronic Interaction Is Responsible for Initial Charge Separation in Ruthenium Complexes $[Ru(Bpy)_3]^{2+}$ and $[Ru(Phen)_3]^{2+}$. *Commun. Chem.* **2019**, *2* (1), 108.
(65) Brennaman, M. K.; Meyer, T. J.; Papanikolas, J. M. $[Ru(Bpy)_2Dppz]^{2+}$ Light-Switch Mechanism in Protic Solvents as Studied through Temperature-Dependent Lifetime Measurements. *J. Phys. Chem. A* **2004**, *108* (45), 9938−9944.
(66) Caspar, J. V.; Meyer, T. J. Photochemistry of Tris(2,2'-Bipyridine)Ruthenium(2+) Ion ($Ru(Bpy)_3^{2+}$). Solvent Effects. *J. Am. Chem. Soc.* **1983**, *105* (17), 5583−5590.
(67) de Buyl, F.; Kirsch-De Mesmaeker, A.; Tossi, A.; Kelly, J. M. Medium Dependence of the Spectroscopic and Photophysical Properties of $Ru(Bpy)_2(HAT)^{2+}$. The Effect of Solvent, pH and Binding to Polyelectrolytes. *J. Photochem. Photobiol. A Chem.* **1991**, *60* (1), 27−45.
(68) Jing, Z.; Liu, S.; Zhang, X.; Hong, Y.; Ma, P.; Wang, J.; Niu, J. $[Ru(Bpy)_3]^{2+}$ Derivatives-Incorporated POM@MOFs with Good

https://doi.org/10.1021/acs.inorgchem.6c00560
Inorg. Chem. 2026, 65, 7549−7577

Photocatalytic Activity for Visible-Light-Driven Oxidative Coupling of Amines to Imines. *Inorg. Chem.* **2025**, *64* (15), 7832−7840.
(69) Vaidyalingam, A.; Dutta, P. K. Analysis of the Photodecomposition Products of $Ru(Bpy)_3^{2+}$ in Various Buffers and upon Zeolite Encapsulation. *Anal. Chem.* **2000**, *72* (21), 5219−5224.
(70) Wang, J.; Zhou, S.; Li, B.; Liu, X.; Chen, H.; Wang, H. Improving the Photostability of $[Ru(Bpy)_3]^{2+}$ by Embedment in Silica. *ChemPhotoChem.* **2022**, *6* (10), No. e202200124.
(71) Bourgois, C.; Troian-Gautier, L.; Kitzmann, W. R. Live and Let Dye: The Ongoing Story of $[Ru(Bpy)_3]^{2+}$. *ChemRxiv* **2026**. (accessed 2026−01−28)
(72) Dorn, M.; East, N. R.; Förster, C.; Kitzmann, W. R.; Moll, J.; Reichenauer, F.; Reuter, T.; Stein, L.; Heinze, K. D-d and Charge Transfer Photochemistry of 3d Metal Complexes. In *Comprehensive Inorganic Chemistry III*; Reedijk, J., Ed.; Elsevier: San Diego, 2022.
(73) van Houten, J.; Watts, R. J. Temperature Dependence of the Photophysical and Photochemical Properties of the Tris(2,2'-Bipyridyl)Ruthenium(II) Ion in Aqueous Solution. *J. Am. Chem. Soc.* **1976**, *98* (16), 4853−4858.
(74) Caspar, J. V.; Meyer, T. J. Application of the Energy Gap Law to Nonradiative, Excited-State Decay. *J. Phys. Chem.* **1983**, *87* (6), 952−957.
(75) Kitzmann, W. R.; Bertrams, M.-S.; Boden, P.; Fischer, A. C.; Klauer, R.; Sutter, J.; Naumann, R.; Förster, C.; Niedner-Schatteburg, G.; Bings, N. H.; Hunger, J.; Kerzig, C.; Heinze, K. Stable Molybdenum(0) Carbonyl Complex for Upconversion and Photoredox Catalysis. *J. Am. Chem. Soc.* **2023**, *145* (30), 16597−16609.
(76) Steinke, S. J.; Piechota, E. J.; Loftus, L. M.; Turro, C. Acetonitrile Ligand Photosubstitution in Ru(II) Complexes Directly from the ^{3}MLCT State. *J. Am. Chem. Soc.* **2022**, *144* (44), 20177−20182.
(77) Hummel, K.; Gupta, S.; Marques Silva, A.; Garcia, S. P.; Odhiambo, D. H.; Sygit, D.; Cai, J.; Ward, C.; Kocarek, T.; Sokolov, A. Yu.; Turro, C.; Kodanko, J. J. Cytochrome P450 Induction through the Efficient Photoinduced Release of a Pyridine-Substituted Agent from Ru(II). *J. Am. Chem. Soc.* **2025**, *147* (39), 35198−35202.
(78) Husiev, Y.; Götzfried, S. K.; Hakkennes, M. L. A.; Kotova, D.; Tutein Nolthenius, I.; van de Griend, C.; Johns, A. C.; Abyar, S.; Siegler, M. A.; Kornienko, A.; Bonnet, S. A Sterically Open Ruthenium-Based Photocage Activated by Red and Far-Red Light for a Wide Range of Drugs. *J. Am. Chem. Soc.* **2025**, *147* (48), 44356−44371.
(79) Hakkennes, M. L. A.; Regeni, I.; Husiev, Y.; Andreeva, V. D.; Siegler, M. A.; Buda, F.; Bonnet, S. Structure over States: Planarity, Not Energy, Dictates Photoactivation in Ru(II) PACT Agents. *J. Am. Chem. Soc.* **2025**, *147* (39), 35767−35787.
(80) Busemann, A.; Rieger, L.; Cunningham, R. M.; Davidse, S. C.; Regeni, I.; Flaspohler, I.; Schmidt, C.; Zhou, X.-Q.; van Rixel, V.; Siegler, M. A.; Ott, I.; Le Dévédec, S. E.; Wagenknecht, H.-A.; DeRose, V. J.; Bonnet, S. Visualizing the Invisible: Dual Click Imaging of Ruthenium-Based Photoactivated Chemotherapy Agents and Their DNA Synthesis Inhibition in Fixed Cancer Cells. *J. Am. Chem. Soc.* **2025**, *147* (46), 42500−42510.
(81) Soupart, A.; Alary, F.; Heully, J.-L.; Dixon, I. M. On the Possible Coordination on a ^{3}MC State Itself? Mechanistic Investigation Using DFT-Based Methods. *Inorganics* **2020**, *8* (2), 15.
(82) Chan, A. Y.; Perry, I. B.; Bissonnette, N. B.; Buksh, B. F.; Edwards, G. A.; Frye, L. I.; Garry, O. L.; Lavagnino, M. N.; Li, B. X.; Liang, Y.; Mao, E.; Millet, A.; Oakley, J. V.; Reed, N. L.; Sakai, H. A.; Seath, C. P.; MacMillan, D. W. C. Metallaphotoredox: The Merger of Photoredox and Transition Metal Catalysis. *Chem. Rev.* **2022**, *122* (2), 1485−1542.
(83) Twilton, J.; Le, C.; Zhang, P.; Shaw, M. H.; Evans, R. W.; MacMillan, D. W. C. The Merger of Transition Metal and Photocatalysis. *Nat. Rev. Chem.* **2017**, *1* (7), No. 0052.
(84) Marzo, L.; Pagire, S. K.; Reiser, O.; König, B. Visible-Light Photocatalysis: Does It Make a Difference in Organic Synthesis? *Angew. Chem., Int. Ed.* **2018**, *57* (32), 10034−10072.
(85) Maurer, A. B.; Piechota, E. J.; Meyer, G. J. Excited-State Dipole Moments of Homoleptic $[Ru(Bpy')_3]^{2+}$ Complexes Measured by Stark Spectroscopy. *J. Phys. Chem. A* **2019**, *123* (41), 8745−8754.
(86) Maurer, A. B.; Meyer, G. J. Stark Spectroscopic Evidence That a Spin Change Accompanies Light Absorption in Transition Metal Polypyridyl Complexes. *J. Am. Chem. Soc.* **2020**, *142* (15), 6847−6851.
(87) De Kreijger, S.; Glaser, F.; Troian-Gautier, L. From Photons to Reactions: Key Concepts in Photoredox Catalysis. *Chem. Catalysis* **2024**, *4* (11), No. 101110.
(88) Shaw, M. H.; Twilton, J.; MacMillan, D. W. C. Photoredox Catalysis in Organic Chemistry. *J. Org. Chem.* **2016**, *81* (16), 6898−6926.
(89) Talbott, E. D.; Burnett, N. L.; Swierk, J. R. Mechanistic and Kinetic Studies of Visible Light Photoredox Reactions. *Chem. Phys. Rev.* **2023**, *4* (3), No. 031312.
(90) Glaser, F.; Kerzig, C.; Wenger, O. S. Multi-Photon Excitation in Photoredox Catalysis: Concepts, Applications, Methods. *Angew. Chem., Int. Ed.* **2020**, *59* (26), 10266−10284.
(91) Speight, I. R.; Ardila-Fierro, K. J.; Hernández, J. G.; Emmerling, F.; Michalchuk, A. A. L.; García, F.; Colacino, E.; Mack, J. Ball Milling for Mechanochemical Reactions. *Nat. Rev. Methods Primers* **2025**, *5* (1), 29.
(92) Ravetz, B. D.; Tay, N. E. S.; Joe, C. L.; Sezen-Edmonds, M.; Schmidt, M. A.; Tan, Y.; Janey, J. M.; Eastgate, M. D.; Rovis, T. Development of a Platform for Near-Infrared Photoredox Catalysis. *ACS Cent. Sci.* **2020**, *6* (11), 2053−2059.
(93) Horsewill, S. J.; Cao, C.; Dabney, N.; Yang, E. S.; Faulkner, S.; Scott, D. J. Isolation of the Elusive $[Ru(Bipy)_3]^+$: A Key Intermediate in Photoredox Catalysis. *Chem. Commun.* **2023**, *59* (99), 14665−14668.
(94) Byskov, C. S.; Weber, J. M.; Nielsen, S. B. Gas-Phase Spectroscopy of Singly Reduced Tris(Bipyridine)Ruthenium Ions, $Ru(Bipy)_3^+$. *Phys. Chem. Chem. Phys.* **2015**, *17* (8), 5561−5564.
(95) Goez, M.; Kerzig, C.; Naumann, R. An "All-Green" Catalytic Cycle of Aqueous Photoionization. *Angew. Chem., Int. Ed.* **2014**, *53* (37), 9914−9916.
(96) Xue, Y.; Sun, L.; Wang, Z.; Chao, D. Activating Purely Organic Molecules for Selective CO_2 Reduction through Photogeneration of Super-Reducing Species. *J. Mol. Struct.* **2026**, *1354*, No. 144862.
(97) Singh, P.; Lal, N.; Shaikh, A. C. Solvated Electrons: Dynamic Reductant in Visible Light Photoredox Catalysis. *Adv. Synth. Catal.* **2024**, *366* (9), 1906−1921.
(98) Yoo, B. I.; Kim, Y. J.; You, Y.; Yang, J. W.; Kim, S. W. Birch Reduction of Aromatic Compounds by Inorganic Electride $[Ca_2N]^{+\bullet}e^-$ in an Alcoholic Solvent: An Analogue of Solvated Electrons. *J. Org. Chem.* **2018**, *83* (22), 13847−13853.
(99) Wang, X.; Qiu, L.; Chen, Z.; Chen, H.; Wang, J.; Zhang, Y.; Xu, Y.; Kong, D.; Zhang, M.; Gu, C. New Insights into the Reductive Destruction of Per- and Polyfluoroalkyl Substances in Hydrated Electron-Based Systems. *Environ. Sci. Technol.* **2025**, *59* (11), 5786−5795.
(100) Biswas, S.; Yamijala, S. S. R. K. C.; Wong, B. M. Degradation of Per- and Polyfluoroalkyl Substances with Hydrated Electrons: A New Mechanism from First-Principles Calculations. *Environ. Sci. Technol.* **2022**, *56* (12), 8167−8175.
(101) Zimmerman, H. E. A Mechanistic Analysis of the Birch Reduction. *Acc. Chem. Res.* **2012**, *45* (2), 164−170.
(102) Tan, S.; Wang, R.; Wang, K.; Yang, Z.; Chen, Y.; Zhang, Y. Unravelling the Structure-Dependent Defluorination Mechanisms of per- and Polyfluoroalkyl Substances by Hydrated Electrons in UV/Sulfite. *Nat. Water* **2025**, *3* (6), 734−745.
(103) Goez, M.; von Ramin-Marro, D.; Othman Musa, M. H.; Schiewek, M. Photoionization of $[Ru(Bpy)_3]^{2+}$: A Catalytic Cycle with Water as Sacrificial Donor. *J. Phys. Chem. A* **2004**, *108* (6), 1090−1100.
(104) Naumann, R.; Kerzig, C.; Goez, M. Laboratory-Scale Photoredox Catalysis Using Hydrated Electrons Sustainably Gen-

https://doi.org/10.1021/acs.inorgchem.6c00560
Inorg. Chem. 2026, 65, 7549−7577

erated with a Single Green Laser. *Chem. Sci.* **2017**, *8* (11), 7510−7520.
(105) Kerzig, C.; Goez, M. Combining Energy and Electron Transfer in a Supramolecular Environment for the "Green" Generation and Utilization of Hydrated Electrons through Photoredox Catalysis. *Chem. Sci.* **2016**, *7* (6), 3862−3868.
(106) Naumann, R.; Lehmann, F.; Goez, M. Generating Hydrated Electrons for Chemical Syntheses by Using a Green Light-Emitting Diode (LED). *Angew. Chem., Int. Ed.* **2018**, *57* (4), 1078−1081.
(107) Naumann, R.; Goez, M. A Green-LED Driven Source of Hydrated Electrons Characterized from Microseconds to Hours and Applied to Cross-Couplings. *Chem.—Eur. J.* **2018**, *24* (39), 9833−9840.
(108) Naumann, R.; Lehmann, F.; Goez, M. Micellized Tris-(Bipyridine)Ruthenium Catalysts Affording Preparative Amounts of Hydrated Electrons with a Green Light-Emitting Diode. *Chem.—Eur. J.* **2018**, *24* (50), 13259−13269.
(109) Naumann, R.; Goez, M. First Micelle-Free Photoredox Catalytic Access to Hydrated Electrons for Syntheses and Remediations with a Visible LED or Even Sunlight. *Chem.—Eur. J.* **2018**, *24* (66), 17557−17567.
(110) Gomollón-Bel, F. Ten Chemical Innovations That Will Change Our World: IUPAC identifies emerging technologies in Chemistry with potential to make our planet more sustainable. *Chemistry International* **2019**, *41* (2), 12−17.
(111) Millward, F.; Zysman-Colman, E. Mechanophotocatalysis: A Generalizable Approach to Solvent-Minimized Photocatalytic Reactions for Organic Synthesis. *Angew. Chem., Int. Ed.* **2024**, *63* (13), No. e202316169.
(112) Briš, A.; Margetić, D.; Štrukil, V. Mechanochemical Ball Milling as an Emerging Tool in Chemical Recycling and Upcycling of Waste Polymers. *Green Chem.* **2025**, *27* (45), 14401−14435.
(113) Millward, F.; Zysman-Colman, E. Mechanometallaphotoredox Catalysis: Utilizing Increased Throughput Mechanochemistry to Develop Solvent-Minimized Aryl Amination and $C(Sp^2)$-$C(Sp^3)$ Cross-Coupling Reactions with Increased Tolerance to Aerobic Conditions. *J. Am. Chem. Soc.* **2025**, *147* (26), 22919−22931.
(114) Stolle, A.; Szuppa, T.; Leonhardt, S. E. S.; Ondruschka, B. Ball Milling in Organic Synthesis: Solutions and Challenges. *Chem. Soc. Rev.* **2011**, *40* (5), 2317−2329.
(115) Pattanayak, P.; Saha, S.; Chatterjee, T.; Ranu, B. C. Sustainable and Solvent-Free Synthesis of Molecules of Pharmaceutical Importance by Ball Milling. *Chem. Commun.* **2025**, *61* (2), 247−265.
(116) Beillard, A.; Bantreil, X.; Métro, T.-X.; Martinez, J.; Lamaty, F. Alternative Technologies That Facilitate Access to Discrete Metal Complexes. *Chem. Rev.* **2019**, *119* (12), 7529−7609.
(117) Lukin, S.; Užarević, K.; Halasz, I. Raman Spectroscopy for Real-Time and in Situ Monitoring of Mechanochemical Milling Reactions. *Nat. Protoc.* **2021**, *16* (7), 3492−3521.
(118) Lukin, S.; Germann, L. S.; Friščić, T.; Halasz, I. Toward Mechanistic Understanding of Mechanochemical Reactions Using Real-Time In Situ Monitoring. *Acc. Chem. Res.* **2022**, *55* (9), 1262−1277.
(119) Gracin, D.; Štrukil, V.; Friščić, T.; Halasz, I.; Užarević, K. Laboratory Real-Time and In Situ Monitoring of Mechanochemical Milling Reactions by Raman Spectroscopy. *Angew. Chem., Int. Ed.* **2014**, *53* (24), 6193−6197.
(120) Ban, V.; Sadikin, Y.; Lange, M.; Tumanov, N.; Filinchuk, Y.; Černý, R.; Casati, N. Innovative in Situ Ball Mill for X-Ray Diffraction. *Anal. Chem.* **2017**, *89* (24), 13176−13181.
(121) Halasz, I.; Kimber, S. A. J.; Beldon, P. J.; Belenguer, A. M.; Adams, F.; Honkimäki, V.; Nightingale, R. C.; Dinnebier, R. E.; Friščić, T. In Situ and Real-Time Monitoring of Mechanochemical Milling Reactions Using Synchrotron X-Ray Diffraction. *Nat. Protoc.* **2013**, *8* (9), 1718−1729.
(122) Luttringer, F.; Lavayssiere, M.; Rastoder, E.; Salov, N.; Gravelet, T.; Quintin, F.; Pinaud, J.; Lamaty, F.; Bantreil, X. Mechanosynthesis of Ruthenium Trisbipyridyl Complexes and Application in Photoredox Catalysis in a Ball-Mill. *RSC Mechanochem.* **2025**, *2* (1), 108−115.
(123) Rastoder, E.; Michel, T.; Lamaty, F.; Bantreil, X. Ball-Milling for Efficient Synthesis of Pyridine-Containing Iron(II) Photosensitizers. *RSC Mechanochem.* **2024**, *1* (1), 116−122.
(124) Štrukil, V.; Sajko, I. Mechanochemically-Assisted Solid-State Photocatalysis (MASSPC). *Chem. Commun.* **2017**, *53* (65), 9101−9104.
(125) Munir, T.; Aneggi, E.; Baratta, W.; Genesin, L.; Zuccaccia, D.; Trigatti, F. Rapid and Efficient Solid-State Mechanosynthesis of Bipyridine Metal Complexes. *Chem.—Eur. J.* **2025**, *31* (38), No. e202501214.
(126) Glaser, F.; De Kreijger, S.; Achilleos, K.; Satheesh, L. N.; Ripak, A.; Chantry, N.; Bourgois, C.; Quiquempoix, S.; Scriven, J.; Rubens, J.; Vander Wee-Léonard, M.; Daenen, M.; Gillard, M.; Elias, B.; Troian-Gautier, L. A Compendium of Methodically Determined Ground- and Excited-State Properties of Homoleptic Ruthenium(II) and Osmium(II) Photosensitizers. *ChemPhotoChem.* **2024**, *8* (12), No. e202400134.
(127) Fantacci, S.; Ronca, E.; De Angelis, F. Impact of Spin−Orbit Coupling on Photocurrent Generation in Ruthenium Dye-Sensitized Solar Cells. *J. Phys. Chem. Lett.* **2014**, *5* (2), 375−380.
(128) Juwita, R.; Liao, J.-M.; Chen, C.-Y.; Tsai, H.-H. G. Enhancing Near-Infrared Absorption in Terpyridyl Ru/Os Complexes with Ancillary Ligands to Activate Spin-Forbidden Transitions in Dye-Sensitized Solar Cells: A TDDFT Investigation. *J. Phys. Chem. A* **2024**, *128* (5), 880−894.
(129) Robertson, N. Optimizing Dyes for Dye-Sensitized Solar Cells. *Angew. Chem., Int. Ed.* **2006**, *45* (15), 2338−2345.
(130) Kinoshita, T.; Fujisawa, J.; Nakazaki, J.; Uchida, S.; Kubo, T.; Segawa, H. Enhancement of Near-IR Photoelectric Conversion in Dye-Sensitized Solar Cells Using an Osmium Sensitizer with Strong Spin-Forbidden Transition. *J. Phys. Chem. Lett.* **2012**, *3* (3), 394−398.
(131) Bednářová, E.; Grotjahn, R.; Lin, C.; Xie, K. A.; Karube, Y.; Owen, J. S.; Joe, C. L.; Lainhart, B. C.; Sherwood, T. C.; Rovis, T. From Structure to Function: Designing Iridium Catalysts with Spin-Forbidden Excitation for Low-Energy Light-Driven Reactions. *J. Am. Chem. Soc.* **2025**, *147* (15), 12511−12522.
(132) Chacktas, G.; Pfund, B.; Kerackian, T.; Yaltseva, P.; Villeneuve, M.; Durand, D.; Fabre, N.; Fiorini-Debuisschert, C.; Cintrat, J.-C.; Wenger, O. S.; Romero, E. Evidence of Spin-Forbidden Excitation of $[Ru(Bpy)_3]^{2+}$ and Application in Red-Light-Driven Photocatalysis. *ACS Catal.* **2025**, *15* (16), 13938−13947.
(133) Mato, M.; Fernández-González, X.; D'Avino, C.; Tomás-Gamasa, M.; Mascareñas, J. L. Bioorthogonal Synthetic Chemistry Enabled by Visible-Light Photocatalysis. *Angew. Chem., Int. Ed.* **2024**, *63* (47), No. e202413506.
(134) Knutson, S. D.; Buksh, B. F.; Huth, S. W.; Morgan, D. C.; MacMillan, D. W. C. Current Advances in Photocatalytic Proximity Labeling. *Cell Chem. Biol.* **2024**, *31* (6), 1145−1161.
(135) Angerani, S.; Winssinger, N. Visible Light Photoredox Catalysis Using Ruthenium Complexes in Chemical Biology. *Chem.—Eur. J.* **2019**, *25* (27), 6661−6672.
(136) Fancy, D. A.; Kodadek, T. Chemistry for the Analysis of Protein−Protein Interactions: Rapid and Efficient Cross-Linking Triggered by Long Wavelength Light. *Proc. Natl. Acad. Sci. U.S.A.* **1999**, *96* (11), 6020−6024.
(137) Sato, S.; Morita, K.; Nakamura, H. Regulation of Target Protein Knockdown and Labeling Using Ligand-Directed $Ru(Bpy)_3$ Photocatalyst. *Bioconjugate Chem.* **2015**, *26* (2), 250−256.
(138) Nakane, K.; Sato, S.; Niwa, T.; Tsushima, M.; Tomoshige, S.; Taguchi, H.; Ishikawa, M.; Nakamura, H. Proximity Histidine Labeling by Umpolung Strategy Using Singlet Oxygen. *J. Am. Chem. Soc.* **2021**, *143* (20), 7726−7731.
(139) D'Avino, C.; Gutiérrez, S.; Feldhaus, M. J.; Tomás-Gamasa, M.; Mascareñas, J. L. Intracellular Synthesis of Indoles Enabled by Visible-Light Photocatalysis. *J. Am. Chem. Soc.* **2024**, *146* (5), 2895−2900.

https://doi.org/10.1021/acs.inorgchem.6c00560
Inorg. Chem. 2026, 65, 7549−7577

(140) Gao, Z.; Li, Y.; Xing, J.; Lu, Y.; Shao, Q.; Hu, J.; Zhao, S.; He, W.; Sun, B. Transition Metal Ru(II) Catalysts Immobilized Nanoreactors for Conditional Bioorthogonal Catalysis in Cells. *ACS Appl. Mater. Interfaces* **2024**, *16* (13), 15870−15878.
(141) Pieslinger, G. E.; Ramírez-Wierzbicki, I.; Cadranel, A. The Excited-State Creutz−Taube Ion. *Angew. Chem., Int. Ed.* **2022**, *61* (49), No. e202211747.
(142) Creutz, C.; Taube, H. Direct Approach to Measuring the Franck-Condon Barrier to Electron Transfer between Metal Ions. *J. Am. Chem. Soc.* **1969**, *91* (14), 3988−3989.
(143) Hu, K.; Blair, A. D.; Piechota, E. J.; Schauer, P. A.; Sampaio, R. N.; Parlane, F. G. L.; Meyer, G. J.; Berlinguette, C. P. Kinetic Pathway for Interfacial Electron Transfer from a Semiconductor to a Molecule. *Nat. Chem.* **2016**, *8* (9), 853−859.
(144) Piechota, E. J.; Sampaio, R. N.; Troian-Gautier, L.; Maurer, A. B.; Berlinguette, C. P.; Meyer, G. J. Entropic Barriers Determine Adiabatic Electron Transfer Equilibrium. *J. Phys. Chem. C* **2019**, *123* (6), 3416−3425.
(145) Sampaio, R. N.; Piechota, E. J.; Troian-Gautier, L.; Maurer, A. B.; Hu, K.; Schauer, P. A.; Blair, A. D.; Berlinguette, C. P.; Meyer, G. J. Kinetics Teach That Electronic Coupling Lowers the Free-Energy Change That Accompanies Electron Transfer. *Proc. Natl. Acad. Sci. U.S.A.* **2018**, *115* (28), 7248−7253.
(146) Piechota, E. J.; Troian-Gautier, L.; Sampaio, R. N.; Brennaman, M. K.; Hu, K.; Berlinguette, C. P.; Meyer, G. J. Optical Intramolecular Electron Transfer in Opposite Directions through the Same Bridge That Follows Different Pathways. *J. Am. Chem. Soc.* **2018**, *140* (23), 7176−7186.
(147) Rutherford, T. J.; Van Gijte, O.; Kirsch-De Mesmaeker, A.; Keene, F. R. Stereoisomers of Mono-, Di-, and Triruthenium(II) Complexes Containing the Bridging Ligand 1,4,5,8,9,12-Hexaazatriphenylene and Studies of Their Photophysical Properties. *Inorg. Chem.* **1997**, *36* (20), 4465−4474.
(148) Leveque, J.; Elias, B.; Moucheron, C.; Kirsch-De Mesmaeker, A. Dendritic Tetranuclear Ru(II) Complexes Based on the Nonsymmetrical PHEHAT Bridging Ligand and Their Building Blocks: Synthesis, Characterization, and Electrochemical and Photophysical Properties. *Inorg. Chem.* **2005**, *44* (2), 393−400.
(149) Kirsch-De Mesmaeker, A.; Moucheron, C.; Boutonnet, N. Mono- and Polynuclear Ruthenium(II) Complexes, Photo-Probes and Reagents for Targeted DNA Sites. *J. Phys. Org. Chem.* **1998**, *11* (8−9), 566−576.
(150) Weaver, T. R.; Meyer, T. J.; Adeyemi, S. A.; Brown, G. M.; Eckberg, R. P.; Hatfield, W. E.; Johnson, E. C.; Murray, R. W.; Untereker, D. Chemically Significant Interactions between Ruthenium Ions in Oxo-Bridged Complexes of Ruthenium(III). *J. Am. Chem. Soc.* **1975**, *97* (11), 3039−3048.
(151) Cadranel, A.; Oviedo, P. S.; Alborés, P.; Baraldo, L. M.; Guldi, D. M.; Hodak, J. H. Electronic Energy Transduction from $\{Ru(Py)_4\}$ Chromophores to Cr(III) Luminophores. *Inorg. Chem.* **2018**, *57* (6), 3042−3053.
(152) Oviedo, P. S.; Pieslinger, G. E.; Cadranel, A.; Baraldo, L. M. Exploring the Localized to Delocalized Transition in Non-Symmetric Bimetallic Ruthenium Polypyridines. *Dalton Trans.* **2017**, *46* (45), 15757−15768.
(153) Abate, P. O.; Juárez, V. M.; Baraldo, L. M. Coupling between Two Ru(Bda) Catalysts Bridged by a *Trans*-Dicyano Complex. *Dalton Trans.* **2024**, *53* (4), 1575−1585.
(154) Coe, B. J.; Meyer, T. J.; White, P. S. Cyano-Bridged Complexes of Trans-Tetrakis(Pyridine)Ruthenium(II). *Inorg. Chem.* **1995**, *34* (14), 3600−3609.
(155) Balzani, V.; Barigelletti, F.; Belser, P.; Bernhard, S.; De Cola, L.; Flamigni, L. Rigid Rodlike Dinuclear Ru/Os Complexes of a Novel Bridging Ligand. Intercomponent Energy and Electron-Transfer Processes. *J. Phys. Chem.* **1996**, *100* (42), 16786−16788.
(156) Campagna, S.; Denti, G.; Serroni, S.; Juris, A.; Venturi, M.; Ricevuto, V.; Balzani, V. Dendrimers of Nanometer Size Based on Metal Complexes: Luminescent and Redox-Active Polynuclear Metal Complexes Containing up to Twenty-Two Metal Centers. *Chem.—Eur. J.* **1995**, *1* (4), 211−221.
(157) Schoonover, J. R.; Bignozzi, C. A.; Meyer, T. J. Application of Transient Vibrational Spectroscopies to the Excited States of Metal Polypyridyl Complexes. *Coord. Chem. Rev.* **1997**, *165*, 239−266.
(158) Balzani, V.; Juris, A.; Venturi, M.; Campagna, S.; Serroni, S. Luminescent and Redox-Active Polynuclear Transition Metal Complexes. *Chem. Rev.* **1996**, *96* (2), 759−834.
(159) Gust, D.; Kramer, D.; Moore, A.; Moore, T. A.; Vermaas, W. Engineered and Artificial Photosynthesis: Human Ingenuity Enters the Game. *MRS Bull.* **2008**, *33* (4), 383−387.
(160) Cotic, A.; Veys, K.; Escudero, D.; Cadranel, A. Unusually High Energy Barriers for Internal Conversion in a $\{Ru(Bpy)\}$ Chromophore. *Phys. Chem. Chem. Phys.* **2022**, *24* (43), 26428−26437.
(161) Hankache, J.; Wenger, O. S. Photoinduced Electron Transfer in Covalent Ruthenium−Anthraquinone Dyads: Relative Importance of Driving-Force, Solvent Polarity, and Donor−Bridge Energy Gap. *Phys. Chem. Chem. Phys.* **2012**, *14* (8), 2685−2692.
(162) Bonn, A. G.; Yushchenko, O.; Vauthey, E.; Wenger, O. S. Photoinduced Electron Transfer in an Anthraquinone−$[Ru(Bpy)_3]^{2+}$−Oligotriarylamine−$[Ru(Bpy)_3]^{2+}$−Anthraquinone Pentad. *Inorg. Chem.* **2016**, *55* (6), 2894−2899.
(163) Opperman, K. A.; Mecklenburg, S. L.; Meyer, T. J. Intramolecular, Photoinduced Electron Transfer in Ruthenium(II) Bipyridine-Quinone Complexes. *Inorg. Chem.* **1994**, *33*, 5295−5301.
(164) Borgström, M.; Johansson, O.; Lomoth, R.; Baudin, H. B.; Wallin, S.; Sun, L.; Åkermark, B.; Hammarström, L. Electron Donor−Acceptor Dyads and Triads Based on Tris(Bipyridine)Ruthenium(II) and Benzoquinone: Synthesis, Characterization, and Photoinduced Electron Transfer Reactions. *Inorg. Chem.* **2003**, *42* (17), 5173−5184.
(165) Indelli, M. T.; Orlandi, M.; Chiorboli, C.; Ravaglia, M.; Scandola, F.; Lafolet, F.; Welter, S.; Cola, L. D. Electron Transfer Across Modular Oligo-*p*-Phenylene Bridges in $Ru(Bpy)_2(Bpy-Ph_n-DQ)^{4+}$ (n = 1−5) Dyads. Unusual Effects of Bridge Elongation. *J. Phys. Chem. A* **2012**, *116* (1), 119−131.
(166) Geisser, B.; Ponce, A.; Alsfasser, R. pH-Dependent Excited-State Dynamics of $[Ru(Bpy)_3]^{2+}$-Modified Amino Acids: Effects of an Amide Linkage and Remote Functional Groups. *Inorg. Chem.* **1999**, *38* (9), 2030−2037.
(167) Kise, K. J.; Bowler, B. E. A Ruthenium(II) Tris(Bipyridyl) Amino Acid: Synthesis and Direct Incorporation into an α-Helical Peptide by Solid-Phase Synthesis. *Inorg. Chem.* **2002**, *41* (2), 379−386.
(168) Geißer, B.; Alsfasser, R. A Peptide Approach to Covalently Linked $[Ru(Bipy)_3]^{2+}$−Ferrocene and $[Ru(Bipy)_3]^{2+}$−Tyrosine Conjugates. *Inorg. Chim. Acta* **2003**, *344*, 102−108.
(169) Luo, G.-F.; Biniuri, Y.; Chen, W.-H.; Neumann, E.; Fadeev, M.; Marjault, H.-B.; Bedi, A.; Gidron, O.; Nechushtai, R.; Stone, D.; Happe, T.; Willner, I. Artificial Photosynthesis with Electron Acceptor/Photosensitizer-Aptamer Conjugates. *Nano Lett.* **2019**, *19* (9), 6621−6628.
(170) Polese, A.; Mondini, S.; Bianco, A.; Toniolo, C.; Scorrano, G.; Guldi, D. M.; Maggini, M. Solvent-Dependent Intramolecular Electron Transfer in a Peptide-Linked $[Ru(Bpy)_3]^{2+}$−C_{60} Dyad. *J. Am. Chem. Soc.* **1999**, *121* (14), 3446−3452.
(171) Closs, G. L.; Miller, J. R. Intramolecular Long-Distance Electron Transfer in Organic Molecules. *Science* **1988**, *240* (4851), 440−447.
(172) Soltau, S. R.; Niklas, J.; Dahlberg, P. D.; Poluektov, O. G.; Tiede, D. M.; Mulfort, K. L.; Utschig, L. M. Aqueous Light Driven Hydrogen Production by a Ru−Ferredoxin−Co Biohybrid. *Chem. Commun.* **2015**, *51* (53), 10628−10631.
(173) Brändlin, M.; Pfund, B.; Wenger, O. S. Photoinduced Double Charge Accumulation in a Molecular Compound. *Nat. Chem.* **2025**, *17* (11), 1777−1784.
(174) Sampaio, R. N.; Troian-Gautier, L.; Meyer, G. J. A Charge-Separated State That Lives for Almost a Second at a Conductive

https://doi.org/10.1021/acs.inorgchem.6c00560
Inorg. Chem. 2026, 65, 7549−7577

Metal Oxide Interface. *Angew. Chem., Int. Ed.* **2018**, *57* (47), 15390−15394.
(175) Wang, Z.; Hu, Y.; Zhang, S.; Sun, Y. Artificial Photosynthesis Systems for Solar Energy Conversion and Storage: Platforms and Their Realities. *Chem. Soc. Rev.* **2022**, *51* (15), 6704−6737.
(176) Silver, S. C.; Niklas, J.; Du, P.; Poluektov, O. G.; Tiede, D. M.; Utschig, L. M. Protein Delivery of a Ni Catalyst to Photosystem I for Light-Driven Hydrogen Production. *J. Am. Chem. Soc.* **2013**, *135* (36), 13246−13249.
(177) Ozawa, H.; Haga, M.; Sakai, K. A Photo-Hydrogen-Evolving Molecular Device Driving Visible-Light-Induced EDTA-Reduction of Water into Molecular Hydrogen. *J. Am. Chem. Soc.* **2006**, *128* (15), 4926−4927.
(178) Sakai, K.; Ozawa, H. Homogeneous Catalysis of Platinum(II) Complexes in Photochemical Hydrogen Production from Water. *Coord. Chem. Rev.* **2007**, *251* (21), 2753−2766.
(179) Rau, S.; Walther, D.; Vos, J. G. Inspired by Nature: Light Driven Organometallic Catalysis by Heterooligonuclear Ru(II) Complexes. *Dalton Trans.* **2007**, *9*, 915−919.
(180) Rau, S.; Schäfer, B.; Gleich, D.; Anders, E.; Rudolph, M.; Friedrich, M.; Görls, H.; Henry, W.; Vos, J. G. A Supramolecular Photocatalyst for the Production of Hydrogen and the Selective Hydrogenation of Tolane. *Angew. Chem., Int. Ed.* **2006**, *45* (37), 6215−6218.
(181) Lei, P.; Hedlund, M.; Lomoth, R.; Rensmo, H.; Johansson, O.; Hammarström, L. The Role of Colloid Formation in the Photo-induced H_2 Production with a Ru^{II}−Pd^{II} Supramolecular Complex: A Study by GC, XPS, and TEM. *J. Am. Chem. Soc.* **2008**, *130* (1), 26−27.
(182) Pfeffer, M. G.; Schäfer, B.; Smolentsev, G.; Uhlig, J.; Nazarenko, E.; Guthmuller, J.; Kuhnt, C.; Wächtler, M.; Dietzek, B.; Sundström, V.; Rau, S. Palladium versus Platinum: The Metal in the Catalytic Center of a Molecular Photocatalyst Determines the Mechanism of the Hydrogen Production with Visible Light. *Angew. Chem., Int. Ed.* **2015**, *54* (17), 5044−5048.
(183) Kuss-Petermann, M.; Wenger, O. S. Electron Transfer Rate Maxima at Large Donor−Acceptor Distances. *J. Am. Chem. Soc.* **2016**, *138* (4), 1349−1358.
(184) Neumann, S.; Kerzig, C.; Wenger, O. S. Quantitative Insights into Charge-Separated States from One- and Two-Pulse Laser Experiments Relevant for Artificial Photosynthesis. *Chem. Sci.* **2019**, *10* (21), 5624−5633.
(185) Ha-Thi, M.-H.; Pham, V.-T.; Pino, T.; Maslova, V.; Quaranta, A.; Lefumeux, C.; Leibl, W.; Aukauloo, A. Photoinduced Electron Transfer in a Molecular Dyad by Nanosecond Pump−Pump−Probe Spectroscopy. *Photochem. Photobiol. Sci.* **2018**, *17* (7), 903−909.
(186) Flamigni, L.; Baranoff, E.; Collin, J.-P.; Sauvage, J.-P.; Ventura, B. Light Intensity Effects on Photoinduced Charge Separation Parameters in a Molecular Triad Based on an Iridium(III) Bis(Terpyridine) Unit. *ChemPhysChem* **2007**, *8* (13), 1943−1949.
(187) Wang, D.; Sampaio, R. N.; Troian-Gautier, L.; Marquard, S. L.; Farnum, B. H.; Sherman, B. D.; Sheridan, M. V.; Dares, C. J.; Meyer, G. J.; Meyer, T. J. Molecular Photoelectrode for Water Oxidation Inspired by Photosystem II. *J. Am. Chem. Soc.* **2019**, *141* (19), 7926−7933.
(188) Hanson, K.; Torelli, D. A.; Vannucci, A. K.; Brennaman, M. K.; Luo, H.; Alibabaei, L.; Song, W.; Ashford, D. L.; Norris, M. R.; Glasson, C. R. K.; Concepcion, J. J.; Meyer, T. J. Self-Assembled Bilayer Films of Ruthenium(II)/Polypyridyl Complexes through Layer-by-Layer Deposition on Nanostructured Metal Oxides. *Angew. Chem., Int. Ed.* **2012**, *51* (51), 12782−12785.
(189) Farnum, B. H.; Wee, K.-R.; Meyer, T. J. Self-Assembled Molecular p/n Junctions for Applications in Dye-Sensitized Solar Energy Conversion. *Nat. Chem.* **2016**, *8* (9), 845−852.
(190) Robb, A. J.; Knorr, E. S.; Watson, N.; Hanson, K. Metal Ion Linked Multilayers on Mesoporous Substrates: Energy/Electron Transfer, Photon Upconversion, and More. *J. Photochem. Photobiol. A Chem.* **2020**, *390*, No. 112291.
(191) Ungashe, S. B.; Wilson, W. L.; Katz, H. E.; Scheller, G. R.; Putvinski, T. M. Synthesis, Self-Assembly, and Photophysical Dynamics of Stacked Layers of Porphyrin and Viologen Phosphonates. *J. Am. Chem. Soc.* **1992**, *114* (22), 8717−8719.
(192) Katz, H. E. Multilayer Deposition of Novel Organophosphonates with Zirconium(IV). *Chem. Mater.* **1994**, *6* (12), 2227−2232.
(193) Bangle, R. E.; Schneider, J.; Piechota, E. J.; Troian-Gautier, L.; Meyer, G. J. Electron Transfer Reorganization Energies in the Electrode−Electrolyte Double Layer. *J. Am. Chem. Soc.* **2020**, *142* (2), 674−679.
(194) Bangle, R. E.; Schneider, J.; Conroy, D. T.; Aramburu-Trošelj, B. M.; Meyer, G. J. Kinetic Evidence That the Solvent Barrier for Electron Transfer Is Absent in the Electric Double Layer. *J. Am. Chem. Soc.* **2020**, *142* (35), 14940−14946.
(195) Hoque, M. A.; Gil-Sepulcre, M.; de Aguirre, A.; Elemans, J. A. A. W.; Moonshiram, D.; Matheu, R.; Shi, Y.; Benet-Buchholz, J.; Sala, X.; Malfois, M.; Solano, E.; Lim, J.; Garzón-Manjón, A.; Scheu, C.; Lanza, M.; Maseras, F.; Gimbert-Suriñach, C.; Llobet, A. Water Oxidation Electrocatalysis Using Ruthenium Coordination Oligomers Adsorbed on Multiwalled Carbon Nanotubes. *Nat. Chem.* **2020**, *12* (11), 1060−1066.
(196) Matheu, R.; Garrido-Barros, P.; Gil-Sepulcre, M.; Ertem, M. Z.; Sala, X.; Gimbert-Suriñach, C.; Llobet, A. The Development of Molecular Water Oxidation Catalysts. *Nat. Rev. Chem.* **2019**, *3* (5), 331−341.
(197) Duan, L.; Bozoglian, F.; Mandal, S.; Stewart, B.; Privalov, T.; Llobet, A.; Sun, L. A Molecular Ruthenium Catalyst with Water-Oxidation Activity Comparable to That of Photosystem II. *Nat. Chem.* **2012**, *4* (5), 418−423.
(198) Burstall, F. H. Optical Activity Dependent on Co-Ordinated Bivalent Ruthenium. *J. Chem. Soc.* **1936**, 173−175.
(199) Univ Australian Nouveaux complexes métalliques et leur procédé de préparation. BE617989A, November 23, 1962. https://patents.google.com/patent/BE617989A/en?oq=BE617989A (accessed Nov 09, 2025).
(200) *The brilliant history of photoredox catalysis*. https://www.nature.com/articles/d42473-019-00033-7 (accessed Oct 27, 2025).
(201) Grimm, I.; Hauer, S. T.; Schulte, T.; Wycich, G.; Collins, K. D.; Lovis, K.; Candish, L. Upscaling Photoredox Cross-Coupling Reactions in Batch Using Immersion-Well Reactors. *Org. Process Res. Dev.* **2020**, *24* (6), 1185−1193.
(202) Harper, K. C.; Moschetta, E. G.; Bordawekar, S. V.; Wittenberger, S. J. A Laser Driven Flow Chemistry Platform for Scaling Photochemical Reactions with Visible Light. *ACS Cent. Sci.* **2019**, *5* (1), 109−115.
(203) Harper, K. C.; Zhang, E.-X.; Liu, Z.-Q.; Grieme, T.; Towne, T. B.; Mack, D. J.; Griffin, J.; Zheng, S.-Y.; Zhang, N.-N.; Gangula, S.; Yuan, J.-L.; Miller, R.; Huang, P.-Z.; Gage, J.; Diwan, M.; Ku, Y.-Y. Commercial-Scale Visible Light Trifluoromethylation of 2-Chlorothiophenol Using CF_3I Gas. *Org. Process Res. Dev.* **2022**, *26* (2), 404−412.
(204) Faatz, E.; Finke, A.; Josel, H.-P.; Prencipe, G.; Quint, S.; Windfuhr, M. Chapter 15. Automated Immunoassays for the Detection of Biomarkers in Body Fluids. *Detection Science* **2019**, 443−470.
(205) Zanut, A.; Fiorani, A.; Canola, S.; Saito, T.; Ziebart, N.; Rapino, S.; Rebeccani, S.; Barbon, A.; Irie, T.; Josel, H.-P.; Negri, F.; Marcaccio, M.; Windfuhr, M.; Imai, K.; Valenti, G.; Paolucci, F. Insights into the Mechanism of Coreactant Electrochemiluminescence Facilitating Enhanced Bioanalytical Performance. *Nat. Commun.* **2020**, *11* (1), 2668.
(206) Orellana, G.; García-Fresnadillo, D. Environmental and Industrial Optosensing with Tailored Luminescent Ru(II) Polypyridyl Complexes. In *Optical Sensors: Industrial Environmental and Diagnostic Applications*; Narayanaswamy, R.; Wolfbeis, O. S., Eds.; Springer: Berlin, Heidelberg, 2004; pp 309−357.
(207) Lo, K. P.; Groger, H. P.; Luo, S.; Churchill, R. J. Loss Compensation Using Digital-Signal Processing in Fiber-Optic

https://doi.org/10.1021/acs.inorgchem.6c00560
Inorg. Chem. 2026, 65, 7549−7577

Fluorescence Sensors. US6207961B1, March 27, 2001. https://patents.google.com/patent/US6207961B1/en?oq=+US+Patent+6207961 (accessed Nov 02, 2025).
(208) Sasso, M. G.; Quina, F. H.; Bechara, E. J. H. Ruthenium(II) Tris(Bipyridyl) Ion as a Luminescent Probe for Oxygen Uptake. *Anal. Biochem.* **1986**, *156* (1), 239−243.
(209) Oguzlar, S.; Zeyrek Ongun, M. Enhancing the O_2 Sensitivity of $[Ru(Bpy)_3]^{2+}$ Dye by Incorporating SnO_2 and Ni:SnO_2. *J. Mater. Sci: Mater. Electron* **2024**, *35* (13), 920.
(210) Shulze, J. E. Fiber Optic Catheter System with Fluorometric Sensor and Integral Flexure Compensation. US5012809A, May 7, 1991. https://patents.google.com/patent/US5012809A/en?oq=US+Patent+5012809 (accessed Nov 02, 2025).
(211) Kaneko, M.; Nakamura, H. Oxygen Concentration Probe. WO1988000339A1, January 14, 1988. https://patents.google.com/patent/WO1988000339A1/en?oq=ES2007362 (accessed Nov 02, 2025).
(212) Walt, D. R.; Barnard, S. M. Imaging Fiber Optic Array Sensors, Apparatus, and Methods for Concurrently Detecting Multiple Analytes of Interest in a Fluid Sample. US5244636A, September 14, 1993. https://patents.google.com/patent/US5244636A/en?oq=US+Patent+5244636 (accessed Nov 02, 2025).
(213) *Ocean Optics Catalog of Products*. https://www.oceanoptics.com/catalog/ (accessed Nov 02, 2025).
(214) Monro, S.; Colón, K. L.; Yin, H.; Roque, J.; Konda, P.; Gujar, S.; Thummel, R. P.; Lilge, L.; Cameron, C. G.; McFarland, S. A. Transition Metal Complexes and Photodynamic Therapy from a Tumor-Centered Approach: Challenges, Opportunities, and Highlights from the Development of TLD1433. *Chem. Rev.* **2019**, *119* (2), 797−828.
(215) Kulkarni, G.; Kassouf, W.; Richards, K.; Jayram, G.; Rendon, R.; Shore, N.; Agarwal, P.; Inman, B.; Saltzstein, D.; Kramalowsky, E.; Kamat, A.; O'Donnell, M.; Mandel, A.; Dumoulin-White, R.; Black, P. C. Pd12−13 Interim Analysis Of Light-Activated Tld-1433 In A Phase Ii Clinical Study Of Bcg-Unresponsive Non-Muscle Invasive Bladder Cancer Carcinoma In-Situ. *J. Urol.* **2025**, *213* (5S), No. e393.
(216) Chettri, A.; Roque, J. A., III; Schneider, K. R. A.; Cole, H. D.; Cameron, C. G.; McFarland, S. A.; Dietzek, B. It Takes Three to Tango: The Length of the Oligothiophene Chain Determines the Nature of the Long-Lived Excited State and the Resulting Photocytotoxicity of a Ruthenium(II) Photodrug. *ChemPhotoChem.* **2021**, *5* (5), 421−425.
(217) Shi, G.; Monro, S.; Hennigar, R.; Colpitts, J.; Fong, J.; Kasimova, K.; Yin, H.; DeCoste, R.; Spencer, C.; Chamberlain, L.; Mandel, A.; Lilge, L.; McFarland, S. A. Ru(II) Dyads Derived from α-Oligothiophenes: A New Class of Potent and Versatile Photosensitizers for PDT. *Coord. Chem. Rev.* **2015**, *282*−*283*, 127−138.
(218) Förster, C.; Heinze, K. Photophysics and Photochemistry with Earth-Abundant Metals - Fundamentals and Concepts. *Chem. Soc. Rev.* **2020**, *49*, 1057−1070.
(219) Kronenberger, S.; Naumann, R.; Förster, C.; East, N. R.; Klett, J.; Heinze, K. A Manganese(I) Complex with a 190 Ns Metal-to-Ligand Charge Transfer Lifetime. *Nat. Commun.* **2025**, *16* (1), 7850.
(220) Sinha, N.; Wegeberg, C.; Häussinger, D.; Prescimone, A.; Wenger, O. S. Photoredox-Active Cr(0) Luminophores Featuring Photophysical Properties Competitive with Ru(II) and Os(II) Complexes. *Nat. Chem.* **2023**, *15* (12), 1730−1736.
(221) Kjær, K. S.; Kaul, N.; Prakash, O.; Chábera, P.; Rosemann, N. W.; Honarfar, A.; Gordivska, O.; Fredin, L. A.; Bergquist, K.-E.; Häggström, L.; Ericsson, T.; Lindh, L.; Yartsev, A.; Styring, S.; Huang, P.; Uhlig, J.; Bendix, J.; Strand, D.; Sundström, V.; Persson, P.; Lomoth, R.; Wärnmark, K. Luminescence and Reactivity of a Charge-Transfer Excited Iron Complex with Nanosecond Lifetime. *Science* **2019**, *363* (6424), 249−253.
(222) Chan, A. Y.; Ghosh, A.; Yarranton, J. T.; Twilton, J.; Jin, J.; Arias-Rotondo, D. M.; Sakai, H. A.; McCusker, J. K.; MacMillan, D. W. C. Exploiting the Marcus Inverted Region for First-Row Transition Metal-Based Photoredox Catalysis. *Science* **2023**, *382* (6667), 191−197.
(223) Barth, A. T.; Fajardo, J.; Sattler, W.; Winkler, J. R.; Gray, H. B. Electronic Structures and Photoredox Chemistry of Tungsten(0) Arylisocyanides. *Acc. Chem. Res.* **2023**, *56* (14), 1978−1989.
(224) Gafni, A.; Steinberg, I. Z. Optical Activity and Lifetime Measurements of Tris-(2,2′-Bipyridine) Ruthenium (II) Bromide: Evidence for Some Singlet-Singlet Emission. *Isr. J. Chem.* **1976**, *15* (1−2), 102−105.
(225) Sittel, S.; Neuner, J.; Grenz, J. M.; Förster, C.; Naumann, R.; Heinze, K. Gram-Scale Photocatalysis with a Stable and Recyclable Chromium(III) Photocatalyst in Acetonitrile and in Water. *Adv. Synth. Catal.* **2025**, *367* (10), No. e202500075.
(226) Treiling, S.; Wang, C.; Förster, C.; Reichenauer, F.; Kalmbach, J.; Boden, P.; Harris, J. P.; Carrella, L. M.; Rentschler, E.; Resch-Genger, U.; Reber, C.; Seitz, M.; Gerhards, M.; Heinze, K. Luminescence and Light-Driven Energy and Electron Transfer from an Exceptionally Long-Lived Excited State of a Non-Innocent Chromium(III) Complex. *Angew. Chem., Int. Ed.* **2019**, *58* (50), 18075−18085.
(227) Hamze, R.; Peltier, J. L.; Sylvinson, D.; Jung, M.; Cardenas, J.; Haiges, R.; Soleilhavoup, M.; Jazzar, R.; Djurovich, P. I.; Bertrand, G.; Thompson, M. E. Eliminating Nonradiative Decay in Cu(I) Emitters: 99% Quantum Efficiency and Microsecond Lifetime. *Science* **2019**, *363* (6427), 601−606.
(228) Reichenauer, F.; Wang, C.; Förster, C.; Boden, P.; Ugur, N.; Báez-Cruz, R.; Kalmbach, J.; Carrella, L. M.; Rentschler, E.; Ramanan, C.; Niedner-Schatteburg, G.; Gerhards, M.; Seitz, M.; Resch-Genger, U.; Heinze, K. Strongly Red-Emissive Molecular Ruby $[Cr(Bpmp)_2]^{3+}$ Surpasses $[Ru(Bpy)_3]^{2+}$. *J. Am. Chem. Soc.* **2021**, *143* (30), 11843−11855.
(229) Jin, T.; Sinha, N.; Wagner, D. S.; Prescimone, A.; Häussinger, D.; Wenger, O. S. Making Mo(0) a Competitive Alternative to Ir(III) in Phosphors and Photocatalysts. *J. Am. Chem. Soc.* **2025**, *147* (5), 4587−4594.
(230) Dee, C.; Zinna, F.; Kitzmann, W. R.; Pescitelli, G.; Heinze, K.; Di Bari, L.; Seitz, M. Strong Circularly Polarized Luminescence of an Octahedral Chromium(III) Complex. *Chem. Commun.* **2019**, *55* (87), 13078−13081.
(231) Jiménez, J.-R.; Doistau, B.; Cruz, C. M.; Besnard, C.; Cuerva, J. M.; Campaña, A. G.; Piguet, C. Chiral Molecular Ruby $[Cr(Dqp)_2]^{3+}$ with Long-Lived Circularly Polarized Luminescence. *J. Am. Chem. Soc.* **2019**, *141*, 13244−13252.
(232) Jiménez, J.-R.; Poncet, M.; Míguez-Lago, S.; Grass, S.; Lacour, J.; Besnard, C.; Cuerva, J. M.; Campaña, A. G.; Piguet, C. Bright Long-Lived Circularly Polarized Luminescence in Chiral Chromium(III) Complexes. *Angew. Chem., Int. Ed.* **2021**, *60* (18), 10095−10102.
(233) Muthig, A. M. T.; Mrózek, O.; Ferschke, T.; Rödel, M.; Ewald, B.; Kuhnt, J.; Lenczyk, C.; Pflaum, J.; Steffen, A. Mechano-Stimulus and Environment-Dependent Circularly Polarized TADF in Chiral Copper(I) Complexes and Their Application in OLEDs. *J. Am. Chem. Soc.* **2023**, *145* (8), 4438−4449.
(234) Alowakennu, M. M.; Ghosh, A.; McCusker, J. K. Direct Evidence for Excited Ligand Field State-Based Oxidative Photoredox Chemistry of a Cobalt(III) Polypyridyl Photosensitizer. *J. Am. Chem. Soc.* **2023**, *145* (38), 20786−20791.
(235) Yaltseva, P.; Maisuradze, T.; Prescimone, A.; Kupfer, S.; Wenger, O. S. Structural Control of Metal-Centered Excited States in Cobalt(III) Complexes via Bite Angle and π−π Interactions. *J. Am. Chem. Soc.* **2025**, *147* (32), 29444−29456.
(236) Stevenson, S. M.; Shores, M. P.; Ferreira, E. M. Photooxidizing Chromium Catalysts for Promoting Radical Cation Cycloadditions. *Angew. Chem., Int. Ed.* **2015**, *54* (22), 6506−6510.
(237) Stevenson, S. M.; Higgins, R. F.; Shores, M. P.; Ferreira, E. M. Chromium Photocatalysis: Accessing Structural Complements to Diels-Alder Adducts with Electron-Deficient Dienophiles. *Chem. Sci.* **2017**, *8* (1), 654−660.
(238) Sittel, S.; Naumann, R.; Heinze, K. Molecular Rubies in Photoredox Catalysis. *Front. Chem.* **2022**, *10*, No. 887439.
(239) Bürgin, T. H.; Glaser, F.; Wenger, O. S. Shedding Light on the Oxidizing Properties of Spin-Flip Excited States in a CrIII

https://doi.org/10.1021/acs.inorgchem.6c00560
Inorg. Chem. 2026, 65, 7549−7577

Polypyridine Complex and Their Use in Photoredox Catalysis. *J. Am. Chem. Soc.* **2022**, *144* (31), 14181−14194.
(240) Castellano, F. N.; Rosko, M. C. Steric and Electronic Influence of Excited-State Decay in Cu(I) MLCT Chromophores. *Acc. Chem. Res.* **2024**, *57* (19), 2872−2886.
(241) Beaudelot, J.; Oger, S.; Peruško, S.; Phan, T.-A.; Teunens, T.; Moucheron, C.; Evano, G. Photoactive Copper Complexes: Properties and Applications. *Chem. Rev.* **2022**, *122* (22), 16365−16609.
(242) Fischer, A. C.; Förster, C.; Kitzmann, W. R.; Heinze, K. A Blessing and a Curse: Remote Ligand Functionalization Modulates ^{3}MLCT Relaxation in Group 6 Tricarbonyl Complexes. *Inorg. Chem.* **2025**, *64* (12), 6100−6114.
(243) Büldt, L. A.; Wenger, O. S. Chromium(0), Molybdenum(0), and Tungsten(0) Isocyanide Complexes as Luminophores and Photosensitizers with Long-Lived Excited States. *Angew. Chem., Int. Ed.* **2017**, *56* (21), 5676−5682.
(244) Zhang, Y.; Leary, D. C.; Belldina, A. M.; Petersen, J. L.; Milsmann, C. Effects of Ligand Substitution on the Optical and Electrochemical Properties of (Pyridinedipyrrolide)Zirconium Photosensitizers. *Inorg. Chem.* **2020**, *59* (20), 14716−14730.
(245) Zhang, Y.; Lee, T. S.; Petersen, J. L.; Milsmann, C. A Zirconium Photosensitizer with a Long-Lived Excited State: Mechanistic Insight into Photoinduced Single-Electron Transfer. *J. Am. Chem. Soc.* **2018**, *140* (18), 5934−5947.
(246) Qiao, Y.; Cheisson, T.; Manor, B. C.; Carroll, P. J.; Schelter, E. J. A Strategy to Improve the Performance of Cerium(III) Photocatalysts. *Chem. Commun.* **2019**, *55* (28), 4067−4070.
(247) Swierk, J. R. The Cost of Quantum Yield. *Org. Process Res. Dev.* **2023**, *27* (7), 1411−1419.
(248) Kitzmann, W. R.; Moll, J.; Heinze, K. Spin-Flip Luminescence. *Photochem. Photobiol. Sci.* **2022**, *21* (7), 1309−1331.
(249) Wang, C.; Otto, S.; Dorn, M.; Heinze, K.; Resch-Genger, U. Luminescent TOP Nanosensors for Simultaneously Measuring Temperature, Oxygen, and pH at a Single Excitation Wavelength. *Anal. Chem.* **2019**, *91* (3), 2337−2344.
(250) Bayliss, S. L.; Laorenza, D. W.; Mintun, P. J.; Kovos, B. D.; Freedman, D. E.; Awschalom, D. D. Optically Addressable Molecular Spins for Quantum Information Processing. *Science* **2020**, *370* (6522), 1309−1312.
(251) Fataftah, M. S.; Bayliss, S. L.; Laorenza, D. W.; Wang, X.; Phelan, B. T.; Wilson, C. B.; Mintun, P. J.; Kovos, B. D.; Wasielewski, M. R.; Han, S.; Sherwin, M. S.; Awschalom, D. D.; Freedman, D. E. Trigonal Bipyramidal V^{3+} Complex as an Optically Addressable Molecular Qubit Candidate. *J. Am. Chem. Soc.* **2020**, *142* (48), 20400−20408.
(252) Laorenza, D. W.; Mullin, K. R.; Weiss, L. R.; Bayliss, S. L.; Deb, P.; Awschalom, D. D.; Rondinelli, J. M.; Freedman, D. E. Coherent Spin-Control of S = 1 Vanadium and Molybdenum Complexes. *Chem. Sci.* **2024**, *15* (34), 14016−14026.
(253) Yue, M.; He, J.; Zou, C.; Chang, X.; Lu, W. Phosphorescent Fac-Bis(Triarylisocyanide) W(0) and Mo(0) Complexes. *Inorg. Chem.* **2024**, *63* (7), 3267−3282.
(254) Arrico, L.; Di Bari, L.; Zinna, F. Quantifying the Overall Efficiency of Circularly Polarized Emitters. *Chem.—Eur. J.* **2021**, *27* (9), 2920−2934.
(255) MacKenzie, L. E.; Pal, R. Circularly Polarized Lanthanide Luminescence for Advanced Security Inks. *Nat. Rev. Chem.* **2021**, *5* (2), 109−124.
(256) Stachelek, P.; MacKenzie, L.; Parker, D.; Pal, R. Circularly Polarised Luminescence Laser Scanning Confocal Microscopy to Study Live Cell Chiral Molecular Interactions. *Nat. Commun.* **2022**, *13* (1), 553.
(257) Aiello, C. D.; Abendroth, J. M.; Abbas, M.; Afanasev, A.; Agarwal, S.; Banerjee, A. S.; Beratan, D. N.; Belling, J. N.; Berche, B.; Botana, A.; Caram, J. R.; Celardo, G. L.; Cuniberti, G.; Garcia-Etxarri, A.; Dianat, A.; Diez-Perez, I.; Guo, Y.; Gutierrez, R.; Herrmann, C.; Hihath, J.; Kale, S.; Kurian, P.; Lai, Y.-C.; Liu, T.; Lopez, A.; Medina, E.; Mujica, V.; Naaman, R.; Noormandipour, M.; Palma, J. L.; Paltiel, Y.; Petuskey, W.; Ribeiro-Silva, J. C.; Saenz, J. J.; Santos, E. J. G.; Solyanik-Gorgone, M.; Sorger, V. J.; Stemer, D. M.; Ugalde, J. M.; Valdes-Curiel, A.; Varela, S.; Waldeck, D. H.; Wasielewski, M. R.; Weiss, P. S.; Zacharias, H.; Wang, Q. H. A Chirality-Based Quantum Leap. *ACS Nano* **2022**, *16* (4), 4989−5035.
(258) Furlan, F.; Moreno-Naranjo, J. M.; Gasparini, N.; Feldmann, S.; Wade, J.; Fuchter, M. J. Chiral Materials and Mechanisms for Circularly Polarized Light-Emitting Diodes. *Nat. Photonics* **2024**, *18*, 658−668.
(259) VanOrman, Z. A.; Kitzmann, W. R.; Reponen, A.-P. M.; Deshpande, T.; Jöbsis, H. J.; Feldmann, S. Chiral Light−Matter Interactions in Solution-Processable Semiconductors. *Nat. Rev. Chem.* **2025**, *9*, 208−223.
(260) Lunkley, J. L.; Shirotani, D.; Yamanari, K.; Kaizaki, S.; Muller, G. Extraordinary Circularly Polarized Luminescence Activity Exhibited by Cesium Tetrakis(3-Heptafluoro-Butylryl-(+)-Camphorato) Eu(III) Complexes in EtOH and $CHCl_3$ Solutions. *J. Am. Chem. Soc.* **2008**, *130* (42), 13814−13815.
(261) Poncet, M.; Cuevas-Contreras, L.; Ye, Y.; Guénée, L.; Cruz, C. M.; Piguet, C.; Jiménez, J.-R. Exploring the Role of the Nephelauxetic Effect in Circularly Polarized Luminescence of Chiral Chromium(III) Complexes. *J. Am. Chem. Soc.* **2025**, *147* (27), 23827−23833.
(262) Haxel, G. B.; Hedrick, J. B.; Orris, G. J. *Rare EarthElements—Critical Resources for High Technology*; U.S. Geolocial Survey, 2002, Fact Sheet 087-02.
(263) Glaser, F.; Aydogan, A.; Elias, B.; Troian-Gautier, L. The Great Strides of Iron Photosensitizers for Contemporary Organic Photoredox Catalysis: On Our Way to the Holy Grail? *Coord. Chem. Rev.* **2024**, *500*, No. 215522.
(264) Lee, A.; Son, M.; Deegbey, M.; Woodhouse, M. D.; Hart, S. M.; Beissel, H. F.; Cesana, P. T.; Jakubikova, E.; McCusker, J. K.; Schlau-Cohen, G. S. Observation of Parallel Intersystem Crossing and Charge Transfer-State Dynamics in $[Fe(Bpy)_3]^{2+}$ from Ultrafast 2D Electronic Spectroscopy. *Chem. Sci.* **2023**, *14* (45), 13140−13150.
(265) Leis, W.; Argüello Cordero, M. A.; Lochbrunner, S.; Schubert, H.; Berkefeld, A. A Photoreactive Iron(II) Complex Luminophore. *J. Am. Chem. Soc.* **2022**, *144* (3), 1169−1173.
(266) Ripak, A.; De Kreijger, S.; Sampaio, R. N.; Vincent, C. A.; Cauët, É.; Jabin, I.; Tambar, U. K.; Elias, B.; Troian-Gautier, L. Photosensitized Activation of Diazonium Derivatives for C−B Bond Formation. *Chem. Catal.* **2023**, *3* (2), No. 100490.
(267) Glaser, F.; De Kreijger, S.; Troian-Gautier, L. Two Birds, One Stone: Microsecond Dark Excited-State Lifetime and Large Cage Escape Yield Afforded by an Iron−Anthracene Molecular Dyad. *J. Am. Chem. Soc.* **2025**, *147* (10), 8559−8567.
(268) Wellauer, J.; Pfund, B.; Becker, I.; Meyer, F.; Prescimone, A.; Wenger, O. S. Iron(III) Complexes with Luminescence Lifetimes of up to 100 Ns to Enhance Upconversion and Photocatalysis. *J. Am. Chem. Soc.* **2025**, *147* (10), 8760−8768.
(269) Glaser, F.; Beneventi, G. M.; Cadranel, A.; Troian-Gautier, L. Beyond Common Energy Transfer: Intramolecular Electron Transfer Cascade Controls Triplet Population of a Long-Lived Iron-Anthracene Molecular Dyad. *ACS Cent. Sci.* **2025**, *11* (10), 1870−1881.
(270) Wellauer, J.; Pattuwage, M. L.; Doeven, E. H.; Connell, T. U.; Wenger, O. S.; Francis, P. S. Rethinking the Excited-State Redox Properties of Iron(III) Complexes for LMCT Photoredox Catalysis. *J. Am. Chem. Soc.* **2025**, *147* (32), 29304−29314.
(271) Losada, I. B.; Ryde, U.; Persson, P. Understanding Anomalous Cage-Escape Dynamics in Photoredox Processes Driven by a Fe(III) N-Heterocyclic Carbene Complex. *J. Am. Chem. Soc.* **2025**, *147* (35), 31509−31520.
(272) Wegeberg, C.; Calvet, N. A.; Krafft, M.; Chábera, P.; Yartsev, A.; Persson, P. Captivating Bimolecular Photoredox Dynamics of a Ligand-to-Metal Charge Transfer Complex. *Chem. Sci.* **2025**, *16* (46), 21975−21990.
(273) De Kreijger, S.; Ripak, A.; Elias, B.; Troian-Gautier, L. Investigation of the Excited-State Electron Transfer and Cage Escape Yields Between Halides and a Fe(III) Photosensitizer. *J. Am. Chem. Soc.* **2024**, *146* (15), 10286−10292.

https://doi.org/10.1021/acs.inorgchem.6c00560
Inorg. Chem. 2026, 65, 7549−7577

(274) Ripak, A.; Vega Salgado, A. K.; Valverde, D.; Cristofaro, S.; de Gary, A.; Olivier, Y.; Elias, B.; Troian-Gautier, L. Factors Controlling Cage Escape Yields of Closed- and Open-Shell Metal Complexes in Bimolecular Photoinduced Electron Transfer. *J. Am. Chem. Soc.* **2024**, *146* (32), 22818−22828.
(275) Goodwin, M. J.; Dickenson, J. C.; Ripak, A.; Deetz, A. M.; McCarthy, J. S.; Meyer, G. J.; Troian-Gautier, L. Factors That Impact Photochemical Cage Escape Yields. *Chem. Rev.* **2024**, *124* (11), 7379−7464.
(276) Wang, L.; Zhao, Z.; Zhan, G.; Fang, H.; Yang, H.; Huang, T.; Zhang, Y.; Jiang, N.; Duan, L.; Liu, Z.; Bian, Z.; Lu, Z.; Huang, C. Deep-Blue Organic Light-Emitting Diodes Based on a Doublet d−f Transition Cerium(III) Complex with 100% Exciton Utilization Efficiency. *Light Sci. Appl.* **2020**, *9* (1), 157.
(277) Wang, C.; Wegeberg, C.; Wenger, O. S. First-Row d^6 Metal Complex Enables Photon Upconversion and Initiates Blue Light-Dependent Polymerization with Red Light. *Angew. Chem., Int. Ed.* **2023**, *62* (43), No. e202311470.
(278) Jin, P.; Xu, X.; Yan, Y.; Hammecke, H.; Wang, C. Luminescent Fe(III) Complex Sensitizes Aerobic Photon Upconversion and Initiates Photocatalytic Radical Polymerization. *J. Am. Chem. Soc.* **2024**, *146* (51), 35390−35401.
(279) Doettinger, F.; Sagaya, J.; Morselli, G.; Wenger, O. S. Homomolecular Photon Upconversion in a Perylene-Decorated Iron(III) Complex. *J. Am. Chem. Soc.* **2025**, *147* (46), 43013−43028.
(280) Wang, C.; Reichenauer, F.; Kitzmann, W. R.; Kerzig, C.; Heinze, K.; Resch-Genger, U. Efficient Triplet-Triplet Annihilation Upconversion Sensitized by a Chromium(III) Complex via an Underexplored Energy Transfer Mechanism. *Angew. Chem., Int. Ed.* **2022**, *61* (27), No. e202202238.
(281) Hernández-Castillo, D.; Eder, I.; González, L. Guidelines to Calculate Non-Radiative Deactivation Mechanisms of Ruthenium Tris(Bipyridine) Derivatives. *Coord. Chem. Rev.* **2024**, *510*, No. 215819.
(282) Gao, Z.-Z.; Xu, Y.-Y.; Wang, Z.-K.; Wang, H.; Zhang, D.-W.; Li, Z.-T. Porous $[Ru(Bpy)_3]^{2+}$-Cored Metallosupramolecular Polymers: Preparation and Recyclable Photocatalysis for the Formation of Amides and 2-Diazo-2-Phenylacetates. *ACS Appl. Polym. Mater.* **2020**, *2* (11), 4885−4892.

https://doi.org/10.1021/acs.inorgchem.6c00560
Inorg. Chem. 2026, 65, 7549−7577